UNIVERSIDAD COMPLUTENSE DE MADRID
FACULTY OF CHEMICAL SCIENCES
DEPARTMENT OF BIOCHEMISTRY AND MOLECULAR BIOLOGY

Characterization of phasin PhaF interactions in the model polyhydroxyalkanoate-accumulating bacterium, *Pseudomonas putida* KT2440

Caracterización de las interacciones de la fasina PhaF en la bacteria modelo acumuladora de polihidroxialcanoatos, *Pseudomonas putida* KT2440

PhD THESIS

NATALIA ANDREA TARAZONA LIZCANO

Madrid, 2019

UNIVERSIDAD COMPLUTENSE DE MADRID
FACULTY OF CHEMICAL SCIENCES
DEPARTMENT OF BIOCHEMISTRY AND MOLECULAR BIOLOGY

Characterization of phasin PhaF interactions in the model polyhydroxyalkanoate-accumulating bacterium, *Pseudomonas putida* KT2440

Caracterización de las interacciones de la fasina PhaF en la bacteria modelo acumuladora de polihidroxialcanoatos, *Pseudomonas putida* KT2440

PhD THESIS

NATALIA ANDREA TARAZONA LIZCANO

DIRECTOR

MARÍA AUXILIADORA PRIETO JIMÉNEZ

SPANISH NATIONAL RESEARCH COUNCIL -CSIC
BIOLOGICAL RESEARCH CENTER -CIB

Madrid, 2019

Nothing is invented, for it's written in nature first.
Originality consists of returning to the origin.

Antoni Gaudí

To my loving family

ACKNOWLEDGEMENTS

Some years ago, I engaged into the biggest adventure of my life, flying away from my nest looking for the “scientific dream”. Today is the day! Today is the day I dreamt about so many nights. The day I am going to remember my whole life. However, birds do not fly alone, and I have to close this dissertation by reflecting on the people who have supported and helped me so much throughout this period.

I would first like to thank my thesis advisor Auxi Prieto. She allowed this thesis to be my own work, but she always shepherded me in the right direction whenever she thought I needed it. She always knew how to keep me motivated but she also knew how to manage my over-excitement in those moments when I was caught up in (wrongly) interpretations of experimental findings. I could not have imagined having a more valuable mentor for my PhD study.

Second, I would like to acknowledge the sources of my research funding: the European Union's Horizon 2020 research and innovation program (n° 633962), the Community of Madrid (P2013/MIT2807), the Spanish Ministry of the Economy (BIO2017-83448-R and BIO2016-79323-R), and the Department of Science Technology and Innovation (Colciencias, Colombia). Special thanks to the Spanish National Research Council (CSIC), the Biological Research Center (CIB) and its facilities for all the scientific support.

I would like to thank Dr. Germán Rivas and Dr. Mercedes Jiménez for opening the doors of their group and contributing to my processional development at CIB. Many thanks to Dr. Olga Revelles, Dr. Jesús Sanz and Dr. Beatriz Maestro for their assistance to some of my research projects and for their insightful comments. I am also grateful to the “Rubenes 1.0”. To Jose Luis, Eduardo, Ernesto and Pedro for being our mentors and the rulers of our big “family”. They have provided me personal and professional guidance and taught me how to overcome scientific difficulties.

My research would have been impossible without the aid and support of the Rubenes 2.0. Bea, Juan, and Gonzalo. They are the pillars of our group, the ones every PhD student runs to when an experimental advice is needed. I thank them for being so patient and for always caring about my research.

Special thanks to Bea, she has always being like a sister to me in science and in life. Her wisdom helped me to overcome many hard obstacles I had to face. I wish the world were more crowded with people like her. Bea, Ana V., Lidem, and Lorein managed to open their very closed and exclusive club to me and to make me feel part of their small family. I am especially thankful to them for all the laughs and all the love I had in the last years.

Ana V. was not only a laughs partner, but also she manage to be an essential part of this thesis. The smooth running of the “Rubenes” laboratory is much more a testimony to her efforts than of any others.

Very special gratitude goes to my lab mates; I was rewarded with a friendly and cheerful group of fellow students and postdocs. Cristina took me in the first years of my PhD and taught me how to move around the lab and around Madrid. She was always there for deep scientific discussions, beers and sports sections too. Arantxa and Maria Manoli knew how to keep me entertained all this years with their huge repertoire of anecdotes and stories. Maria was always a good companion for after work wine and laugh sections. Her strength is inspiring for me and I am deeply thankful for all her advices and for always be so straightforward when I needed.

Erika had always a big smile for me and she did a good job cheering me up in some of my lowest moments. Ana Maria was a mentor to me in the protein arena and quickly she became my confidant and the keeper of special secrets. Alberto was always a good company for coffee breaks because his energy and good attitude are so contagious. I could not be more thankful to him for being so supportive and open his ears and heart to me. I am also thankful for sharing so many special moments with Natalia H, Virginia, Manuel and Ryan and for these five years full of science and fun.

My sincere thanks to Dr. Andreas Lendlein and Dr. Schulz for awarded me a six months internship at Helmholtz Institute in Berlin. It has been the coldest winter of my life, but also one of the greatest and more exciting personal challenges I had to face. Special thanks go to Rainhard for being such a patience colleague and coach. I would also like to thank the rest of my labmates in Berlin, Shivam, Anne and Thanga. Their support and knowledge got me through my stay at the institute.

I am also thankful to Peter, Diego and Lucia for being my best friends during all these years. I cannot be more grateful to them for all the memories we built together and all the love. I could not have survived Madrid without them. Lorena has to be mentioned here, she was such an amazing company for me during my PhD and I thank her for all the special moments we shared.

I cannot finish without thanking my dearest “Fidolovers”, the best roommates everyone could have. They were like a family to me and I would never forget all the happy moments that we got to spend together. Special thanks to Mariana for those balcony moments trying to decipher “human behavior and the meaning of life”.

A huge gratitude goes for Alex. He could also feel this thesis as his achievement. He was always there in the happiest and saddest moments and always had the right words to make me keep going.

Finally, last but by no means least, I must express my very heartfelt gratitude to my parents and to my sisters for providing me with unfailing support during my years of study. Being away home has being difficult but their love for me and their continuous encouragement have made this thesis possible. Tatiana, Adriana and Yessenia, the best friends I have in the world, "*all our dream-worlds may come true*".

INDEX

ABBREVIATIONS

AFM	atomic force microscopy
A-W interface	air-water interface
BACTH	bacterial two-hybrid system
BAM	Brewster angle microscopy
BioF	N-terminal domain of PhaF
BLItz	biolayer interferometry system
cAMP	cyclic adenosine monophosphate
CCM	coiled-coil motif
Cs^{-1}	compressibility modulus
Cya	adenylate cyclase from *Bordetella pertussis*
EGFP	enhanced green fluorescent protein
EMSA	electrophoretic mobility shift assays
GAPs	granule-associated proteins
GFP	green fluorescent protein
IPTG	isopropyl-β-D-thiogalactopyranoside
IR	infrared
LB	Luria-Bertani medium
lcl-PHA	long-chain-length polyhydroxyalkanoates
LS	Langmuir-Schaefer
MBP	maltose-binding protein
mcl-PHA	medium-chain-length polyhydroxyalkanoates
MMA	mean molecular area
Mn	number average molecular weight
MS	mass sprectrometry
MWCO	molecular weight limit cut-off
NMR	nuclear magnetic resonance spectroscopy
ONPG	o-nitrophenol-β-galactoside
P4HB	poly(4-hydroxybutyrate)
PBS	phosphate buffered saline
P_{C1}	promoter region of *phaC1*
PCL	poly(ε-caprolactone)
PCR	polymerase chain reaction
PHA	polyhydroxyalkanoates
PHB	poly(3-*R*-hydroxybutyrate)
PHBHV	poly[(3-*R*-hydroxybutyrate)-*co*-(3-*R*-hydroxyvalerate)]
PHHx	poly(3-*R*-hydroxyhexanoate)
PHO	poly(3-*R*-hydroxyoctanoate)

PHOHHx	poly[(3-*R*-hydroxyoctanoate)-*co*-(3-*R*-hydroxyhexanoate)]
P_I	promoter region of *phaI*
PLA	poly(L-lactide)
PLGA	poly[(lactide-*co*-glycolide)]
PM-IRRAS	polarization modulated infrared absorption spectroscopy
PPIs	protein-protein interactions
PSM	peptide-spectrum match
RGD	integrin-binding motif (arginine-glycine-aspartic acid)
scl-PHA	short-chain-length polyhydroxyalkanoates
SDS-PAGE	sodium dodecyl sulfate-polyacrylamide gel electrophoresis
TEM	transmission electron microscopy
X-gal	5-bromo-4-chloro-3-indolyl-β-D-galactopyranoside
ZIP	leucine zipper-like motif of phasins
ZIPF	leucine zipper-like motif of phasin PhaF
ZIPI	leucine zipper-like motif of phasin PhaI
β-gal	β-galactosidase
π-A	surface pressure-area

SUMMARY

The discovery of bacterial polyhydroxyalkanoates (PHA) in the cytoplasm of *Bacillus megaterium* by Lemoigne (Lemoigne, 1926) unveiled a new class of *in vivo* synthesized polymers with adjustable properties and different applications (as plastics, in medical devices, etc.); it also provided impetus to research on proteins involved in PHA accumulation.

Interest in phasins emerged through two major observations: i) that they bind to PHA, potentially establishing a network-like protein layer on the surface of intracellular PHA granules; and ii) that their concentration can reach 5% (wt/wt) of the total protein content of PHA-accumulating cells (Wieczorek et al., 1995; Maestro and Sanz, 2017). Soon after it was found that these proteins are almost exclusively produced when PHA is synthesized (York et al., 2002), and that they play important roles in its biogenesis, helping to ensure optimal cell fitness. For example, phasins have been found to engage in the physical stabilization of PHA granules at the polymer-cytoplasm interface, and to participate in the control of the number and size of these granules, their segregation into daughter cells, and their mobilization (reviewed in (Mezzina and Pettinari, 2016; Maestro and Sanz, 2017)).

Although these proteins are highly diverse in sequence, they share structural features such as a majority amphipathic α-helix composition, and all show intrinsic disorder in absence of PHA. Structural models have additionally revealed them to possess coiled-coil regions that might be important in the establishment of protein-protein interactions (Maestro et al., 2013). However, experimental evidence of coiled-coil mediated oligomerization in these proteins has been lacking.

In the first chapter of this PhD thesis, structure prediction analyses are used to characterize the coiled-coil domains of phasins PhaF and PhaI produced by the model PHA-accumulating bacterium *Pseudomonas putida* KT2440. Their oligomerization is examined using biolayer interferometry and the *in vivo* two-hybrid (BACTH) system. The interaction capacity of a series of coiled-coil mutant phasins is also explored. The results confirm the formation of PhaF and PhaI complexes, and establish the involvement of a predicted short leucine zipper-like coiled-coil (ZIP), which contains “ideal” residues located within the hydrophobic core, in the oligomer's stability. The substitution of key residues (leucines or valines) in PhaI ZIP (ZIPI) for alanine is shown to reduce oligomerization efficiency by around 75%. These results indicate that coiled-coil motifs are essential in PhaF-PhaI interactions, and that the correct oligomerization of the phasins requires the formation of a stable hydrophobic interface between them. Since this motif is present in most phasins produced by PHA-accumulating bacteria, the

present results provide valuable insights into how PHA granule stability might be modified to fulfil diverse applications.

In spite of the high sequence similarity shared by PhaF and PhaI, the deletion of *phaF* is well known to have a notable impact on overall cell physiology, resulting in a non-homogeneous population in terms of PHA content and granule localization, and in the reduction of the expression of *phaC1* (PHA synthase) and *phaI* (Prieto et al., 1999; Galán et al., 2011; Dinjaski and Prieto, 2013). This is most likely due to the presence of the C-terminal or DNA binding domain in PhaF, which is absent in PhaI. Taking into account this observations, and the protein concentration at the surface of the granule, it was hypothesized in this work that PhaF might participate in extensive networks of protein–protein interactions that assemble and disassemble in obedience to specific cellular signals.

The second chapter discusses the comprehensive approach followed to identify candidates for novel interactions of PhaF. Mass spectrometry-coupled recombinant His_6-PhaF interaction/pull-down (affinity chromatography) experiments were used to screen for *P. putida* KT2440 proteins that interact with PhaF. Six were identified as forming complexes with PhaF, including two PHA-related proteins: phasin PhaI (UniProt Q88D20), and the transcriptional regulator PhaD (Q88D22). When these results were correlated with PHA granule proteome results, also accomplished in this Thesis, four of the latter six proteins were again identified. The most interesting finding, however, was the interaction between the PHA regulator protein PhaD and PhaF in the pull-down assay. PhaD functions as an activator of *phaC1* and *phaI* transcription. It binds to 25 and 29 bp target regions of the P_{C1} and P_I promoters respectively (which lie upstream of *phaC1* and *phaI* genes) (de Eugenio et al., 2010). Remarkably, the absence of PhaD in the PHA granules, corroborated by *in vivo* localization of a PhaD-GFP fusion protein, suggests the existence of a novel mechanism in which the PhaD-PhaF complex participates in the regulatory system controlling *pha* genes expression.

In vivo BACTH (two-hybrid) interaction assays confirmed the interaction of PhaF and PhaD. Electrophoretic mobility shift analysis of the *phaI* promoter revealed the formation of a DNA-PhaD-PhaF complex that migrates to a position on the gel different to those reached when the P_I DNA fragment is complexed with the two proteins individually. Based on these results, it might be concluded that PhaF and PhaD act in harmony to control the expression of *pha* genes.

The disclosure of *in vivo* roles for phasins over recent years has opened up a new field of research which holds the promise of developing innovative applications based on these proteins. The strong affinity of phasins for PHA (and other hydrophobic materials) has already led to the development of affinity tags for use in low-cost recombinant protein purification, specific drug delivery vehicles, and cell sorting techniques.

Additionally, their amphiphilic nature means phasins have uses as biosurfactants (Wei et al., 2011) and the functionalization of biomaterials through coating their surfaces in combination with cell signal molecules (Dong et al., 2010; Xie et al., 2013; Gao et al., 2014).

Despite the remarkable properties of phasins, and their recently explored use in the surface coating of biomaterials, we know little about their robustness and stability at interfaces, or about their adsorption behavior with respect to PHA (their natural substrates). Neither has the alteration of the molecular conformation of either during the functionalization process been addressed. The Langmuir technique was therefore used to study the interaction of PhaF with PHA by mimicking the native environment, thus providing insights into the structure of the PHA-PhaF complex. The results could help to improve control over phasin-coated material production.

The Langmuir technique, combined with *in situ* microscopy and spectroscopic methods, revealed PhaF to form stable and robust monolayers at different temperatures, with an almost flat orientation of its alpha-helix at the air-water interface. The adsorption of PhaF onto preformed PHA monolayers yielded stable mixed-layers below a surface pressure of π = ~15.7 mN/m. Further PhaF adsorption induced a molecular reorganization of the film. In the prospective of the assumption made in this work, the surface of granules being formed merely by proteins, these results let us conclude that elevated concentrations of PhaF function as a surfactant, separating PHA into "granules" in hydrophilic environments as occurs in the cytoplasm of bacterial cells.

Furthermore, PHA polymers with stronger surface hydrophobicity are here shown to be more appropriate substrates for PhaF-mediated functionalization than less hydrophobic polyesters like PLGA, poly[(lactide-*co*-glycolide)]. The observed orientation of the main axis of the protein in relation to both polyester surfaces ensures the best exposure of the hydrophobic residues. A suitable coating strategy for producing PHA-functionalized materials is thus unveiled. The Langmuir technique also allowed for the preparation of monomolecular films of PhaF that were successfully transferred to solid substrates and characterized by atomic force microscopy (AFM). This chapter presents the first thorough analysis of the surface properties of PhaF, and the results obtained help to improve our understanding of already used PHA-based biomaterials, and perhaps other polyester-based biomaterials.

RESUMEN

El descubrimiento de polihidroxialcanoatos de origen bacteriano (PHA) en el citoplasma de *Bacillus megaterium* por Lemoigne (Lemoigne, 1926), no solo reveló una nueva clase de polímeros sintetizados *in vivo* con propiedades modulables y diferentes aplicaciones (como plásticos, en dispositivos médicos, etc.); sino que también impulsó la investigación sobre proteínas involucradas en la acumulación de PHA.

El interés en las fasinas (phasins en inglés) surgió principalmente por dos observaciones: i) son proteínas que se unen al PHA, posiblemente estableciendo una capa proteica en forma de red en la superficie de los gránulos de PHA; y ii) su concentración puede alcanzar un 5% en peso del contenido total de proteína en las células que acumulan PHA (Wieczorek et al., 1995; Maestro and Sanz, 2017). Poco después, se descubrió que estas proteínas se producen casi exclusivamente en función de la síntesis de PHA (York et al., 2002), y que desempeñan un papel importante en su biogénesis, ayudando además a garantizar el estado óptimo de las células. Por ejemplo, se ha descrito que en la interfaz polímero-citoplasma las fasinas participan en la estabilización física de los gránulos de PHA, y que participan en el control del número y tamaño de los gránulos, la segregación de los mismos a las células hijas durante la división celular y su posterior movilización o degradación (revisado en (Mezzina y Pettinari, 2016; Maestro y Sanz, 2017).

Aunque Las fasinas tienen una secuencia muy diversa, comparten ciertas características estructurales como una alta composición de α-helices anfipáticas, y se presentan como proteínas intrínsecamente desordenadas en ausencia de PHA. Diferentes modelos estructurales en fasinas también han revelado que poseen regiones de oligomerización de tipo *coiled-coil* que podrían ser importantes en el establecimiento de interacciones proteína-proteína (Maestro et al., 2013). Sin embargo, aún no se ha demostrado experimentalmente que el proceso de oligomerización de las fasinas está mediado por motivos estructurales de tipo *coiled-coil*.

En el primer capítulo de esta Tesis doctoral, se han utilizado análisis de predicción de estructura para caracterizar los dominios *coiled-coil* presentes en las fasinas PhaF y PhaI, producidas por la bacteria modelo acumuladora de PHA, *Pseudomonas putida* KT2440. La oligomerización de estas proteínas se ha explorado utilizando las técnicas de interferometría de biocapa y el sistema de doble híbrido *in vivo* (BACTH). También se ha investigado la interacción entre fasinas con mutaciones en los motivos *coiled-coil*. Estos resultados confirman la formación de complejos entre PhaF y PhaI, y establecen la participación de los *coiled-coils* identificados en estas fasinas (ZIP), los cuales contienen residuos "ideales" (leucinas o valinas) ubicados dentro del núcleo hidrofóbico, en la

estabilización de los oligomeros. La sustitución de estos residuos por alanina en el *coiled-coil* de la proteina PhaI (ZIPI) produjo una reducción en la eficiencia de la oligomerización aproximadamente un 75%. Por lo tanto, estos resultados indican que los motivos *coiled-coil* son esenciales para las interacciones PhaF-PhaI, y que la correcta oligomerización de las fasinas requiere la formación de una interfaz hidrofóbica estable entre ellas. Dado que este motivo está presente en la mayoría de las fasinas producidas por bacterias que acumulan PHA, estos resultados brindan información valiosa que podrá ser usada para la modificación de la estabilidad de los gránulos de PHA para satisfacer diversas aplicaciones.

A pesar de la alta similitud en la secuencia de aminoácidos entre PhaF y PhaI, se ha demostrado previamente que la deleción de *phaF* tiene un impacto significativo en la fisiología celular en términos generales, resultando en una población celular no homogénea en cuanto al contenido de PHA y localización de los gránulos, y en la reducción de la expresión de los genes *phaC1* (PHA sintasa) y *phaI* (Prieto et al., 1999; Galán et al., 2011; Dinjaski and Prieto, 2013). Se ha propuesto que estos efectos se deben a la presencia del C-terminal, o dominio de unión al ADN en PhaF, ausente en PhaI. Teniendo en cuenta estas observaciones, y la alta concentración de la proteína en la superficie del gránulo, en esta Tesis se planteó la hipótesis que PhaF podría participar en múltiples interacciones proteína-proteína que se ensamblan y desmontan en respuesta a señales celulares específicas.

El segundo capítulo de este trabajo discute un enfoque integral, dirigido hacia la identificación de candidatos que podrían establecer nuevas interacciones con la fasina PhaF. La búsqueda de proteínas de *P. putida* KT2440 que interaccionan con PhaF se realizó con un sistema de *pull-down* o cromatografía de afinidad (usando His_6-PhaF recombinante), acoplado a espectrometría de masas. Se lograron identificar 6 proteínas que podrían estar formando complejos con PhaF, incluidas dos proteínas relacionadas con PHA: la fasina PhaI (UniProt Q88D20) y el regulador transcripcional PhaD (Q88D22). Al correlacionar estos resultados con los obtenidos en el proteoma de los gránulos de PHA, 4 de estas 6 proteínas fueron identificadas de nuevo. Sin embargo, el hallazgo más interesante de estos experimentos fue la interacción entre PhaF y la proteína reguladora de PHA PhaD en los ensayos de *pull-down*. PhaD funciona como un activador de la trascripción de *phaC1* y de *phaI*, esta proteína se une a regiones diana de 25 y 29 pb ubicadas en los promotores P_{C1} y P_I, respectivamente (los cuales se encuentran *upstream phaC1* y *phaI*) (de Eugenio et al., 2010). Destacablemente, la ausencia de PhaD en los gránulos de PHA, corroborada mediante ensayos de localización *in vivo* usando la fusión PhaD-GFP, sugiere la existencia de un nuevo mecanismo en el que el complejo PhaD-PhaF podría estar participando en el sistema regulador que controla la expresión de genes del cluster de *pha*. La interacción entre PhaF y PhaD fue confirmada

in vivo mediante ensayos de doble híbrido (BACTH). Ensayos de desplazamiento de movilidad electroforética del promotor de *phaI* revelaron la formación de un complejo ADN-PhaD-PhaF que migra a una posición en el gel diferente a las observadas cuando el fragmento de ADN (P_I) forma complejos con cada una de las proteínas individualmente. Teniendo en cuenta estos resultados, podría concluirse que PhaF y PhaD actúan en armonía para controlar la expresión de genes *pha*.

Los hallazgos de los diversos roles *in vivo* de las fasinas durante los últimos años, ha abierto un nuevo campo de investigación que presagia el desarrollo de aplicaciones innovadoras basadas en estas proteínas. La alta afinidad de las fasinas por el PHA (y otros materiales hidrófobos) ya ha dado lugar al desarrollo de, *tags* de afinidad para la purificación rentable de proteínas recombinantes, sistemas para el transporte de fármacos, y técnicas de selección celular. Adicionalmente, debido a su naturaleza anfifílica, se ha descrito el uso estas proteínas como biosurfactantes (Wei et al., 2011) y en la funcionalización de biomateriales mediante el recubrimiento de sus superficies en conjunto con moléculas de señalización celular (Dong et al., 2010; Xie et al., 2013; Gao et al. al., 2014).

A pesar de las propiedades singulares de las fasinas y su uso reciente en el recubrimiento de la superficie de biomateriales, se conoce poco sobre su robustez y su estabilidad en interfaces, o sobre su proceso de adsorción al PHA, su sustrato natural. Tampoco se ha abordado la alteración de la conformación molecular de los dos componentes (proteína y polímero) durante el proceso de funcionalización. Por lo tanto, en esta Tesis se usó la técnica de Langmuir para estudiar la interacción entre PhaF y PHA, imitando el entorno nativo del gránulo, proporcionando de esta manera información sobre la estructura del complejo PhaF-PHA. Más aún, estos resultados pretenden ayudar a mejorar el control sobre la producción de materiales recubiertos con fasinas.

La técnica de Langmuir, combinada con microscopía *in situ* y métodos espectroscópicos permitió identificar la formación de monocapas (films) de PhaF, estables y robustas a diferentes temperaturas, las cuales se forman con una orientación casi plana de su α-hélice con respecto a la interfaz. La adsorción de PhaF en monocapas de PHA preformadas resultó en la formación de films mixtos, estables por debajo de una presión superficial de π = ~15.7 mN/m. La adsorción de un mayor número de moléculas de PhaF provocó la reorganización molecular del film. En la perspectiva de la suposición realizada en este trabajo, en donde la superficie de los gránulos se encuentra formada únicamente por proteínas, estos resultados nos permiten concluir que PhaF funciona como surfactante a altas concentraciones, separando el PHA en "gránulos" en ambientes hidrofílicos *in vitro*, tal como ocurre en el citoplasma bacteriano.

También se demuestra en este capítulo, que los poliésteres con una mayor hidrofobicidad de superficie, como el PHA, son sustratos más apropiados para la funcionalización mediada por PhaF, comparados con poliésteres menos hidrofóbicos cómo el PLGA (copolímero de ácido láctico y glicólico). La orientación del eje principal de la proteína en relación con la superficie de los dos poliésteres, garantiza una exposición óptima de los residuos hidrófobos. De este modo, este trabajo revela una estrategia de recubrimiento adecuada para producir materiales de PHA funcionalizados. La técnica de Langmuir también permitió la preparación de films monomoleculares de PhaF que se transfirieron con éxito a sustratos sólidos para su posterior caracterización por microscopía de fuerza atómica (AFM). Esta Tesis doctoral presenta el primer análisis exhaustivo de las propiedades superficiales de la fasina PhaF, y con estos resultados se obtiene una mejor comprensión de los biomateriales basados en PHA que han sido previamente descritos, y quizás de otros materiales basados en diferentes poliésteres.

I. INTRODUCTION

1. Bacterial subcellular structures

Bacterial cells are small, crowded places, historically thought devoid of any organized subcellular architecture. This dogma, however, has been challenged by the growing evidence for compartmentalization involving highly ordered subcellular structures in the form of protein- and lipid-bound organelles. Such compartmentalization allows bacteria to gain functionalities that provide them with selective advantages (Murat et al., 2010; Govindarajan and Amster-Choder, 2016). A closer look at the organization of these structures has, in fact, revealed an outstanding degree of intracellular differentiation associated with distinct subsets of proteins; examples include the coat of *Bacillus* endospores (which consists of approximately 30 proteins; Figure 1A) (Driks, 2002), the membrane of magnetosomes produced by magnetotactic bacteria (Figure 1B) (Barber-Zucker and Zarivach, 2017), and the lipid-protein envelope of chlorosomes of photosynthetic bacteria (Figure 1C) (Bryant and Liu, 2013). Among the most intriguing examples of these subcellular structures are polyhydroxyalkanoate (PHA) granules - *in vivo* polymerized polyesters that accumulate as intracellular inclusions (Figure 1D). A number of proteins have been identified on the surface of these granules, including components of the PHA metabolic machinery. These multicomponent structures are known as carbonosomes - a name that makes plain their multifunctionality (Jendrossek, 2009).

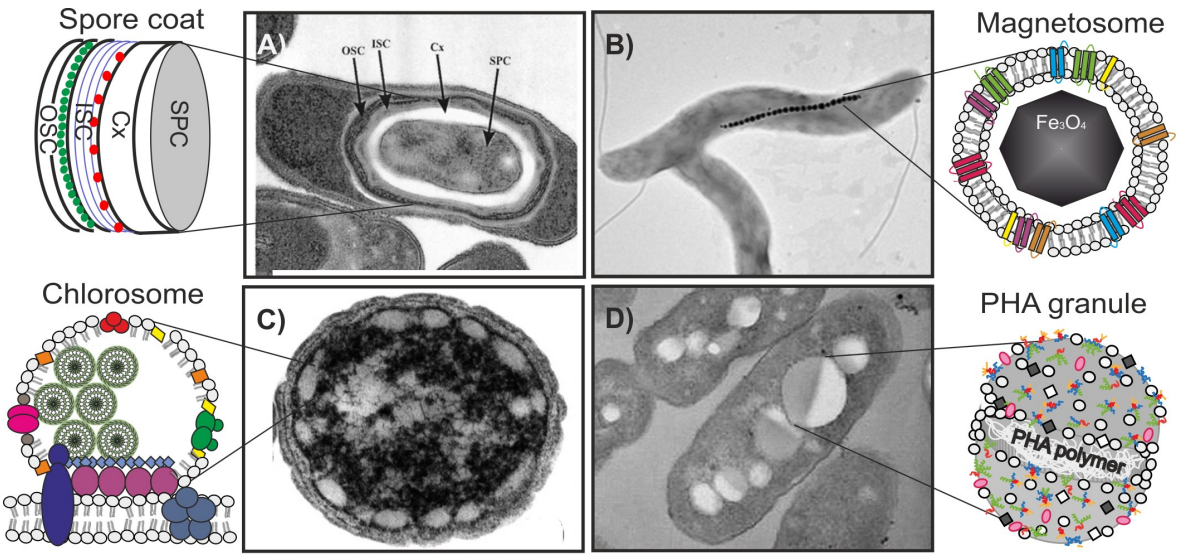

Figure 1. Examples of bacterial subcellular structures. A) Transmission electron microscopy (TEM) image of *Bacillus subtilis* endospores taken from (Erlendsson et al., 2004). The diagram of the spore coat, which comprises approximately 30 protein species, was adapted from (Driks, 2002). Abbreviations: OSC, outer spore coat; ISC, inner spore coat; Cx, cortex; SPC, spore core. **B)** TEM image of magnetosomes synthesized by

Magnetospirillum magnetotacticum (Shimoshige et al., 2015). Magnetosomes consist of crystals of the magnetic iron oxide magnetite (Fe_3O_4) enclosed by a lipid bilayer, which contains a specific set of about 30 proteins (Barber-Zucker and Zarivach, 2017). **C)** TEM image from the green sulphur bacterium *Chlorobaculum tepidium* (Bryant and Liu, 2013). The synthesized bacteriochlorophyll (BChl) is assembled into large antenna-like structures known as chlorosomes (diagram adapted from (Bryant and Liu, 2013)). Around 10 proteins are found in the chlorosome envelope. **D)** TEM image of *P. putida* KT2440 with PHA granules (Galán et al., 2011). The hydrophobic polymer core (PHA) is surrounded by structural and functional proteins, and presumably by a lipid monolayer.

A systems view of the bacterial cell understands the different subcellular domains not as completely segregated but as connected through a complex network of interactions in which "*everything connects to everything*" (Govindarajan and Amster-Choder, 2016). Networks of physical interactions among proteins are at the core of all cellular processes, enabling cells to execute diverse complex functions in a concerted and coordinated manner. Understanding the structures and operational modes of these networks is one of the great challenges of microbiology. Within this context, this thesis (Results section 1 and 2) assesses protein-protein interactions (PPIs) within the PHA carbonosome produced by the model PHA-accumulating bacterium *Pseudomonas putida* KT2440 (Nikel et al., 2014; Prieto et al., 2016).

2. Polyhydroxyalkanoates: unique structures inside cells

2.1. General overview

Microbially-produced PHA are fully biodegradable polyesters of (*R*)-hydroxyalkanoic acid monomers. Given their natural origin and tailored physicochemical properties, PHA have attracted much attention as alternative polymeric materials. More than 300 species of Gram-positive and Gram-negative bacteria, as well as different genera of archaea, accumulate PHA as carbon/energy stores in response to excess carbon when other essential nutrients, such as nitrogen or phosphorus, are limited (Lu et al., 2009). They can be stored at high concentration in bacterial cells; as insoluble cytoplasmic inclusions (see Introduction section 2.4) they do not significantly alter osmotic status (Uchino et al., 2007). The monomeric composition of PHA varies widely across bacterial species and even within individual bacteria. This depends on the substrate (e.g., hydrocarbons, sugars, fatty acids, etc.) and metabolic pathways used in their synthesis, and the substrate

specificities of the enzymes supplying the monomers to be polymerized (Sudesh et al., 2000). Given the stereospecificity of the polymerizing enzyme PHA synthase (PhaC), the resulting polymers have only the *R* configuration; Figure 2 shows the general chemical structure of PHA. More than 150 types of PHA monomer have been identified, allowing for a huge range of polymers with different mechanical properties extending from rigid plastics to elastic rubbers (Li et al., 2016).

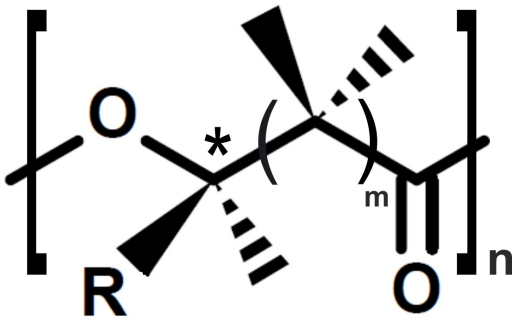

R = alkyl groups (C1-C13)

m = 1-3

n = 100-30000

Figure 2. General structure of polyhydroxyalkanoates. An ester bond is formed by the reaction between the carboxyl group of a monomer and the hydroxyl group of the next. All monomeric units have an asymmetric carbon centre (*), *R* enantiomer configuration; and most commonly aliphatic side-chains (R). Examples of mcl monomeric units: R = C_3H_7, m = 1: 3-*R*-hydroxyhexanoate (HHx); R = C_5H_{11}, m = 1: 3-*R*-hydroxyoctanoate (HO).

Depending on the number of carbons in their monomers, PHA may be classified into 3 groups. The first encompasses short-chain-length PHA (scl-PHA) with 3 to 5 carbon atoms, e.g., poly(3-*R*-hydroxybutyrate) (PHB) and poly(4-hydroxybutyrate) (P[4HB]). These are obtained from several bacteria, including *Ralstonia eutropha* H16 (also known as *Cupriavidus necator* H16), the most thoroughly investigated producer of scl-PHA. The second group includes the medium-chain-length PHA (mcl-PHA), which consist of monomers with 6-14 carbon atoms, e.g., poly(3-*R*-hydroxyhexanoate) (PHHx) and poly(3-*R*-hydroxyoctanoate) (PHO), mainly produced by *Pseudomonas* spp. (Rai et al., 2011). It is worth to mention that during mcl-PHAs biosynthesis, fatty acids (substrate) are degraded by the removal of a C2 unit (in the form of acetyl-CoA) in each turn of the β-oxidation cycle. Most mcl-PHA are therefore copolymers containing monomers with 2 carbon atoms fewer than possessed by the carbon source in the growth culture (Zinn and Hany, 2005). The last group, the long-chain-length PHA (lcl-PHA), includes monomers with more than 14 carbon atoms, such as those produced by *Shewanella oneidensis* (Hazer et al., 2012).

PHA monomers may have saturated, unsaturated, straight, cyclic or branched side-chains (R). In general, these side chains are aliphatic. However, when cultivated on unconventional substrates, certain microorganisms (mainly fluorescent pseudomonads) are able to synthesize PHA with aromatic, halogenic or alkoxy pendant functional groups (Kim and Lenz, 2001). Some of these functional side chains allow for post-synthesis chemical or enzymatic modification; and biopolymers with properties customized for special applications can therefore be produced .

PHA are either homopolyesters (which consist of only 1 type of monomer) or heteropolyesters. The latter are grouped into copolyesters (monomers with different backbones or side chains) such us poly[(3-*R*-hydroxybutyrate)-*co*-(3-*R*-hydroxyvalerate)] (PHBHV) or poly[(3-*R*-hydroxyoctanoate)-*co*-(3-*R*-hydroxyhexanoate)] (PHOHHx), and terpolyesters (monomers differing in both their side chains and backbones) such as poly [(3-*R*-hydroxybutyrate)-*co*-(3-*R*-hydroxyvalerate)-*co*-(4-hydroxybutyrate)] (PHBHV4HB) (Kim and Lenz, 2001; Mozejko-Ciesielska et al., 2017). Additionally, bacteria can be made to produce random and block copolymers by changing the precursors in the culture medium and the growth conditions (Pederson et al., 2006; Wang et al., 2017).

One of the most remarkable features of PHA is that they are efficiently degraded in the environment by many soil microorganisms. This degradation occurs through the action of PHA depolymerases (PhaZ) that hydrolyze the ester bonds of the polymer into water-soluble monomers and oligomers. Microorganisms then metabolize these degradation products into water and carbon dioxide (Jendrossek and Handrick, 2002; Lim et al., 2005). Summarizing, the structural diversity, plastic properties, biodegradability and sustainable production possibilities of PHA have attracted interest in them for use in medicine, agriculture, and the packaging, pharmaceutical and food industries, among others (Rai et al., 2011; Koller, 2018).

This thesis focuses on the study of *P. putida* KT2440 as a model mcl-PHA accumulating bacteria. *P. putida* KT2440 was developed as a biosafe strain, and its 'Generally Recognized As Safe' credentials (Federal Register, 1982) have allowed its use as a prototype microorganism in the development of environmental and industrial applications (Nikel et al., 2014). It is a TOL plasmid-cured and a spontaneous restriction-deficient derivative of *P. putida* mt-2; the latter makes *P. putida* KT2440 a good recipient organism for use in gene transfer experiments (Regenhardt et al., 2002). Moreover, the sequencing of its genome (Nelson et al., 2002), plus genome-scale metabolic modelling (Puchalka et al., 2008; Nogales et al., 2008), has led to the production of flexible cellular factories with bio-industrial uses and could help to improve our understanding of the physiology underlying mcl-PHA accumulation and other metabolic processes (Prieto et al., 2016).

Compared to scl-PHA, mcl-PHA polyesters have elastomeric and thermal properties

that make them generally superior as bioplastics for rubber and viscoelastic applications (Sudesh et al., 2000). These polymers have been shown suitable for tissue engineering, in which flexible biomaterials are required (Sudesh et al., 2000; Rai et al., 2011). Among these, PHOHHx, which was employed in the work pertaining to this thesis (Results section 3), is obtained by feeding *P. putida* KT2440 with octanoic acid (C8), and contains randomly distributed PHHx and PHO (monomer molar ratio 94 and 6 %, respectively).

2.2. PHA influence on bacterial fitness

The physiology behind PHA production is of substantial interest given the widespread ability of bacteria to produce these polymers and their impact on many cell activities. These polyesters are synthesized from *R*-3-hydroxyacyl-CoA, which can be produced from different intermediates of fatty acid metabolism (Rehm, 2010; Prieto et al., 2016). PHA have commonly been considered bacterial reservoirs of carbon and energy that help the cell survive periods when nutrients are scarce. However, it has been shown in *P. putida* KT2442 (a spontaneous rifampicin-resistant mutant of *P. putida* KT2440 (Franklin et al., 1981)), that the PHA cycle has a strong influence on cell physiology, balancing the stored carbon/biomass/number of cells as function of carbon availability. In contrast, when cultured under PHA production-favourable conditions (i.e., excess carbon and low nitrogen concentrations), a *P. putida* KT2442 PHA-deficient mutant, which carries a disrupted form of the gene for PhaC, wastes resources by releasing CO_2 instead of generating PHA (and therefore biomass) (Escapa et al., 2012).

In *Pseudomonas* spp. and the prototype PHB (scl-PHA)-producer *R. eutropha*, the PHA cycle enhances the resistance of bacterial cells to stress conditions such as osmotic shock, ultraviolet radiation, desiccation, and thermal and oxidative stress (Ruiz et al., 2004; Ayub et al., 2009; Obruca et al., 2016). One of the proposed mechanisms that invest bacteria with such resistance is the stringent response, which involves guanosine penta- and tetra-phosphates [(p)ppGpp] and other nucleotides. When nutrients are scarce, (p) ppGpp destabilizes RNA polymerase σ^{70}, reducing the transcription of housekeeping genes and thereby increasing the availability of the polymerase to bind to other σ factors related to stress tolerance, such as σ^{54} (RpoN) or σ^{38} (RpoS). Under such stress conditions, the expression of the gene coding for the RpoS factor increases, leading to general stress resistance. A direct correlation between PHA degradation, (p)ppGpp accumulation and intracellular RpoS levels has been reported in *P. putida* GPo1 (previously referred as *P. oleovorans* GPo1) (Ruiz et al., 2001; Ruiz et al., 2004).

PHA also plays an important role in syntrophic interactions between consortia of organisms in different ecosystems. For example, PHA may be degraded in biologically active environments and the consumption of the resulting monomers be of advantage to other microorganisms in the same habitat by providing them with an extra source of

carbon and energy (Kadouri et al., 2005; Prieto et al., 2016). Figure 3 summarizes the influence of PHA on bacterial environmental fitness.

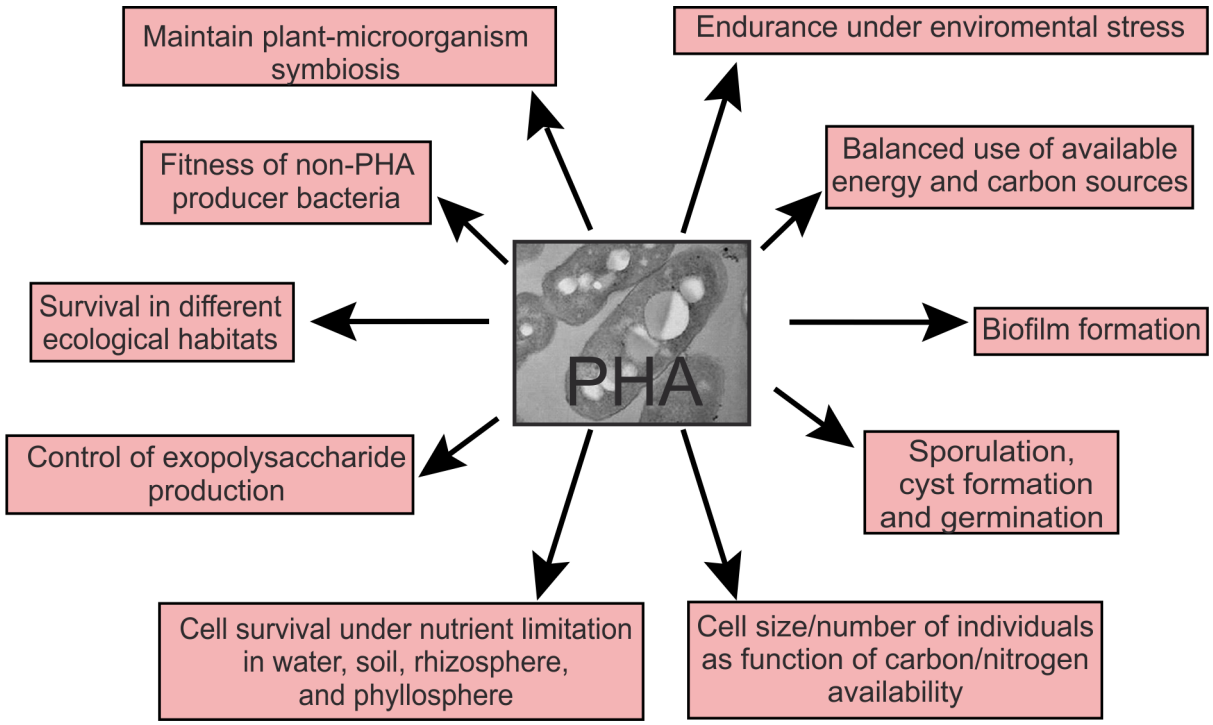

Figure 3. Physiological functions of PHA. With the goal of surviving in nutrient-poor ecosystems, bacteria use PHA metabolism to increase their ability to endure physical and chemical stresses. PHA can be used as a carbon source under nutrient deficiency conditions, and function as a source of energy (reducing equivalents) that can be mobilized to respond to the stress. Figure modified from (Prieto et al., 2016).

2.3. PHA cycle and regulation in *Pseudomonas*

PHA production and utilization (mobilization) proceeds in a continuous cycle in which the simultaneous activities of PHA synthases and depolymerases ensure a carbon flux that balances the energy and carbon needs of the cells by maintaining a PHA turnover (Ren et al., 2009; de Eugenio et al., 2010; Arias et al., 2013). This cycle is interconnected with the main central pathways that converge in acetyl-CoA. Mcl-PHA monomers can be synthesized from both fatty acids via β-oxidation (PHA structural related sources), and from PHA-unrelated carbon sources (e.g., sugars) via *de novo* fatty acid synthesis (Kniewel et al., 2017).

P. putida produces mcl-PHA, based on a gene cluster (*pha* cluster) containing 2 operons that are transcribed in opposite directions. The *phaC1ZC2D* operon encodes 2 synthases or polymerases (PhaC1 and PhaC2) that incorporate *R*-3-hydroxyacyl-CoA monomers into the PHA polymer, plus a depolymerase (PhaZ) that catalyzes the hydrolysis of PHA, plus the PhaD transcriptional regulator (Huisman et al., 1991; de

Eugenio et al., 2007; de Eugenio et al., 2010). The *phaFI* operon is located downstream of *phaC1ZC2D* and codes for the PhaF and PhaI phasins (Figure 4) (Prieto et al., 1999). This cluster is very well conserved among the mcl-PHA-producing strains, and most of the products of the *pha* cluster are localized on the surface of PHA granules as described later.

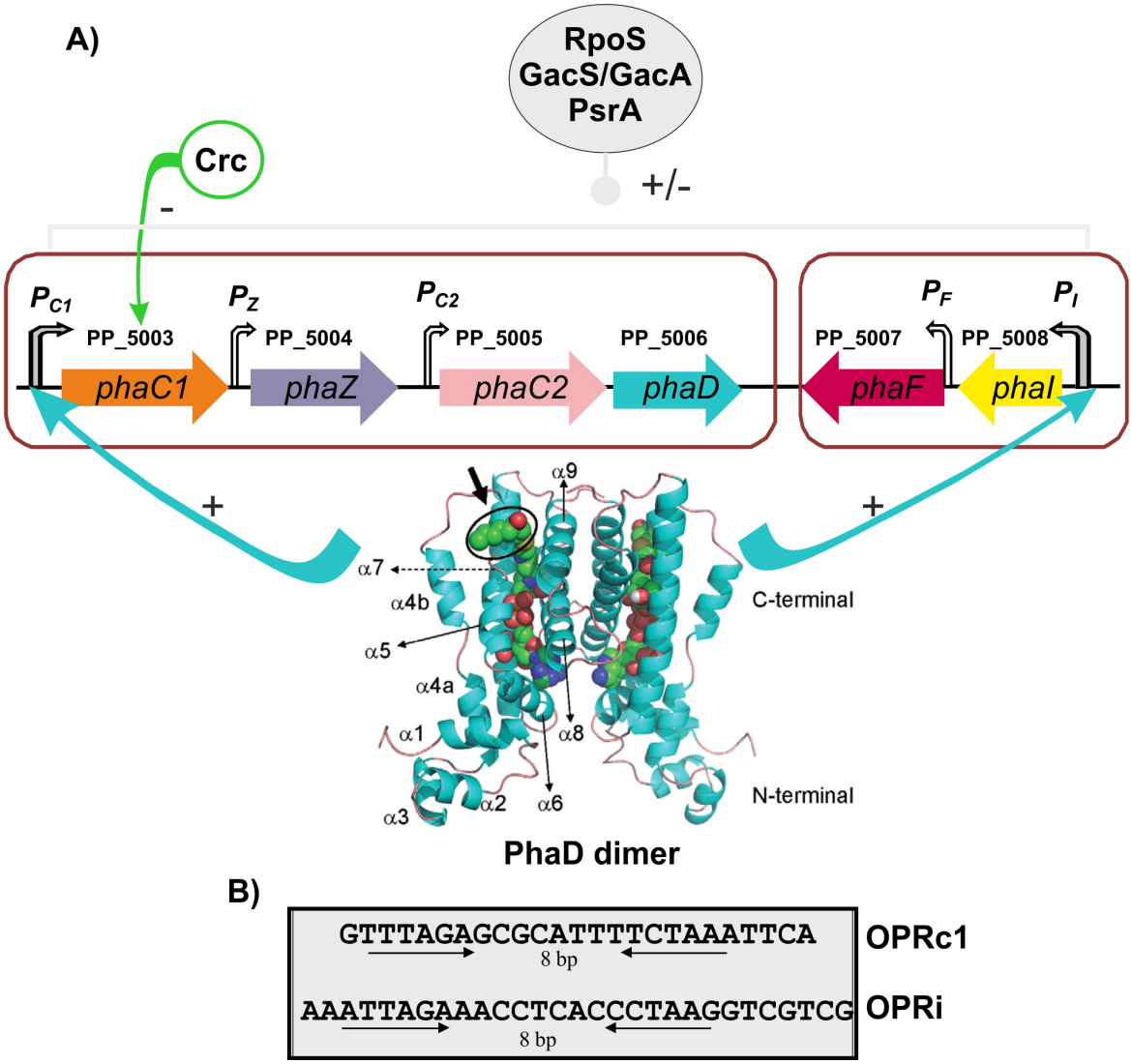

Figure 4. Regulation of *pha* gene expression in pseudomonads. A) Diagram of the *pha gene* cluster in *P. putida* KT2440 and its regulatory components. Both operons, *phaC1ZC2D* and *phaIF*, are under the control of the regulator PhaD. The modelled PhaD structure suggests the existence of a dimer, with each monomer composed of 2 domains consisting of 9 α-helices. The black arrow shows one of the putative PhaD effectors (hydroxyoctanoyl-CoA) that might fit inside the molecule's crevice (surrounded by helices α5 - α8) without steric impediment. Despite our increasing knowledge of PHA regulation, the specific roles of the global transcriptional regulators Crc, RpoS and the GacS/GacA system on the synthesis and degradation of the polymer are still to be elucidated. **B)** Sequences of the PhaD-binding sites at P_{C1} and P_I promoters (OPRc1 and OPRi, respectively). Inverted black arrows indicate the palindromic sequences.

According to the data from translational fusions with the *lacZ* reporter gene, the *pha* locus in *P. putida* contains 5 functional promoters upstream of the *phaC1*, *phaZ*, *phaC2*, *phaF* and *phaI* genes (denoted P_{C1}, P_Z, P_{C2}, P_F and P_I), indicating the co-existence of a variety of polycistronic transcription units. However, real-time quantitative polymerase chain reaction (RT-qPCR) has revealed that P_{C1} and P_I are the most active promoters of the *pha* cluster, allowing the transcription of both operons (de Eugenio et al., 2010).

The biosynthetic machinery for PHA accumulation involves multiple regulatory mechanisms comprising interactions between polyesters, metabolites, enzymes, the bacterial nucleoid, and regulators. In fact, the accumulation of PHA in *Pseudomonas* is subject to extensive regulation at the transcriptional and post-transcriptional levels by specific and global regulatory factors (Figure 4A), as well as at the enzymatic level, including the regulation of the carbon flow in different pathways that provide PHA precursors (Escapa et al., 2012; Kniewel et al., 2017). At the transcriptional level, both operons (*phaC1ZC2D* and *phaIF*) are under the control of the regulator protein PhaD, which belongs to the TetR family of transcriptional regulators. Unlike most characterized members of this family, PhaD functions as an activator and not as a repressor of transcription (de Eugenio et al., 2010). It binds to a region of 25 bp (OPRc1) at P_{C1} promoter and a 29 bp region (OPRi) at P_I promoter. Both sequences contain a single binding site formed by inverted half sites of 6 bp separated by 8 bp (Figure 4B).The *in silico* 3D model of PhaD structure, based on information for similar regulators belonging to the TetR family, suggests it to exist as a dimer. Each monomer would be composed of 2 domains made up of 9 α-helices. This model proposes the effector of PhaD to be a CoA intermediate of fatty acid β-oxidation (Figure 4A, black arrow)**;** however, the true effector remains uncertain (de Eugenio et al., 2010).

Recent evidence suggests that the expression of the genes in the *pha* cluster is also subject to the influence of global regulatory systems, although most mechanisms are not fully understood. De la Rosa et al. (2014) reported PHA synthesis to be controlled by catabolite repression control (Crc) protein, a global regulator that optimizes carbon metabolism by inhibiting the expression of genes involved in the use of non-preferred carbon sources. Under balanced C/N conditions (which are not optimal for PHA accumulation), Crc was shown to inhibit the translation of *phaC1* mRNA via its interaction with a specific sequence A*n*AA*n*AA located immediately downstream of the AUG start codon (where *n* represents any nucleotide). This results in a reduction in the PHA content of the cell (De la Rosa et al., 2014). The RpoS global regulator has also been suggested involved in the regulation of the P_{C1} promoter. Experiments in *P. putida,* using the P_{C1}*::lacZ* translational fusion, showed that *rpoS* mutation increased the expression driven by the P_{C1} promoter. PHA synthesis is also affected by the two-component GacS/

GacA global regulatory system (global antibiotic and cyanide control), as described in *P. putida* CA-3. GacS is a sensor kinase and GacA its cognate regulator that activates the expression of small RNAs (sRNAs). These sRNAs and the RsmA (sRNA-binding protein) cooperatively regulate protein synthesis, together constituting the Gac/Rsm system. A *gacS* mutation in *P. putida* CA-3 prevents the translation of *phaC1* mRNA by a non-conventional mechanism yet to be fully understood (Ryan et al., 2013).

A link between PHA accumulation and the transcriptional regulators of the central metabolic routes (such as the glycerol pathway) that provide substrates for PHA synthesis via *de novo* fatty acid synthesis and the β-oxidation pathway, has also been reported (Escapa et al., 2013; Fonseca et al., 2014). For instance, in *P. putida* KT2440, the transcriptional repressor of the β-oxidation route, PsrA, negatively regulates the expression of genes related to fatty acid metabolism. It has been suggested that PsrA binds to the promoter region of the *fadBA* operon inhibiting its expression in *P. putida.* This explains why a *psrA* mutant strain showed increased β-oxidation and a reduction in its PHA content when using fatty acids as a growth and polymer precursor. Moreover, in *P. putida* it has been shown that the RpoS factor is regulated by PsrA, indicating the indirect regulation of PsrA via RpoS (Fonseca et al., 2014).

2.4. PHA carbonosomes

PHA are stored as densely packed, hydrophobic, water-insoluble inclusions known as carbonosomes, within the cytoplasm of cells (Figure 5) (Jendrossek and Pfeiffer, 2014). The size, number, and distribution of carbonosomes vary considerably among bacterial species. These structures are typically 100-500 nm in diameter, and there may be 1 to around 10 inclusions per cell (mean 5–6) (Beeby et al., 2011). In pseudomonads, carbonosomes account for nearly 70 % of the cell's dry weight and fill up most of the intracellular space (Jendrossek, 2009; Galán et al., 2011).

The chemical composition of the carbonosomes of *Bacillus megaterium* - 97.7 % PHB, 1.87 % protein, 0.46 % lipids - was the first to be described (Griebel et al., 1968). The existence of a lipid component in the carbonosomes of bacteria, however, remains uncertain; experimental evidence exists that both supports (Mayer and Hoppert, 1997; Dennis et al., 2003) and refutes (Bresan et al., 2016) its presence. Proteins (and lipids) form a membranous coat that surrounds the hydrophobic PHA core and stabilizes the transition between the hydrophobic core and its hydrophilic surroundings.

The presence of structural and functional proteins bound to the carbonosomes has been demonstrated in a variety of bacterial species. Known as granule-associated proteins (GAPs), these can be roughly classified into 4 types: PHA synthases, PHA depolymerases, phasins, and other proteins (Steinbüchel et al., 1995) - including transcriptional regulators, hydrolases, and reductases etc. involved in PHA monomer synthesis.

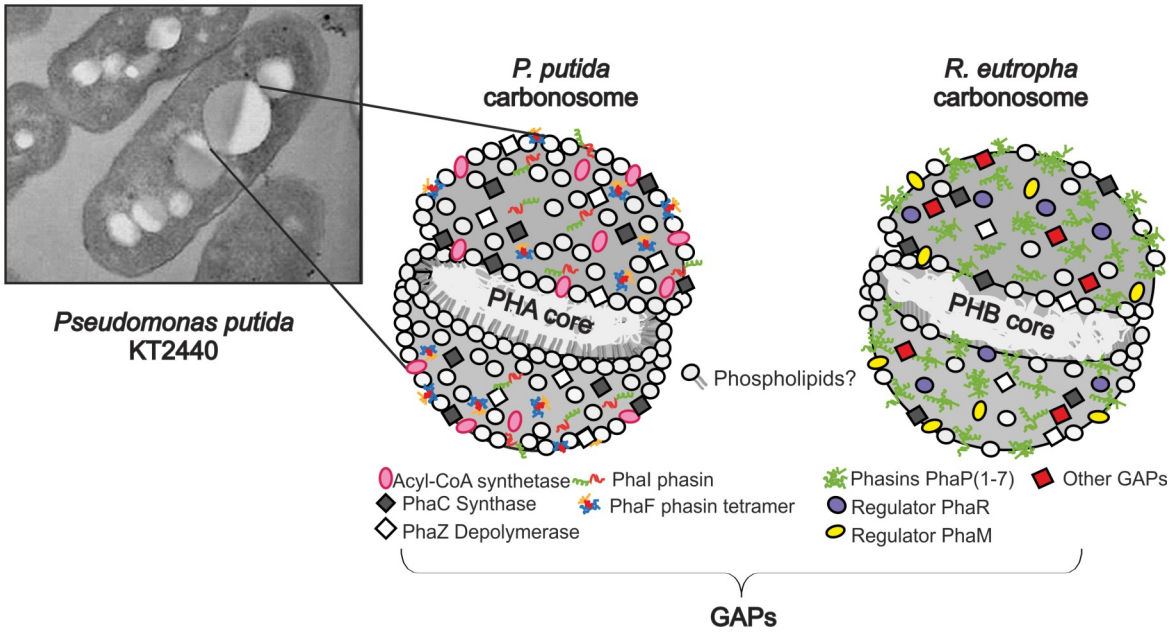

Figure 5. PHA carbonosomes. Diagram of PHA granules from *P. putida* K2440 (mcl-PHA) and the prototype PHB (scl-PHA) producer, *R. eutropha* H16. Structural and functional proteins (GAPs) and phospholipids making up the surface layer are indicated.

Early evidence of GAPs was obtained from the electrophoresis of isolated PHA granules and immunoblotting (Fuller et al., 1992; Steinbüchel et al., 1995; Prieto et al., 1999), and later by immuno-gold-labelling, transmission electron microscopy (Gerngross et al., 1993; Wieczorek et al., 1995; Pötter et al., 2002), and fluorescence microscopy using green fluorescent protein (GFP) fusions (Barnard et al., 2005; Uchino et al., 2007; Neumann et al., 2008; Pfeiffer and Jendrossek, 2011; Pfeiffer and Jendrossek, 2012; Hauf et al., 2013; Sznajder et al., 2015; Narancic et al., 2018). Phasins are the predominant GAPs, making up some 5 % (wt/wt) of the total protein content of PHA-accumulating cells (Wieczorek et al., 1995; Sznajder et al., 2015).

In *Pseudomonas* spp., 6 proteins have been classified as GAPs: PhaC1, PhaC2, PhaZ, phasins PhaF and PhaI, and the acyl-CoA synthetase Acs1 (FadD1) (de Eugenio et al., 2007; Sandoval et al., 2007; Ruth et al., 2008; Ren et al., 2009) (Figure 5). The PHB granules of *R. eutropha* H16 are covered by so far identified 15 different GAPs but are most probably depleted of phospholipids (Bresan et al., 2016) (Figure 5). In this strain, several studies have reported the physical interaction or co-localization of PHB granules with 7 phasin proteins, i.e., $PhaP1_{Reu}$-$PhaP7_{Reu}$, as well as with $PhaC1_{Reu}$, $PhaZ1_{Reu}$, the regulators $PhaR_{Reu}$ and $PhaM_{Reu}$, and 4 additional proteins not related to known GAPs (Gerngross et al., 1993; Pötter et al., 2002; Pötter et al., 2004; Pfeiffer and Jendrossek, 2011; Pfeiffer et al., 2011; Pfeiffer and Jendrossek, 2013; Sznajder et al., 2015). Out of

these “GAP-unrelated” proteins, H16_B1632 and H16_A0671, are annotated as potential α/β-hydrolases. The other , H16_A0225 and H16_A2001, are annotated as a putative phospholipase and a hypothetical protein respectively (Sznajder et al., 2015).

Only a few studies on PPIs involving GAPs have been published. Jendrossek's group was the first to report the interactions between GAPs in *R. eutropha* H16 - interactions that were detected in two-hybrid studies and through the use of a bimolecular fluorescence complementation system (BiFC) (Pfeiffer and Jendrossek, 2011; Pfeiffer and Jendrossek, 2013). These studies led to the detection of the homo- and heterooligomerization of phasins, the formation of complexes between phasins and other GAPs (e.g., $PhaP5_{Reu}$-$PhaZ_{Reu}$, $PhaP5_{Reu}$-PhaR), the interaction of PhaR and PhaM with $PhaC1_{Reu}$, and the identification of new phasins (Pfeiffer and Jendrossek, 2011; Pfeiffer and Jendrossek, 2013; Jendrossek and Pfeiffer, 2014). However, no protein interaction studies have been performed on *Pseudomonas* GAPs.

Advances in systems biology and high-throughput ‘omic’ techniques for detecting PPIs provide new opportunities for studying bacterial physiology from a holistic standpoint. In this PhD thesis, PPIs among *P. putida* KT2440 phasins are examined, providing new insights into the functions of phasins. Proteomic analyses are also used to comprehensively characterize the surface of this strain's carbonosomes, providing new information on mcl-PHA granule composition (see Results section 1 and 2).

3. Phasins: the interface-active proteins of PHA carbonosomes

The term phasin originated as an analogy to a class of amphipathic proteins known as oleosins (Steinbüchel et al., 1995). The latter are known to stabilize triacylglycerol inclusions within seeds and pollen by forming a boundary layer at these organs' surfaces (Murphy, 1993). Phasins are low molecular weight proteins present in all known PHA-accumulating bacteria. Although they lack catalytic activity, they are the major components of the interface of PHA granules, and a link exists between PHA accumulation and phasin production (York et al., 2001; Galán et al., 2011).

Phasins have been classified into 4 Pfam families - PF09602, PF09650, PF05597 and PF09361 - based on their phlylogenetic origin and the kind of PHA to which they bind (Table 1). The first family (PF09602) contains phasins found in *Bacillus* species; the second (PF09650) contains a diverse group of mostly uncharacterized proteins belonging to different *Proteobacteria*; the third (PF05597) includes phasins from different members of *Proteobacteria*, *Cyanobacteria* and *Firmicutes*. The characterized

phasins of *Pseudomonas* that accumulate mcl-PHAs, such as PhaF and PhaI from *P. putida*, fall into this group. The fourth family (PF09361) contains the largest number of proteins, which are found in members of the *Alpha-*, *Beta-*, and *Gammaproteobacteria*; the most studied phasin, $PhaP1_{Reu}$ from *R. eutropha* H16, falls into this group.

Table 1. Phasin families according to the Pfam database

Family name	Domain	taxon/taxa	Number of phasins	Domain length (aa)*	Domain coverage (%)**	Identity (%)***	Protein(s)
PF09602	PhaP_Bmeg	*Bacillus*	28	159.9	91.01	23	PhaP from *B. megaterium*
PF09650	PHA_gran_rgn	Diverse	371	90.9	88.08	25	Uncharacterized
PF05597	Phasin	Proteobacteria *Pseudomonas*	467	106.7	73.82	21	group of phasins PhaF from
PF09361	Phasin_2	*Ralstonia,*	1584	98.9	61.54	16	PhaP from

*Mean length of the full domain in aminoacids
**Mean coverage of the sequence by the domain
***Mean identity of alignment

Despite the widespread occurrence of phasins, the low degree of conservation among their amino acid sequences suggests they are not phylogenetically related. However, *in silico* predictions indicate that they share some structural features, such as a preponderant α-helix composition, partially disordered structures, and coiled-coil regions (Mezzina et al., 2014; Maestro and Sanz, 2017).

The 3-dimensional model of PhaF, acquired by homology modelling and making secondary structure predictions, shows PhaF to be composed of 2 domains (Figure 6A). The N-terminal domain of PhaF, known as BioF, consists of a long amphipathic alpha helix (residues 1-142), with a peculiar segregation of hydrophobic/hydrophilic residues (Figure 6B). This latter feature has been suggested responsible for the binding of PhaF to the PHA granule surface. This domain is followed by a structurally disordered C-terminal domain (residues 143-225) predicted to form a superhelix that can be inserted into the major groove of DNA. This domain has a characteristic 8 AAKP-like tandem repeats similar to those found in the DNA binding nucleoid-associated proteins of histone family H1 (Galán et al., 2011; Maestro et al., 2013).

Experiments investigating hydrodynamic, spectroscopic and thermodynamic features indicate that free PhaF oligomerizes to form tetramers in solution, most likely through coiled-coils (Figure 6C). The hydrophobic face of the amphipathic BioF helices thus becomes associated with the PHA granule, either through its lipid coating or the naked polyester itself (Maestro et al., 2013).

PhaI phasin lacks the DNA binding domain, but it shares considerable sequence

similarity with the N-terminal PHA binding domain of PhaF (57 % similarity, 35 % identity), and it cooperates with PhaF in the optimization of PHA synthesis (Dinjaski and Prieto, 2013). No structural information about PhaI or its oligomerization is available. However, in an earlier publication (Maestro et al., 2013), our group predicted that coiled-coil regions likely existed in all the phasins that had been described at that time. It has been proposed that this coiled-coil motif allows the homo-oligomerization and/or the interaction of phasins with other proteins (Maestro et al., 2013; Mezzina et al., 2014).

Recently, the crystal structure of phasin PhaP from *Aeromonas hydrophila* (PF0936 family) revealed the formation of $PhaP_{Ah}$ tetramers with a coiled-coil structure (Zhao et al., 2016). However, the location and extension of coiled-coil regions differs greatly among phasins belonging to different families, and even among phasins of the same family, indicating that oligomerization may take place by different mechanisms.

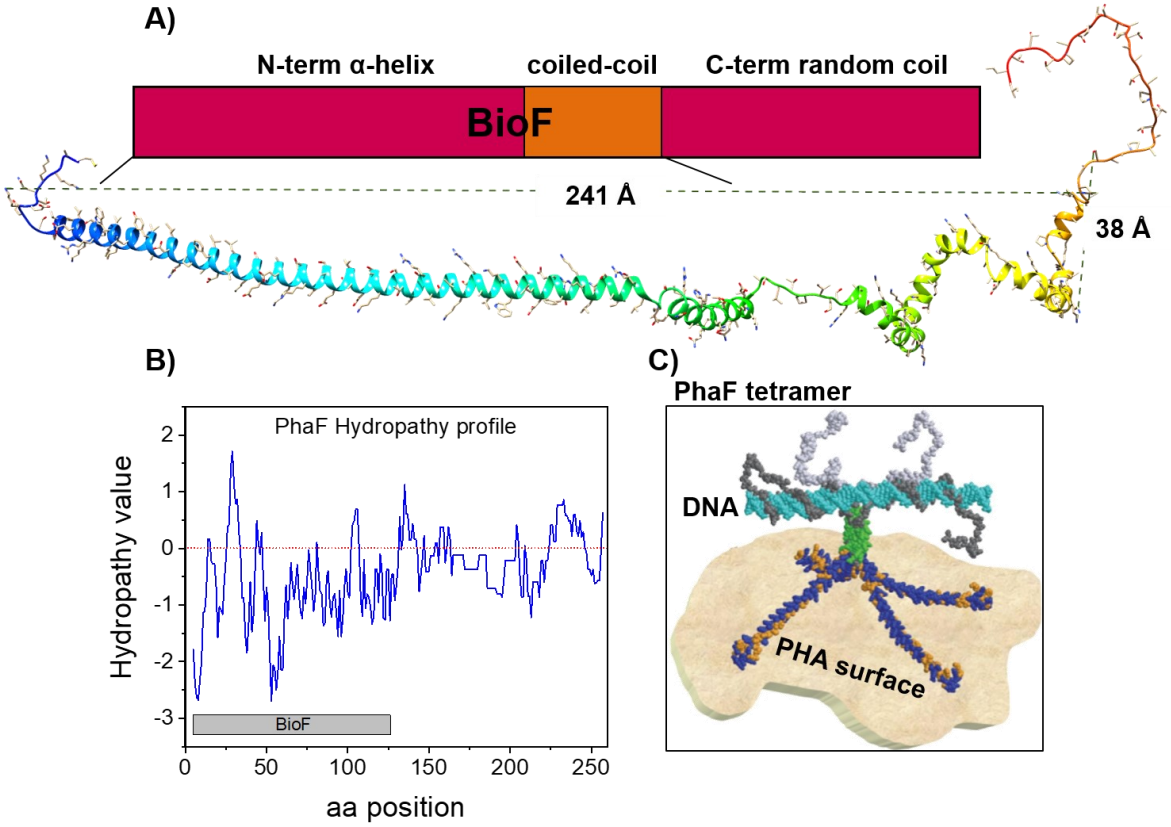

Figure 6. Phasin PhaF from *P. putida* KT2440. A) Predicted structure of a monomer of PhaF (structure provided by Jesus Sanz' group). **B)** Hydropathy profile according to Kyte and Doolittle (Kyte and Doolittle, 1982). **C)** Model of a PhaF tetramer (taken from (Maestro et al., 2013) interacting with the PHA granule and attached to a fragment of nucleoid DNA. The hydrophobic residues in the N-terminal domain are shown in orange; the polar ones are blue. The coiled-coil (predicted as a leucine zipper) is coloured green; the DNA is shown in cyan.

3.1. Phasins biological functions

Sequence versatility among phasins from different species has revealed a set of unanticipated roles for them in the PHA machinery - roles that ensure the optimal fitness of the cell. Quite apart from their structural role in the PHA granule cover, many other functions related to PHA accumulation and degradation have been described for different phasins. For instance, all phasins play a crucial role in the determination of the number and the size of PHA granules. In addition, some phasins have regulatory activity (reviewed in (Mezzina et al., 2014; Maestro and Sanz, 2017)). For example, $PhaP1_{Reu}$ increases the activity of $PhaC1_{Reu}$ *in vitro*, plus the activity of $PhaC1_{Pa}$ and $PhaC2_{Pa}$, produced by *P. aeruginosa* (Qi et al., 2000).

In particular, PhaF has been shown to regulate the expression of the *pha* genes, and to some extent the entire transcriptomic profile. This effect is also believed to be derived from its DNA binding abilities and putative histone-like functionality as shown in Figure 7 (Prieto et al., 1999; Galán et al., 2011). The disruption of the *phaF* gene in *P. putida* KT2442 has been shown to affect PHA production (1.5-fold reduction) and the transcription of the *phaC1* and *phaI* genes. Experiments have shown the transcription level of *phaC1* to decrease approximately 3.5-fold with respect to the wild-type, and that of *phaI* to reach its highest much later in the stationary phase (Galán et al., 2011).

Even though there is no evidence for the specific binding of PhaF to the promoter regions of *pha* genes, preliminary transcriptomic analyses of a *phaF* mutant strain has suggested an indirect regulatory effect on the expression of these genes with the mild downregulation of the *pha* cluster. A wider effect on the *P. putida phaF* mutant transcriptome has also been observed, including an upregulation of acetyl-CoA acetyltransferase (Q88E32), a key enzyme in fatty acid degradation, and other proteins involved in metabolic and regulatory processes (Galán et al., 2011).

PhaF also plays a crucial role in the distribution of PHA granules into the daughter cells upon cell division, most likely via the binding of the PhaF C-terminal domain to DNA. Similar behavior has been observed for the phasin-like PhaM in *R. eutropha* H16 (Wahl et al., 2012). This ensures that the granules are separated together with the chromosomes in a homogeneous fashion (Figure 7). A PhaF-deficient *P. putida* KT2440 strain showed the defective segregation of PHA granules and reduced PHA accumulation compared to the wild-type strain (33 % vs. 63 % cell dry weight of PHA) (Figure 7).

The organization of the granules into a needle array along the long axis of the cell, as observed in the wild-type strain, is also lost (Galán et al., 2011). Other possibilities, such as the interaction of PhaF with other cytoskeletal proteins to facilitate the formation of the needle array and to regulate PHA accumulation, are still to be proven.

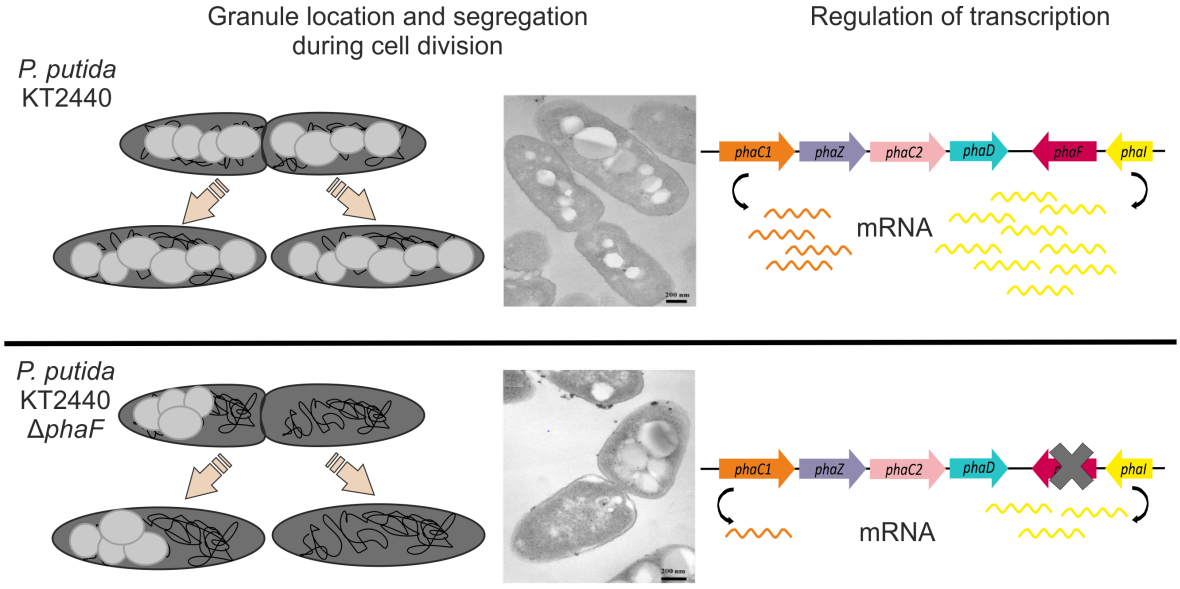

Figure 7. Main functions of phasin PhaF from *P. putida* KT2440. A key role of PhaF is the organization of PHA granules within the cell (left), probably through its interaction with the DNA. Effect of PhaF on the expression levels of *phaI* and *phaC1* (right). The scale bar in the TEM images = 200 nm.

4. Phasins as promising biotechnological tools

The revelation of different roles for phasins *in vivo* has opened a new field of research, and the promise of innovative applications. The main function of phasins is to bind to the polymer-cytoplasm interface of PHA granules; this prevents any negative effect of polyester accumulation on cellular activities, and stops the coalescence of granules (Wieczorek et al., 1995; Maehara et al., 1999; Prieto et al., 1999; Kuchta et al., 2007; Neumann et al., 2008). Although phasin production and location are strictly PHA granule-associated, some phasins have been shown to bind to different hydrophobic substrates *in vivo* and *in vitro*, including lipid inclusions (Hänisch et al., 2006) and natural and synthetic polymers such as poly(L-lactide) (PLA), poly(ε-caprolactone) (PCL), and poly[(lactide-*co*-glycolide)] (PLGA) (Dong et al., 2010; You et al., 2011; Xie et al., 2013). This feature has been exploited for the development of, e.g., affinity tags used in low-cost protein purification, specific drug delivery systems, and cell sorting techniques (Table 2).

The construction of different fully functional chimeric proteins, immobilized *in vivo* on PHA granules, has been made possible via the use of the polypeptide tag BioF (PHA binding domain of PhaF) from *P. putida*. (Moldes et al., 2004; Moldes et al., 2006).

PHA granules carrying BioF-tagged fusion proteins can be easily isolated from bacterial cells by centrifugation, facilitating the production of desired proteins. The purification of the adsorbed protein from the granules can be also achieved by gentle elution with detergents, with no loss of activity (Moldes et al., 2004).

Moldes et al. (2006) used the BioF tag to deliver the Cry1Ab toxin with insecticidal activity into the environment in an eco-friendly manner (Moldes et al., 2006). Similar immobilization platforms have been developed to anchor different proteins of interest to PHA granules produced by different microorganisms (Banki et al., 2005; Barnard et al., 2005; Chen et al., 2014). The main advantage of these strategies is the simultaneous production of the protein and its support in the same bacterial host, greatly reducing production cost (Moldes et al., 2004).

Another phasin-based purification system consists of using a self-cleaving intein fused between $PhaP_{Reu}$ and a target protein (Banki et al., 2005); the entire fusion protein is produced and bound to PHB granules *in vivo*. The target protein is then released via the induction of intein cleavage and collected from the supernatant as the PHB granules precipitate. Wang et al. (2008) improved this system by developing a low-cost *in vitro* system in which phasin fusions and polymer supports are produced separately. This system allowed the successful purification of enhanced green fluorescent protein (EGFP), maltose binding protein (MBP) and β-galactosidase (β-gal) using copolymers of PHB and PHHx for $PhaP_{Ah}$ binding (Wang et al., 2008). In another study, $PhaP_{Reu}$ fused to the sequence for mouse interleukin-2 (IL2, or the myelin oligodendrocyte glycoprotein (MOG), was successfully used in fluorescence-activated cell sorting-based diagnostics (FACS). PHA granules displaying either IL2 or MOG protein (antigens) were used in this system to bind anti-IL2 or anti-MOG antibodies which were conjugated to a fluorescent dye (Bäckström et al., 2007).

Owing to their amphiphilic nature, phasins have also been proposed as biosurfactants. $PhaP_{Ah}$ phasin easily forms emulsions with lubricating oil, diesel, and soybean oil, maintaining a very stable emulsion layer even after 30 days (Wei et al., 2011).

Recently, Chen's group reported the surface modification of PHA via the physical adsorption of phasin $PhaP_{Ah}$ using a coating strategy for the functionalization of polymers for tissue engineering purposes (Dong et al., 2010; Xie et al., 2013; Gao et al., 2014). By coating different films with phasin PhaP-cell binding motif fusions, e.g., the integrin-binding motif arginine-glycine-aspartic acid (RGD), these authors succeeded in reducing PHA surface hydrophobicity, promoting the attachment and proliferation of different cell lines (Dong et al., 2010). Table 2 lists the literature reporting the use of phasins as affinity tags, biosurfactants and coating materials.

Despite the remarkable properties of phasins, little information is available on their robustness and stability at polymeric interfaces or their adsorption behavior with respect to PHA, their natural substrate. In this thesis, the interaction between PhaF and PHA is studied in depth; with the aim of improving the control of the production of phasin-coated materials (see Results section 3).

Table 2. Reported applications of phasins in biotechnology and biomedicine

Strain/ platform	PHA support	Phasin	Fusion protein	Reference
Affinity tag for protein purification				
P. putida	PHOHHx	BioF (N-terminal of phasin PhaF)	Recombinant proteins for research and commercial use -β-galactosidase -Choline binding domain (ChBD) of pneumococcal autolysin LytA	(Moldes et al., 2004)
P. putida	PHOHHx	BioF	-Cry1Ab insect-specific toxin	(Moldes et al., 2006)
	In vitro prepared particles of PHB	BioF	-LytA -β-gal	(Bello-Gil et al., 2017)
Escherichia coli *	PHB	$PhaP1_{Reu}$	-D-hydantoinase (d-HDT), enzyme involved in the synthesis of D-amino acids of commercial interest	(Chen et al., 2014)
E. coli *	PHB	$PhaP1_{Reu}$ Fusion phasin-intein-target protein	Recombinant proteins for research and commercial use -Maltose binding protein (MBP) -β-gal -Chloramphenicol acetyltransferase (CAT) -NusA protein	(Banki et al., 2005)
R. eutropha H16	PHB	$PhaP1_{Reu}$ Fusion phasin-intein-target protein	Recombinant proteins for research and commercial use -GFP -β-gal	(Barnard et al., 2005)
-	*In vitro*-prepared nanoparticles of PHBHHx, PLA and PCL	$PhaP_{Ah}$ Fusion phasin-intein-target protein	Recombinant proteins for research and commercial use -Enhanced GFP (EGFP) -MBP -β-gal	(Wang et al., 2008)

Continuation Table 2. Reported applications of phasins in biotechnology and biomedicine

Strain/ platform	PHA support	Phasin	Fusion protein	Reference
Affinity tag for protein purification				
E. coli *	PHB	$PhaP1_{Reu}$	Diagnostically important antigens -Mouse interleukin□2 (IL2) -Myelinoligodendrocyte glycoprotein (MOG)	(Bäckström et al., 2007)
-	*In vitro*-prepared nanoparticles of PHBHHx packed with hydrophobic drugs	$PhaP1_{Reu}$	Cell ligands -Mannosylated human α1-acid glycoprotein (hAGP), able to bind to the mannose receptor of macrophages -Human epidermal growth factor (hEGF), able to recognize EGF receptors on	(Yao et al., 2008)
Biosurfactant				
A. hydrophila	-	$PhaP_{Ah}$	-	(Wei et al., 2011)
Coating material				
	PHBHHx, PHBHV and PLA casted films	$PhaP_{Ah}$	Cell adhesion motif RGD (Arg-Gly-Asp)	(Dong et al., 2010)
	PLA, PHBPHHx and PHBHVHHx casted films	$PhaP_{Ah}$	Cell adhesion motifs -RGD -Laminin-derived motif IKVAV (Ile–Lys–Val–Ala–Val)	(Xie et al., 2013)
	PHBHV and PHBHHx casted films	$PhaP_{Ah}$	RGD	(Gao et al., 2014)
	PHBHHx casted films	$PhaP_{Ah}$	RGD	(You et al., 2011)

II. MOTIVATION AND AIMS

Knowledge of the interactions between PHA and their biological environment is vital if we are to better understand the polymer biogenesis process and develop added value applications. Interest in phasins has emerged for two main reasons: i) they are bound to PHA granules (carbonosomes), forming a layer on their surface; and ii) their concentration may reach 5 % (wt/wt) of the total protein content of PHA-accumulating cells. These proteins play important roles in PHA biogenesis, ensuring cell fitness. The present thesis aims to:

1. Demonstrate the interaction between phasins from the model PHA-accumulating bacterium *P. putida* KT2440 and identify the oligomerization motif of these proteins.

2. Undertake a comprehensive proteomic study to identify novel interactions of PhaF, helping to explain its different roles in *Pseudomonas*.

3. Study the interaction between PhaF and PHA by mimicking their native environment with the goal of improving the control of production of phasin-coated materials.

III. MATERIALS AND METHODS

1. Bacterial strains, media and growth conditions

Table 3 shows the bacterial strains used throughout this work. Unless otherwise stated *E. coli* and *P. putida* strains were grown aerobically in Luria-Bertani (LB) broth or LB agar (Sambrook and Russell, 2001) at 37 ºC and 30 ºC, respectively. The media were supplemented, when appropriate, with 100 μg/mL ampicillin or 50 μg/mL kanamycin.

E. coli JM109 was used in the cloning steps for protein purification. *E. coli* M15 [pREP4] was used for the high-level production of recombinant His_6-tagged proteins using the pQE32 plasmid, and *E. coli* BL21(DE3) was used to produce recombinant proteins using pET29a(+) and derivative plasmids. The production of recombinant protein in *E. coli* was induced by the addition of 1 mM isopropyl-β-D-thiogalactopyranoside (IPTG). *E. coli* DH10B was used as cloning strain for experiments using the bacterial two-hybrid system (BACTH, for "Bacterial Adenylate Cyclase-based TwoHybrid", Euromedex, France) and to construct GFP-fusions. GFP protein was obtain from pMAB20-GFP-LYTAG plasmid provided by Biomedal S.L, Spain (Dinjaski and Prieto, 2013).

BACTH assays were performed with the reporter strain *E. coli* BTH101 (Cya^-, adenylate cyclase deficient) harbouring the pUT18C and pKT25 plasmid combination on M63 indicator plates containing 13.6 g/L KH_2PO_4, 2 g/L $(NH_4)_2SO_4$, 0.5 mg/L $FeSO_4 \cdot 7H_2O$, 1 mM $MgSO_4$, 2 g/L maltose, 15 g/L agar, 100 μg/mL ampicillin, 50 μg/mL kanamycin, 0.5 mM IPTG and 40 μg/ml 5-bromo-4-chloro-3-indolyl-β-D-galactopyranoside (X-gal) (Euromedex, France).

For PHA accumulation, *P. putida* strains were pre-cultured in LB medium at 30 °C and 200 rpm; overnight growths were washed, transferred at a final OD_{600} 0.3 in M63 0.1 N medium, and grown at 30 °C and 200 rpm as previously described (Moldes et al., 2004). M63 0.1 N is a nitrogen limited minimal medium composed of 13.6 g/L KH_2PO_4, 0.2 g/L $(NH_4)_2SO_4$, 0.5 mg/L $FeSO_4 \cdot 7H_2O$, 1 mM $MgSO_4$ and a solution of trace elements (composition 1000x per liter = 2.78 g $FeSO_4 \cdot 7H_2O$, 1.98 g $MnCl_2 \cdot 4H_2O$, 2.81 g $CoSO_4 \cdot 7H_2O$, 1.47 g $CaCl_2 \cdot 2H_2$, 0.17 g $CuCl_2 \cdot 2H_2O$, and 0.29 g $ZnSO_4 \cdot 7H_2O$). 15 mM octanoic acid was used as carbon source for the production of PHOHHx. Cultures of *P. putida* strains carrying pSEVA238 plasmids (GFP fusions) were induced with 0.5 mM 3 -methylbenzoate.

Table 3. List of strains and plasmids used in this work

Strain/plasmid	Description	Source/Reference
Strains		
E. coli DH10B	Cloning strain	Invitrogen, Thermo Fisher Scientific, USA
E. coli JM109	Cloning strain	Stratagene, Agilent Technologies, USA
E. coli BTH101	Adenylate cyclase (Cya-) deficient strain for BACTH screens	Euromedex, France
E. coli M15[pREP4]	Transformation strain for His_6-protein production from the pQE32 plasmid. Contains pREP4 plasmid, Km^r	Qiagen N. V., Germany
E. coli BL21(DE3)	Strain for PhaI production from the pET29a(+) plasmid; deficient in lon and ompT proteases. Contains the λDE3 lysogen that carries the gene for T7 RNA polymerase	Novagen, Merck KGaA, Germany
P. putida KT2440	TOL plasmid-cured, spontaneous restriction deficient derivative of *P. putida* mt-2	Prieto's lab collection
P. putida KT2440-G	KT2440 derivative strain containing pSEVA238-GFP plasmid	This work
P. putida KT2440-IG	KT2440 derivative strain containing pSEVA238-IG plasmid (*phaI-GFP* fusion)	This work
P. putida KT2440-DG	KT2440 derivative strain containing pSEVA238-DG plasmid (*phaD-GFP* fusion)	This work
Plasmids		
pQE32	Vector for the production of His_6-tagged proteins. ColE1 ori, T5 promoter/*lac* operator element, N-terminal His_6-tag sequence; Amp^r	Qiagen N. V., Germany
pQE32-*phaF*	Plasmid for production of His_6-PhaF; Amp^r	This work
pET29a(+)	Expression vector. F1 ori, T7 promoter/*lac* operator, N-terminal S•Tag™/thrombin configuration, and optional C-terminal His_6-tag sequence; Km^r	Novagen, Merck KGaA, Germany
pETD	Derivative of pET29a(+) for production of thrombin-PhaD-His_6; Km^r	This work
pETI	Derivative of pET29a(+) for production of PhaI. The construction is not in frame with the thrombin or His_6 -tag sequence; Km^r	Prieto's lab collection
pUT18C	BACTH vector designed to produce a given polypeptide fused in-frame at its N-terminal end with the T25 Cya fragment. ColE1 ori; Amp^r	Euromedex, France
pKT25	BACTH vector designed to produce a given polypeptide fused in-frame at its N-terminal end with the T25 Cya fragment. P15 ori; Km^r	Euromedex, France
pUT18C-*zip*, pKT25-*zip*	Derivatives of pUT18C and pKT25 with a 114 bp DNA fragment encoding the Gcn4 leucine zipper (positive control for two-hybrid assays)	Euromedex, France
pUT18C-*phaF*	*phaF* cloned into pUT18C	This work
pKT25-*phaF*	*phaF* cloned into pKT25	This work

Continuation Table 3. List of strains and plasmids used in this work

Strain/plasmid	Description	Source/Reference
Plasmids		
pUT18C-*phaI*	*phaI* cloned into pUT18C	This work
pKT25-*phaI*	*phaI* cloned into pKT25	This work
pUT18C-*phaI*$^{\Delta ZIPI}$	*phaI* deletion mutant of the leucine zipper-like motif (ZIPI) cloned into pUT18C	This work
pUT18C-*phaI*^{V135A}	*phaI*^{V135A} (ZIP mutant) cloned into pUT18C	This work
pUT18C-*phaI*^{L128A,V135A}	*phaI*^{L128A,V135A} (ZIP mutant) cloned into pUT18C	This work
pUT18C-*phaI*^{L128A}	*phaI*^{L128A} (ZIP mutant) cloned into pUT18C	This work
pUT18C-*phaI*^{L121A,L128A,V135A}	*phaI*^{L121A,L128A,V135A} (ZIP mutant) cloned into pUT18C	This work
pUT18C-*ZIPI*	ZIPI cloned into pUT18C	This work
pUT18C-*phaD*	*phaD* cloned into pUT18C	This work
pUT18C-*phaC1*	*phaC1* cloned into pUT18C	This work
pKT25-*phaIC1*	*phaC1* cloned into pKT25	This work
pSEVA238-GFP	Derivative of pSEVA238 (Standar European Vector Architecture) containing GFP protein. pBBR1 ori, XylS-Pm promoter; Km^r	Prieto's lab collection
pSEVA238-IG	pSEVA238-GFP derivative containing *phaI-GFP*	This work
pSEVA238-DG	pSEVA238-GFP derivative containing *phaD-GFP*	This work

Ori, origin of replication; Km^r, kanamycin resistance; Amp^r, ampicillin resistance

2. Molecular biology techniques

Genomic DNA from *P. putida* KT2440 was isolated with the PureLink™ Genomic DNA Mini Kit (Invitrogen, Thermo Fisher Scientific, USA). DNA fragments were purified using the QIAquick PCR purification or QIAquick gel extraction kit (Qiagen N. V., Germany). DNA amplification was executed in the thermocycler Mastercycler Gradient (Eppendorf, Germany). The reaction mixtures contained 1 unit of Phusion® High-Fidelity DNA Polymerase (New England BioLabs, Inc., USA) per 50 µL of reaction, 1X Phusion HF buffer, 200 µM dNTPs, 0.5 µM of each forward and reverse primer, and ~10 ng of template DNA. All oligonucleotides used for PCR amplification are listed in Table 4.

Thermocycling conditions for a routine PCR were as follows: initial denaturation 98 ºC, 30 sec; 30 cycles of 98 ºC 10sec, 60-72 ºC 30 sec (calculated based on the melting temperature of the primer pair using NB Tm calculator), and 72 ºC 15-30 sec per kb of DNA; and final extension 72 ºC 10 min.

Table 4. Oligonucleotides used in this thesis

Oligonucleotides	Sequence 5'À3'
PhaF_pQE32_FWD	gatggatccgagctggcaagaagaacaccg (*Bam*HI)
PhaF_pQE32_REV	atcaagctttcagatcagggtaccggtg (*Hin*dIII*)*
PhaD_pET29_FWD	gtctctcatatgatgaaaacccgcgatcgtatcctt (*Nde*I*)*
PhaD_pET29_REV	taaggtaccccctccaggtacttcactg (*Kpn*I)
PhaI_pET29_FWD	gggtttcatatgatggccaaagtgattgcgaaga (*Nde*I*)*
PhaI_pET29_REV	taaggatcctggtttgtgcgcgacg (*Bam*HI)
pKT25-PhaF_FWD	gctctagagatggctggcaagaagaacacc (*Xba*I)
pKT25-PhaF_REV	cgggatcctcagatcagggtaccggtgc (*Bam*HI)
pUT18C-PhaF_FWD	gctctagagatggctggcaagaagaacacc (*Xba*I)
pUT18C-PhaF_REV	cgggatcctcagatcagggtaccggtgc (*Bam*HI)
pKT25-PhaI_FWD	tgtctagagatggccaaagtgattgcgaagaa (*Xba*I)
pKT25-PhaI_REV	attggatccttatggtttgtgcgcgacgcg (*Bam*HI)
pUT18C-PhaI_FWD	tgtctagagatggccaaagtgattgcgaagaaa (*Xba*I)
pUT18C-PhaI_REV	attggatccttatggtttgtgcgcgacgcg (*Bam*HI)
PhaI^{V135A}_FWD	tgtctagagatggccaaagtgattgcgaagaaaaaagacgaagccctggac (*Xba*I)
PhaI^{V135A}_REV	attggatccttatggtttgtgcgcagcgcgctcaagcagctcatgagcc (*Bam*HI)
PhaI^{L128A,V135A}_FWD	tgtctagagatggccaaagtgattgcgaagaaaaaagacgaagccctggacacgcttggcgagg (*Xba*I)
PhaI^{L128A,V135A}_REV	attggatccttatggtttgtgcgcagcgcgctcaagcagctcatgagcctgttcaagcttgatcgacaacgcct (*Bam*HI)
PhaI^{L128A}_FWD	tgtctagagatggccaaagtgattgcgaagaaaaaagacgaagccctggacacgcttggcgagg (*Xba*I)
PhaI^{L128A}_REV	attggatccttatggtttgtgcgcgacgcgctcaagcagctcatgagcctgttcaagcttgatcgacaacgcct (*Bam*HI)
PhaI^{L121A,L128A,V135A}_FWD	tgtctagagatggccaaagtgattgcgaagaaaaaagacgaagccctggacacgcttggcgagg (*Xba*I)
PhaI^{L121A,L128A,V135A}_REV	attggatccttatggtttgtgcgcagcgcgctcaagcagctcatgagcctgttcaagcttgatcgaagccgcct (*Bam*HI)
pUT18C-PhaD_FWD	gtgtctagagatgaaaacccgcgatc (*Xba*I)
pUT18C-PhaD_REV	attggatccctacccctccaggtact (*Bam*HI)
pUT18C-PhaC1_FWD	gtgtctagagatgagtaacaagaacaacga (*Xba*I)
pUT18C-PhaC1_REV	attggatcctcaacgctcgtgaac (*Bam*HI)
pKT25- PhaC1_FWD	gctctagagatgagtaacaagaacaac (*Xba*I)
pKT25- PhaC1_REV	cgggatcctcaacgctcgtgaacgtaggt (*Bam*HI)
PhaD-GFP_FWD	attctagaaataattttgtttaactttaagaaggagatatacatatgaaaacccgcgatcgtatc (*Xba*I)
PhaD-GFP_REV	tactcgagcccctccaggtacttcact (*Xho*I)
PhaI-GFP_FWD	attctagaaataattttgtttaactttaagaaggagatatacatatggccaaagtgattgcg (*Xba*I)
PhaI-GFP_REV	tactcgagtggtttgtgcgcgacg (*Xho*I)
pI5'	ccggaattcctgccacgctttgcttgaac (*Eco*RI)
pI3'	cgcggatccatgctgtgtacctcatgctc (*Bam*HI)
glpK5'	cacctggctgatctggaagc
glpK3'	ccgtacacttccgaggatgg

Underlined sequence means the restriction site for restriction enzymes shown in brackets.

DNA fragments were purified from agarose gel, using High Pure PCR Product Purification Kit (Roche Diagnostics, Indianapolis). Restriction digestion was carried out with High-Fidelity Restriction Endonucleases (New England BioLabs, Inc., USA). Ligation of DNA fragments was performed with T4 DNA Ligase (New England BioLabs, Inc., USA) overnight at 4 ºC.

For plasmid extraction, the High Pure Plasmid Isolation Kit (Roche Diagnostics, USA) was used. All cloned inserts and DNA fragments were confirmed by DNA sequencing with fluorescently labeled dideoxynucleotide terminators and AmpliTaq FS DNA polymerase (Applied Biosystems Inc., USA) in an ABI Prism 377 automated DNA sequencer (Applied Biosystems Inc., USA). Chemically competent cells of *E. coli* were prepared using a high-efficiency transformation method based on complex condition (TBF method) (Hanahan et al., 1991). *P. putida* cells were made competent utilizing a sucrose-based procedure (Choi et al., 2006). Briefly, cells from an overnight culture grown in LB medium were harvested by centrifugation and the cell pellet was washed at least 3 times with room temperature 300 mM sucrose. The transfer of exogenous DNA molecules into *P. putida* competent cells was achieved by electroporation.

3. Overproduction, purification and fluorescent labelling of proteins

3.1. Purification of PhaF

The universal vector pQE32, which allows the production of an N-terminal His_6-tagged protein under the control of the T5 promoter, was used for His_6-PhaF construction. The 786 bp DNA fragment encoding PhaF was PCR-generated using the oligonucleotides 1 and 2 listed in Table 4, and cloned into the pQE32 vector using the *Bam*HI and *Hin*dIII restriction enzymes to generate the plasmid pQE32-*phaF*. Overproduction of His_6-PhaF protein was achieved in recombinant *E. coli* M15[pREP4] harbouring pQE32-*phaF* by induction with 1 mM IPTG. The culture was grown in LB (Km, Apm), induced at OD_{600nm} of 0.5, and incubated for 16 h at 18 ºC and ~50 rpm to minimize the formation of inclusion bodies. Cells were harvested, resuspended in buffer A (20 mM sodium phosphate pH 7.4, 300 mM NaCl, 30 mM imidazole, 0.1 % Triton X-100, and 1 tablet of Roche cOmplete™ protease inhibitor cocktail per 50 mL of solution), and disrupted by 3 passages through a French pressure cell at 1000 psi.

The mixture of cellular materials (known as homogenate) was centrifuged at 14,800 *g* for 20 min. His_6-PhaF was purified from the soluble fraction of the homogenate by metal ion affinity chromatography (IMAC) using an ÄKTA chromatography system (GE

Healthcare Life Science, USA). The soluble fraction of the homogenate was passed through a column packed with 5 mL of affinity medium Ni-Sepharose (GE Healthcare Life Sciences, USA) precharged with Ni^{2+}, and equilibrated with 50 mL of buffer A. The column was washed with 25 mL of buffer A and then with 75 mL of increasing concentrations of imidazole (30-250 mM) to remove protein bound non-specifically to the column. To reach different concentrations of imidazole, buffer A was mixed with buffer B, which have the same components of buffer A and 500 mM imidazole. His_6-PhaF was eluted at 265 mM imidazole, which competes with the His-tag for binding to the metal-charged resin. Eluted PhaF was dialyzed against 50 mM Tris-HCl pH 7.5 and 300 mM NaCl, or phosphate buffered saline (PBS) pH 7.4 and 140 mM NaCl, and concentrated using Amicon® Ultra 15 mL Centrifugal Filters (Merck KGaA, MilliporeSigma, Germany) with a molecular weight limit cut-off (MWCO) of 10,000 kDa. The NMWCO is defined as the minimum molecular weight of a solute that is 90 % retained by the membrane (Drioli et al., 2015). Prior use, aliquots stored at -20 ºC were centrifuged 5 min at 13,000 *g* to remove aggregates. Protein absorbance was measured in a NanoDrop™ UV-Vis spectrophotometer at 280 nm (Bionova Scientific, Inc. USA).

The protein molar concentration was obtained using $M = A / \varepsilon_{280} \times l$; where A = absorbance 280 nm, ε_{280} = molar extinction coefficient of PhaF (19480 M^{-1} cm^{-1}) and l = path length of the window cuvette (1 cm). PhaF purity was analyzed by 12.5 % SDS-PAGE (sodium dodecyl sulfate-polyacrylamide gel electrophoresis).

3.2. Fluorescent labelling of PhaF

His_6-PhaF labelling was achieved by using Alexa Fluor 647 succinimidyl Ester dye that binds to the primary amines ($R\text{-}NH_2$) of proteins (Invitrogen, Thermo Fisher Scientific, USA). The protein solution (2 mg/mL) was dialized in 50 mM Hepes pH 7.5, 300 mM NaCl, and mixed with Alexa-647 dye. The molar ratio of dye to protein was adjusted to achieve a 1:1 of dye:PhaF. The mixture was incubated for 30 min in a shaker at room temperature protected from light and the reaction was stopped by adding 1M Tris-HCl pH 7.0 at a final concentration of 100 mM. A Hi-Trap desalting column (GE Healthcare Life Science, USA) was used to remove the excess dye by size exclusion chromatography.

The final concentration of the labelled protein was calculated from the absorbance of the sample at 280 nm. To account for absorption of the dye at 280 nm, the protein absorbance was corrected according to: $A_{corr} = (A_{280} - A_{650} \times CF)$; where A_{280} = absorbance of the conjugate solution measured at 280 nm, A_{650} = absorbance at 650 nm (fluorophore), and CF = correction factor of fluorophore (0.03) estimated by the A_{280} / A_{650} of Alexa 647. The protein molar concentration was calculated as explained above.

3.3. Purification of PhaD

The universal vector pET29a(+), which allows the production of a C-terminal His_6-tagged protein with a thrombin cleavage site at the N-terminal, was used for PhaD-His_6 construction. The 615 bp DNA fragment encoding PhaD was PCR-generated using the oligonucleotides numbered 3 and 4 in Table 4, and cloned into the pET29a(+) vector using the *Nde*I and *Kpn*I restriction enzymes to create the plasmid named pET-*phaD*. Overproduction of PhaD-His_6 was achieved in recombinant *E. coli* BL21(DE3) harbouring pET-*phaD* by induction with 1 mM IPTG at an OD_{600} of 0.5 and subsequent incubation for 3 h at 37 ºC. The purification of PhaD-His_6 from the soluble fraction of the homogenate was achieved using the ÄKTA system as explained for His_6-PhaF. After successive washing steps, PhaD-His_6 was eluted from the column at 210 mM imidazole. Purified protein was dialyzed against 50 mM Tris-HCl pH 7.4 and 150 mM NaCl, and then concentrated using Amicon® Ultra 15 mL Centrifugal Filters, with a MWCO of 10,000 kDa (Merck KGaA, MilliporeSigma, Germany).

The protein concentration was measured based on the above mentioned formula (PhaD $\varepsilon_{280} = 15930\ M^{-1}\ cm^{-1}$). The purified protein was kept at -20 ºC until use.

3.4. Production of *E. coli* soluble fraction containing recombinant PhaI protein

Overproduction of His_6-PhaI protein was achieved in recombinant *E. coli* M15 [pREP4] harbouring pQE32-*phaI* by induction with 1 mM IPTG. However, we did not succeed on purifying the protein despite many attempts. Therefore, for PhaF-PhaI *in vitro* interaction test we used the soluble fraction of the homogenate of *E. coli* containing recombinant PhaI protein (without his-tag). The plasmid pET29a(+) carrying the *phaI* gene was constructed as follows: *phaI* was PCR amplified from *P. putida* KT2440 genomic DNA using oligonucleotides engineered with *Nde*I and *Bam*HI restriction sites (numbered 5 and 6 in Table 4). The resulting 420 bp DNA fragment was ligated into the *Nde*I/*Bam*HI double-digested pET29a(+) plasmid, giving rise to plasmid named pETI, which expressed *pha*I under the control of the T7 promoter /lac operator system. *E. coli* BL21(DE3) cells harbouring plasmid pETI were grown in LB medium until the cultures reached an OD_{600} of 0.5, and then induced at 37 ºC for 3 h through the addition of 1 mM IPTG. Cells were harvested by centrifugation at 14,800 *g*, resuspended in 50 mM Tris-HCl pH 7.5 and 300 mM NaCl, and disrupted using a French press cell (2 passages at 1000 psi) to obtain a homogenate. The soluble fraction retrieved from the second round of centrifugation was kept at -20 ºC. For PhaF-PhaI binding experiments, dilutions of the soluble fraction were made in 50 mM Tris-HCl pH 7.5, and the total protein concentration determined by the Bradford assay (Bradford, 1976) using Bio-Rad Protein Assay (Bio-Rad Laboratories, Inc., USA)

4. *In silico* prediction of phasins secondary structure

The secondary structure of pashins was predicted *in silico* using the 1) PredictProtein (PHD) (Rost et al., 2004), 2) JPred (Cole et al., 2008), and 3) multivariate linear regression combination (MLRC) (Guermeur et al., 1999) tools. A consensus prediction for a particular secondary structure was assigned when predicted by at least 2 of these tools. The PONDR-FIT™ and PONDR-VLXT predictors (from the Disprot Database of Protein Disorder) were used to predict disordered/unstructured regions within PhaI. PONDR-VLXT was also used to predict molecular recognition features (MoRFs) - short regions experimentally known to be disordered but which become structured when they co-crystallize with other proteins (Xue et al., 2010). Sequences with a disorder probability of >0.5 were considered disordered.

Coiled-coils were predicted using the method of Lupas et al. (Lupas et al., 1991) and the COILS server, as well as the MARCOIL method (Delorenzi and Speed, 2002). The oligomeric state of the phasin coiled-coils was examined using the LOGICOIL algorithm (Vincent et al., 2013), contemplating a coiled-coil interaction probability threshold of 10 %. If a given sequence score = 1, then there is no evidence for a particular oligomeric state. If the estimate probability is > 1 or < 1 then there is strong or less evidence against a particular oligimeric state, respectively (Vincent et al., 2013). DrawCoil software was used to create a helical wheel diagram for the oligomer interface.

5. Methods for protein-protein interactions

5.1. Biolayer interferometry

PhaF and PhaI binding *in vitro* was determined by biolayer interferometry using the BLItz® System (ForteBio Inc., USA). All binding reactions were performed at 25 °C with 50 mM Tris-HCl pH 7.5 and 300 mM NaCl (assay buffer). Basic kinetic experiments were performed as follows: (i) an initial baseline step using the assay buffer (30 s), followed by (ii) ligand molecule immobilization on the surface of the biosensor (300 s), (iii) a second baseline step (30 s), (iv) an association or analyte binding step (300 s), and finally (v) dissociation in the presence of buffer only (300 s). The binding response was measured as the shift in wavelength caused by a change in the thickness of the biosensor tip, and reported in real time as a sensorgram trace. The density of the ligand on the surface of the biosensor was optimised by testing different concentrations of His_6-PhaF (0, 0.6, 1.2, 2.4, 4.8, 5 μM) following steps i, ii and iv mentioned above.

Once the appropriate ligand concentration was chosen, immobilized His_6-PhaF was exposed to different dilutions of the soluble fraction of *E. coli* BL21(DE3) [pETI] homogenate, containing recombinant PhaI (50, 100 and 200 μg/mL of total protein). *E. coli* BL21(DE3) [pET29a(+)] soluble fraction was used as a negative control at a concentration of 100 μg/mL. Curve fitting and data processing were performed using BLItz Pro software (ForteBio Inc., USA).

5.2. Bacterial Two-Hybrid system (BACTH)

5.2. 1. Plasmid constructs for BACTH tests

In vivo PPIs were detected using the BACTH Kit (Euromedex, France) according to the manufacturer's instructions. A scheme of the technique is presented in Figure 8. It takes advantage of the fact that the catalytic domain of adenylate cyclase (Cya) from *Bordetella pertussis* comprises 2 complementary fragments, T25 and T18 (Figure 8), that are not active when physically separated. When these fragments are fused to interacting polypeptides, X and Y, hetero-dimerization of these hybrid proteins results in functional complementation between T25 and T18 and, therefore, cyclic AMP (cAMP) synthesis (Karimova et al., 1998).

To construct the plasmids for the BACTH assays, the DNA fragments encoding full-length *phaI* and *phaF* (without stop codon) were PCR-amplified from *P. putida* KT2440 using the oligonucleotides numbered 7-14 in Table 4. Purified DNA fragments were digested with *Xba*I and *Bam*HI and cloned into the pUT18C and pKT25 vectors. The resulting recombinant plasmids, named pUT18C-*phaF*, pKT25-*phaF*, pUT18C-*phaI* and pKT25-*phaI*, expressed hybrid proteins in which the phasins were fused at the C-terminal of the T18 and T25 fragments of the *B. pertussis* Cya catalytic domain. In addition, a variant of PhaI that lacked the last 25 residues encoding the coiled-coil ZIPI was synthetically generated and expressed as a T18-$PhaI^{\Delta ZIPI}$ fusion (ATG:biosynthetics GmbH, Germany). All clones were sequenced as a verification step.

To introduce mutations into the ZIPI motif of PhaI, *in vitro* PCR-based site-directed mutagenesis was conducted using Phusion High-Fidelity DNA polymerase (New England BioLabs, Inc., USA). The forward and reverse oligonucleotides numbered 15-22 in Table 4 were designed to introduce desired nucleotide substitutions into a particular region of the amplified DNA. PhaI variants were generated in which the key residues Leu121, Leu128 and V135 were replaced by alanine in different combinations (Figure 17A). Amplified DNA was cloned into pUT18C plasmid yielding the fusions T18-$PhaI^{\Delta ZIPI}$, T18-$PhaI^{V135A}$, T18-$PhaI^{L128A,V135A}$, T18-$PhaI^{L128A}$, and T18-$PhaI^{L121A,L128A,V135A}$. *In vivo* PPIs of PhaF with partners of interest identified by pull-down assays (see below), were corroborated using the BACTH system. The T18 and T25 complementary fragments were fused at their C-terminal with *phaD* and *phaC1* using the vectors pUT18C and pKT25 (oligonucleotides numbered 23-28 in Table 4).

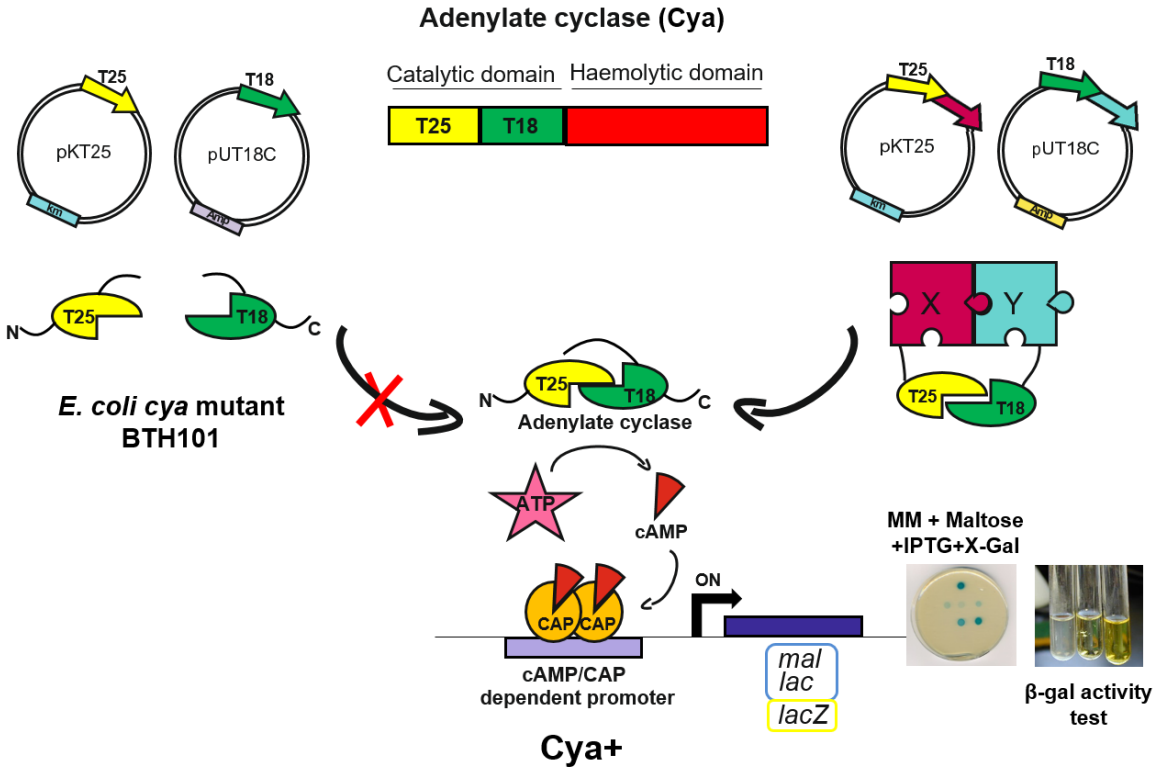

Figure 8. BACTH system scheme. Positive interactions are observed when cAMP is produced by the reconstituted Cya, due to the interaction between T18- and T25-fusion proteins, as showed on the right part of the diagram. cAMP produced by the reconstituted chimeric enzyme binds to the catabolite activator protein, CAP. The cAMP/CAP complex is a pleiotropic regulator of gene transcription in *E. coli*. It turns on the expression of several genes, including genes of the *lac* and *mal* operons, involved in lactose and maltose catabolism. Therefore, *cya* deficient strain *E. coli* BTH101 become able to use lactose or maltose as sole carbon source (Euromedex, France).

5.2. 2. Western blot analyses

Western blot analyses were performed to determine the expression of the different PhaI variants fused to the T18 fragment (T18-PhaI, T18-PhaI$^{\Delta ZIPI}$, T18-PhaI^{V135A}, T18-PhaI^{L128A,V135A}, T18- PhaI^{L128A} and T18-PhaI^{L121A,L128A,V135}). For this, *E. coli* DH10B cells carrying individual plasmids encoding the different fusions were grown at 30 °C in LB medium supplemented with 100 µg/mL ampicillin. The production of the fusion proteins was induced with 0.5 mM of IPTG after 4 h of growth. Samples were taken 48 h after induction, normalized to the optical density at OD_{600}, separated by 15 % SDS-PAGE, and transferred to a PVDF membrane.

The membrane was blocked with a solution of nonfat dry milk (5 %) in PBS-T buffer (10 mM sodium phosphate, 0.15M NaCl and 0.05 % Tween-20) for 1 h, washed

with PBS-T, and incubated 1h with anti-CyaA mouse monoclonal antibody (CyaA 3D1: SC13582 which specifically recognizes a sequence at the C-terminal of the T18 fragment) (Santa Cruz Biotechnology, USA) diluted 1:1000 in PBS-T buffer containing 1 % nonfat dry milk. After washing, the membrane was incubated with Amersham anti-mouse IgG horseradish peroxidase secondary antibody (NA931; diluted 1:5000), and immunoreactive proteins detected using the Amersham ECL system according to the manufacturer's instructions (GE Healthcare Life Science, USA).

5.2. 3 BACTH assays

To study PhaF-PhaI dimerization, plasmids pUT18C-*phaI* and pKT25-*phaF*, or pUT18C-*phaF* and pKT25-*phaI*, were co-transformed into the *E. coli* BTH101 (*cya*) reporter strain, and grown on LB-X-gal indicator plates incubated at 30 °C for 24-48 h. At least 3 randomly selected colonies were further plated on M63 minimal medium supplemented with 0.2 % (w/v) maltose as the sole carbon source for in plate detection of β-gal activity. Quantification of PPIs was achieved by assessment of β-gal activity in liquid cultures using the Miller assay explained below (Miller, 1972).

PhaI or PhaF homo-oligomerization was examined using the T18-PhaI and T25-PhaI or T18-PhaF and T25-PhaF fusions co-expressed in the *cya* strain. Combinations of T25-PhaI or T25-PhaF with T18-PhaI$^{\Delta ZIPI}$, T18-PhaI^{V135A}, T18-PhaI^{L128A}, T18-PhaI^{L128A} or T18-PhaI^{L121A,L128A,V135A} were also co-expressed in *E. coli* BTH101 for testing the role of the coiled-coil in oligomerization. Plasmids pKT25-*phaF* and pUT18C-target proteins (*phaD* and *phaC1*) were co-transformed into the reported strain to verify new PhaF interacting partners. A co-transformant of pKT25-*zip* and pUT18C-*zip* containing a DNA sequence coding for a leucine zipper motif (Gcn4 leucine zipper) was used as a universal positive control. Bacteria harbouring the empty vectors pKT25 and pUT18C were used as negative controls. Negative controls of each fusion co-transformed with an empty plasmid were also used.

5.2. 4. β-galactosidase activity assay

The functional complementation of the interacting proteins in the BACTH system (Euromedex, France) was quantified by β-gal activity in liquid cultures using the Miller assay (Miller, 1972) as recommended by the BACTH kit manufacturer. In brief, *E. coli* BTH101 were grown in 10 mL of LB broth in the presence of 0.5 mM IPTG and the appropriate antibiotics at 30 °C without agitation for 24 h (stationary phase). The liquid cultures were diluted in PM2 assay buffer pH 7.0 (final volume of 1 mL), which is composed of 70 mM Na2HPO4·12$H_2$0, 30 mM NaH_2PO_4·$H_2$0, 1 mM $MgSO_4$, 0.2 mM $MnSO_4$, and 100 mM β-mercaptoethanol. Permeabilization of the cells was achieved

upon addition of 25 µL chloroform plus 50 µL SDS 0.1 %. The β-gal activity was assayed at 28 ºC using 250 µL of o-nitrophenol-β-galactoside (ONPG) substrate solution (0.4 % ONPG in PM2 buffer without β-mercaptoethanol). The reaction was stopped by the addition of 500 µL 1 M Na_2CO_3. The enzymatic activity, A in Units per mL (U/mL), was quantified according to the formula:

$$A = [200*(OD_{420}\text{-}OD_{420} \text{ in control tube / min of incubation})]*\text{dilution factor}$$

Where OD_{420} is the absorbance of the o-nitrophenol that results from hydrolysis of ONPG. A unit of enzymatic activity corresponds to 1 nmol of ONPG hydrolyzed per min at 28 °C. The factor 200 in the above formula is the inverse of the absorption coefficient of o-nitrophenol, which is 0.005 per nmol/mL at pH 11.0 (i.e. after addition of Na_2CO_3). The enzyme activity was finally expressed as U per mg of cell dry weight (U/mg CDW). CDW is determined from the OD_{600} value of the bacterial culture, given that 1 mL of culture at OD_{600} = 1 corresponds to 300 µg of CDW (Euromedex, France).

Under routine conditions, when no interaction occurs, the BTH101 strain basally expresses approximately 150 U/mg CDW. When hybrid proteins interact, β-galactosidase activity ranges between 700 to 7000 U/mg CDW, depending on the efficiency of functional complementation. For statistical analyses, a *p* value of 0.05 was used as the cut-off for significance. If the *p* value was less than 0.05, we rejected the null hypothesis and concluded that a significant difference does exist. Such statistically significant differences are indicated in the figures with an asterisk "*".

5.3. Affinity purification coupled to mass spectrometry: pull-down assays

To identify interacting partners of PhaF, an affinity-purification followed by mass spectrometry (AP-MS) approach was used. Our method involves: i) the incubation of recombinant His_6-PhaF (the bait) with the soluble fraction of *P. putida* KT2440 homogenate, containing putative interacting proteins; ii) binding of His_6-PhaF and interacting proteins to a Ni-Sepharose column; iii) washing away nonspecific proteins; iv) elution of the bound proteins; and v) analyses by SDS-PAGE and MS.

Recombinant His_6-PhaF, the "bait protein" was expressed and purified as described above, and suspended in buffer A (20 mM sodium phosphate pH 7.4, 300 mM NaCl, 30 mM imidazole) (Figure 9). The pool of cellular proteins was prepared as follows: *P.putida* KT2440 was grown in PHA accumulation conditions for 24 h. Cells were harvested, resuspended in buffer A supplemented with Roche cOmplete™ protease inhibitor cocktail (1 tablet per 50 mL of solution) and disrupted by 3 passages through a French pressure cell at 1000 psi. The homogenate was treated with 0.1 mg/mL DNase

(TURBO™ DNase, Ambion, Inc., USA) for 20 min at room temperature. The soluble fraction of the homogenate was separated from PHA granules and other cellular materials by centrifugation at 18,000 *g* for 30 min. The concentration of total protein in the soluble fraction was quantified by Bradford assay.

For pull-down experiments, 100 µg of purified His_6-PhaF was incubated with 1 mg of soluble fraction on a roller shaker during 1 h at ~25 ºC with smooth agitation. The sample was passed through a column packed with affinity medium Ni-Sepharose (GE Healthcare Life Sciences), washed with buffer B and eluted as described above for affinity purification. The PhaF-interacting protein complexes were eluted with 265 mM of imidazole. A pull-down with *P. putida* soluble fraction in the absence of His_6-PhaF was used as a negative control for non-specific binding to the Ni-Sepharose column. All the experiments were performed at least 2 times with different biological samples (3 and 2 biological replicas for the sample and the negative control, respectively). The eluted fractions were analyzed by MS (see section 5.5).

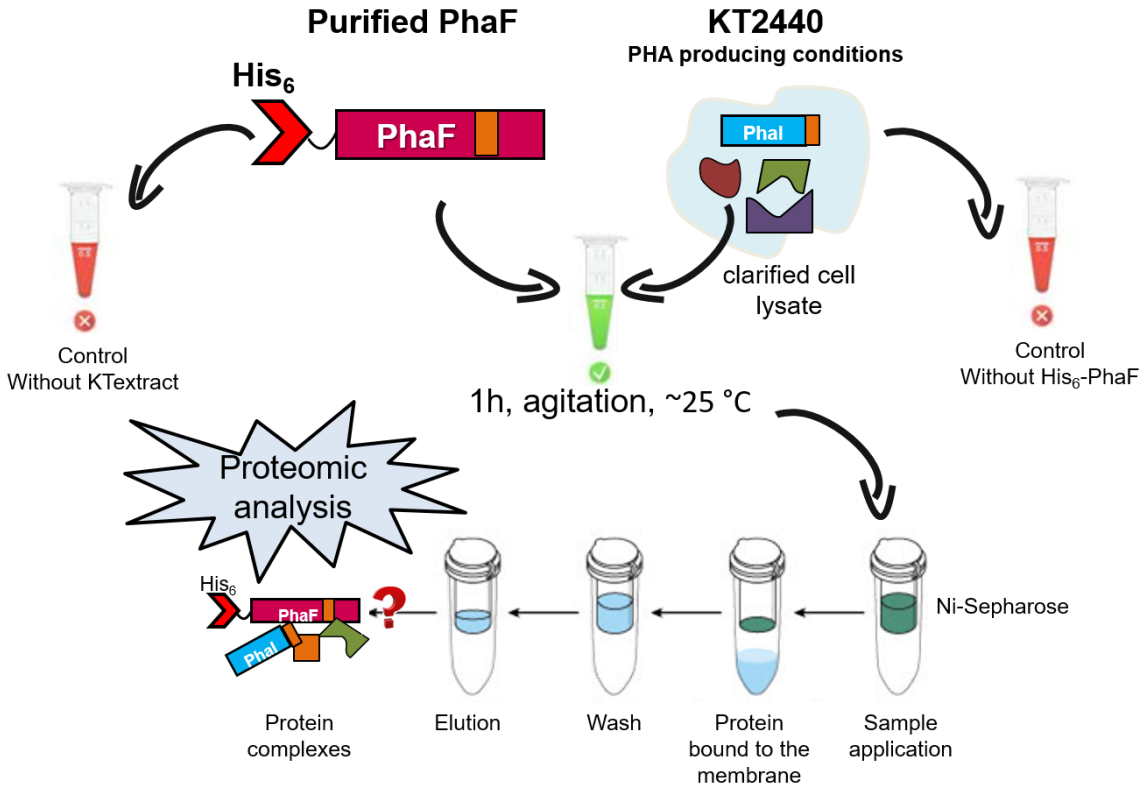

Figure 9. Pull-down coupled to MS. Workflow followed in this work. i) incubation of purified recombinant His_6-PhaF (the bait) with the soluble fraction of *P.putida* KT2440 homogenate, 1 h at ~25 ºC ii) binding of His_6-PhaF and interacting proteins to a Ni-Sepharose column; iii) washing away nonspecific proteins; iv) elution of the bound proteins; and v) proteomic analyses by SDS-PAGE and MS.

A Western blot analysis was performed to detect PhaI in the pull-down assay, as a positive control for a known PhaF interacting partner. The elution fraction containing proteins that co-eluted with PhaF was separated by 15 % SDS-PAGE, and transferred to PVDF membrane and blocked as explained above. The membrane was incubated 2h with rabbit polyclonal antiserum against PhaI diluted 1:5000 in PBS-T buffer containing 1 % nonfat dry milk. The antiserum was generated using SDS-PAGE-separated PhaI material as the antigen, in the same manner that the PhaZ depolymerase antiserum was previously obtained (de Eugenio et al., 2007). After washing, the membrane was incubated with anti-rabit IgG horseradish peroxidase secondary antibody (diluted 1:10000; NA934), and immunoreactive proteins detected using the Amersham ECL system according to the manufacturer's instructions (GE Healthcare Life Science, USA).

5.4. PHA granule-associated proteome

To evaluate whether proteins interacting with PhaF were present or absent in the PHA granule fraction, an analysis of the PHA granule proteome of *P. putida* KT2440 was carried out. The granule fraction extracted from homogenates treated with DNase was washed twice with 150 mM NaCl and suspended in 15 mM Tris-HCl, pH 8. The suspension was layered on 55 % glycerol, followed by centrifugation in a swinging-bucket rotor 1 h at 10,000 *g* (Dinjaski and Prieto, 2013). The PHA granule band was collected from the interface and the centrifugation over glycerol was repeated 2 more times. For comparison, PHA granules were also isolated on a discontinuous sucrose gradient (0.43 and 0.58 M) in 50 mM Tris-HCl pH 8, as previously reported (Moldes et al., 2004). Cell lysate was centrifuged for 3.5 h, 120,000 *g* at 4 ºC, the granule fraction was collected, resuspended in 15 mM Tris-HCl, pH 8, centrifuged for 20 min at 120,000 *g* and stored at -20 ºC. For this second method, the homogenate sample was not treated with DNase prior to granule preparation. The final granule preparations were separated on a 12.5 % SDS-PAGE gel and further analyzed by MS.

5.5. Identification of proteins by MALDI-TOF-TOF peptide mass fingerprinting

Proteome analyses were performed by the proteome core facility of the Biological Research Center of the Spanish National Research Council CIB-CSIC (Madrid, Spain) as described in detail previously (Cristobo et al., 2011). A preparative gel containing 500 µg of each elution sample was run approximately 1 cm and stained with the Colloidal Blue Staining Kit (Invitrogen, Thermo Fisher Scientific, USA) for protein visualization and spot picking. The gel section containing the whole protein fraction was cut-off into 2 vertical slices and subjected to tryptic digestion.

The peptide mixture was loaded onto an Acclaim PepMap 100 precolumn with output to an Acclaim PepMap 100 C18 (3 µm particle size, 75 µm inner diameter x 25 cm length) analytical column eluting directly into the nano-electrospray source (Thermo Fisher Scientific, USA). Samples were analyzed with an LTQ-Orbitrap Velos mass spectrometer (Thermo Fisher Scientific, USA). Fragmented ions were detected at a resolution of up to 60,000. The top 15 most abundant ions in the scan were selected for MS/MS fragmentation. Selected ions were fragmented by collision-induced dissociation with normalized collision energies of 35 %. Spectrums were processed with Discoverer software Version 1.1.1.14. Database searching for protein identification was done using Sequest. Peptide matches were validated using the Percolator algorithm, where a peptide -spectrum match (PSM) was considered correct if it achieved a q value < 0.01 (Käll et al., 2007).

Pearson´s r correlation coefficients were calculated for the MS datasets (number of PSM). It was obtained by dividing the covariance of the comparable variables by the product of their standard deviations. The formula returns a value between -1 and 1; where: 1 indicates a strong positive relationship, -1 indicates a strong negative relationship and results of 0 indicate no relationship at all.

5.6. *In vivo* localization of PhaD-GFP and PhaI-GFP fusions

A variant of the vector pSEVA238 (Standard European Vector Assembly platform) which encodes a green fluorescent protein (GFP) was used for expression of PhaD-GFP and PhaI-GFP fusions in *P. putida* KT2440 (Table 3). The expression system consist of the benzoate/*m*-toluate-responsive XylS regulator of the TOL plasmid of *P. putida* mt-2 and its cognate promoter *Pm*.

The *phaD* and *phaI* fragments were amplified from *P. putida* KT2440 using oligonucleotides 29-32 (Table 4), and cloned in-frame to the N-terminal of GFP. The resulting plasmids, pSEVA238-DG (PhaD-GFP fusion) and pSEVA238-IG (PhaI-GFP fusion) were transformed into *P. putida* KT2440 via electroporation (Choi et al., 2006).

For *in vivo* localization studies, cells carrying *phaD-GFP* or *phaI-GFP* (*P. putida* KT2440-DG and *P. putida* KT2440-IG, respectively) were cultured in LB medium overnight and were transferred to a final OD_{600} 0.3 into M63 0.1 N medium containing 15 mM octanoic acid for PHA production. M63 0.1 N cultures were induced by 0.5 mM 3-methylbenzoate after 2 h of growing at 30 ºC and 200 rpm. GFP fluorescent signal was analyzed microscopically using a Leica AF6000 LX widefield multidimensional microscopy system with Leica LAS AF lite software.

5.7. Electrophoretic mobility shift assay (EMSA)

Electrophoretic mobility shift assays (EMSA) were conducted using purified His_6-PhaF and PhaD-His_6 and unlabeled DNA fragments. The upstream region of *phaI*, PhaI promoter $P_{I,}$ was amplified by PCR using oligonucleotides pI5' and pI3', numbered 33 and 34 in Table 4, to generate a 230 bp fragment. As a non-specific control we used a DNA fragment (177 bp) of the coding region of the housekeeping gene *glpK* (Protein, Q88NX8), which was amplified by glpK5' and glpK3' oligonucleotides (numbered 35 and 36).

For binding reactions, 10 nM of the DNA fragment was incubated with varying amounts of purified proteins in binding buffer (50 mM Tris–HCl pH 7.4, 50 mM NaCl). The reaction samples (10 µl) were incubated at room temperature for 1 h before being electrophoresed on native 5 % polyacrylamide gels. After electrophoresis, DNA fragments were stained with GelRed® (Biotium) and were detected by exposure to UV light.

6. Methods for protein-polymers interaction

6.1. Polymer synthesis, purification and characterization

PHOHHx was synthesized by shake flask cultivation using *P. putida* KT2440 growing in M63 0.1 N medium with a final concentration of 15 mM octanoic acid as carbon source, as detailed in the section: bacterial strains, media and growth conditions. After 12 h of incubation, the cells were harvested, resuspended in NaCl 0.9 % solution, and disrupted tree times by passing through a French pressure cell. The homogenates were centrifuged 30 min at 15,000 *g*, and the pellet fraction containing the PHOHHx granules was dissolved in 10 mL chloroform. To extract water soluble cell components, 2 mL of *MilliQ* water was added, and the organic and aqueous phases were separated by centrifugation at 5,000 *g*. The organic phase was transferred to a clean tube. The process was repeated several times with the homogenates to maximize recovery. Finally, the chloroform solution containing the PHA was precipitated in ice-cold methanol (tenfold excess) under vigorous stirring, and separated by centrifugation (Escapa et al., 2011).

To obtain a polymer with endotoxin units (EU) ≤ 20 EU/g, in agreement with the endotoxin requirements for biomedical applications, successive steps of PHA extraction with chloroform at 40 ºC, filtration and precipitation with cold methanol were performed. Finally, the polymer was dried under vacuum at 40 °C for 48 h (Dinjaski et al., 2014).

The determination of the number average of molecular weight (Mn), and the structural characterization of purified PHA by nuclear magnetic resonance spectroscopy

(NMR) were performed by the Helmholz Zentrum Geesthacht chromatography facilities (Germany). For Mn analyses, a multidetector Gel Permeation Chromatography system was used as reported before (Balk et al., 2017). Briefly, chloroform was used as eluent with a flow rate of 1 mL/min at 35 °C, and 0.2 % toluene as internal standard. Polystyrene samples were used for universal calibration. ^{13}C- and and ^{1}H-NMR measurements were performed at 25 °C in $CDCl_3$ (VWR, 99.8 %) using a Bruker Avance 300 spectrometer (300 MHz). Chemical shifts are referenced against residual solvent signal (7.26 and 77.0 ppm for ^{1}H and ^{13}C, respectively). Spectra were analyzed using the MestReNova software package. The spectra of ^{1}H- and ^{13}C-NMR of the purified PHOHHx and the assignment of the corresponding PHA by comparison with published data (Shen et al., 2011) are depicted in Annex I, Figure A1.

PLGA (M_n: 8370 g/mol; lactide content 68 % by weight) was synthesized by ring-opening copolymerization of *rac*-dilactide and diglycolide using 1,8-octanediol as initiator and the catalyst dibutyltin (IV) oxide as catalyst. The protocol for polymer synthesis and characterization was conducted at HZG as reported before (Mathew et al., 2015).

6.2. PHA supported films

The reaction chambers for the assays were prepared by attaching a plastic ring from an Eppendorf tube on a cleaned glass coverslip using UV glue (Norland optical adhesive 88). Glass coverslips used as supports were cleaned by sonication in 80 % ethanol for 15 min, followed by extensive washing with *MilliQ* water. PHA supported films were prepared by solvent casting of PHA isolated from *P. putida* KT2440 (PHOHHx) on Eppendorf-glass chambers. Different concentrations of PHA dissolved in chloroform plus Nile Red dye (1µg/mL) were spread on the glass surface and vacuum dried until solvent evaporation.

6.2.1. PhaF *in vitro* self-organization on PHA films

To evaluate self-organization of His_6-PhaF on PHA films, Alexa 647-labeled His_6-PhaF in 50 mM Tris-HCl pH 7.5 and 300 mM NaCl, was incubated above the casted films at final concentration of 1µM. The final volume of the assay was 100 µL. The binding of the protein to the substrate was followed after 15 min by confocal microscopy measurements. Images were collected with a Leica TCS-SP2-AOBS inverted confocal microscope. A HCX PL APO 63x oil immersion objective (N.A. = 1.4–1.6; Leica, Mannheim, Germany) was used for all images. Ar (488–514 nm) and He-Ne (633 nm) ion lasers were used to excite Alexa 488 or Nile red and Alexa 647, respectively. Image processing was carried out using LAS AF Lite software.

6.3. PhaF and PHA Langmuir monolayers

In this thesis, we used the Langmuir technique, one of the most known models to investigate and understand molecular interactions at interfaces, to get dipper insights into the PhaF-PHA interaction. In this technique films are formed at the air-water interface (A-W interface) with precise control of the area per molecule and other experimental conditions (Giner-Casares et al., 2014; Schöne et al., 2017) (Figure 10).

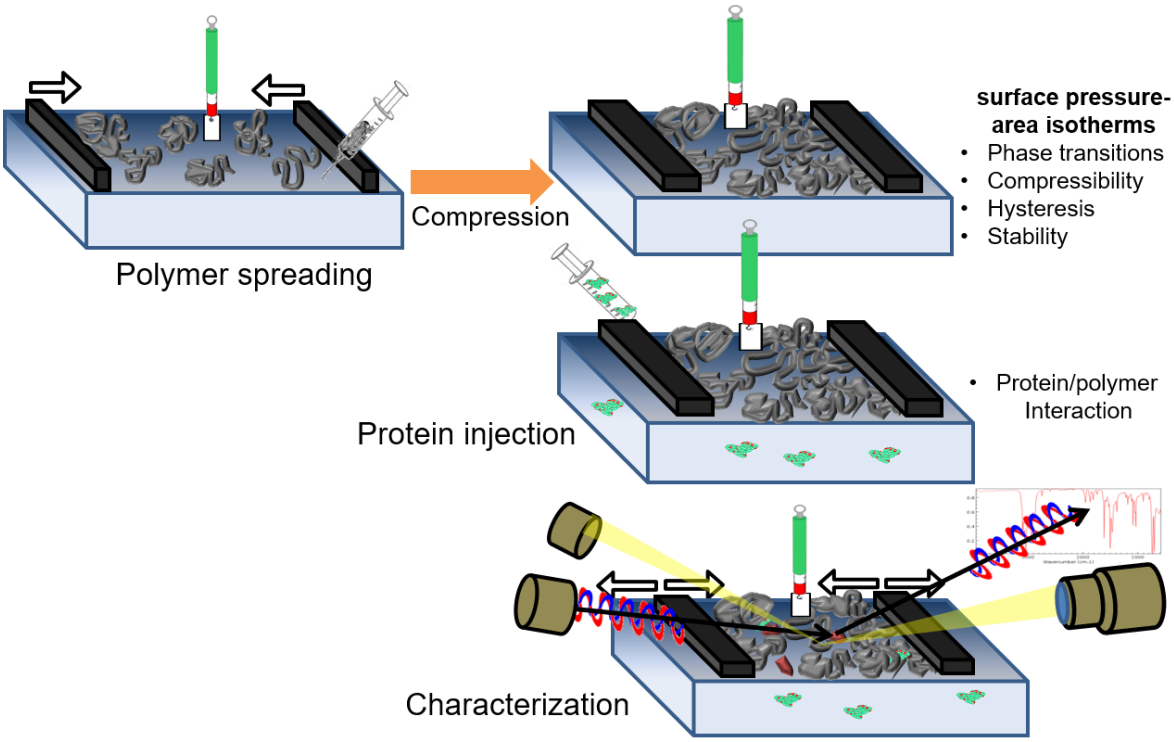

Figure 10. Overview of the Langmuir technique to study polymer-protein interactions. Here, we use PHOHHx to form monolayers at the A-W interface by spreading the polymer solution on top of the water subphase (PBS buffer), as a model system to test the interaction between PhaF and its natural substrate as well as for detecting possible alterations in the molecular conformation of both species during the process. After compressing the polymer monolayer to a desired surface pressure π, the barriers are kept constant and the protein is injected under the polymer layer (into the subphase). The Δπ, caused by the adsorption of PhaF into the polymer surface, is monitored in real time using a Wilhelmy plate. *In situ* characterization of the conformation and morphology of the mixed film (PHOHHx-PhaF) is carried out by PM -IRRAS and BAM microscopy. The formed films can also be transferred to solid substrates for further analyses.

In order to characterize protein adsorption to A-W interfaces, a description of the adsorption isotherm, adsorption and desorption kinetics, conformation of adsorbed proteins, and other physical parameters related to the adsorbed protein layer, such as layer thickness is typically obtained (Hlady et al., 1999). The adsorption of PhaF (from an aqueous subphase) to the polymer is followed by *in situ* methods: Polarization Modulated Infrared Absorption Spectroscopy (PM-IRRAS) and Brewster Angle Microscopy (BAM). The interaction of this protein with a less hydrophobic polymer, PLGA, will be addressed to substantially improve the understanding on the interplay of polymer hydrophilicity and PhaF adsorption. An overview of the technique is shown in Figure 10.

6.3.1. Langmuir surface pressure vs. bulk concentration isotherms: PhaF

The characterization of PhaF adsorption to bare A-W interfaces was first studied using the Langmuir technique approach. Protein monolayers on the A-W interface can be formed either by spreading of protein solution on the water/buffer surface (Langmuir monolayers) or upon surface adsorption of the protein molecules injected into the subphase (Gibbs monolayers) (Tronin et al., 1994; Dukhin et al., 1995; Rogalska et al., 2000). The surface activity of PhaF in different subphases and the minimal concentration of PhaF for Langmuir and Gibbs isotherms was examined in a polytetrafluoroethylene circular trough with an area of ~63 cm^2 and a surface-area/ volume ratio of 0.8 cm^{-1}. A PhaF stock solution (0.7 mg/ml) was added (spreaded or injecteded) in increments into *MilliQ* water or PBS buffer with a Hamilton microsyringe. The surface pressure (understood as the change of the water surface tension) was monitored in real time during the process using a Wilhelmy plate. For each increment, the surface pressure was allowed to reach equilibrium before the measurements.

The surface pressure of compression isotherms of PhaF is given as a function of trough area. Each experiment was performed twice. All presented isotherm data correspond to individual experiment data reproducible with a random measurement error of ~5 % concerning the surface pressure or the mean molecular area (MMA) values for the independently repeated experiments.

6.3.2. Surface pressure vs. area (π-A) and surface adsorption isotherms

π-A isotherms of spread monolayers (Langmuir) on PBS were recorded on a polytetrafluoroethylene Langmuir trough (“Large” or “medium” trough, KSV NIMA, Finland) equipped with Delrin barriers, for controlling the MMA, and a custom-made level compensation system. (KSV LTD, Finland). The system was placed on an active vibration isolation system (halcyonics variobasic 40, Accurion, Germany) within a

cabinet. The changes in the surface tension of the A-W interface (surface pressure) were monitored by a filter paper-based Wilhelmy plate microbalance and recorded as a function of the MMA.

For PHOHHx π-A isotherms, a defined amount of polymer solution in chloroform was deposited drop-wise onto PBS using a microsyringe (Hamilton Co., Reno, NV, USA). Before an experiment was started, the chloroform was allowed to evaporate for 10 min. The Langmuir layers were laterally compressed at constant compression rates of 10 mm/ min. The MMA for PHOHHx was calculated based on the average weight and the molar fraction of the repeating units (HO and HHx) and the surface area of the trough during compression. For PhaF π-A isotherms, PhaF solution in PBS was spread drop by drop onto the buffer subphase with a Hamilton microsyringe. The final concentration was 0.013 μM. A total of 10 min was allowed for the protein to reach equilibrium at the air-buffer interface before compression.

PhaF isotherm was obtained by plotting the surface pressure against the trough area. The compression modulus Cs^{-1} was computed using surface pressure isotherms based on:

$$Cs^{-1} = -\mathrm{A}\left(\frac{\delta\pi}{\delta\mathrm{A}}\right)$$

Where A is the area at the given surface pressure π. A high value means that a monolayer is rigid and densely packed. Adsorption isotherms (Gibbs monolayers) of PhaF were recorded as an increase of the surface pressure, by a Wilhelmy microbalance, as a function of time after injection Δπ(t), without any external mechanical force. The protein was injected into PBS at a final concentration of 0.18 μM. The surface area-dependent adsorption was evaluated using 3 different troughs with surface-area/volume ratios of 1.4, 0.8 and 0.7 cm^{-1}. The temperature of the subphase for PHOHHx and PhaF isotherms was kept constant at 22 ± 0.5 °C, if not noted differently. All isotherm experiments were repeated at least 2 times.

6.3.3. PhaF adsorption into PHA Langmuir films

The adsorption of His_6-PhaF to PHOHHx preformed monolayers was monitored using a constant surface area approach in a circular trough with a lower surface-area/ volume ratio without compression, resulting in an increase of the surface pressure upon protein insertion. PHOHHx Langmuir monolayers were prepared by spreading the polymer solution dropwise at the air-buffer interface, until the desired initial surface pressure (12 mN/m) was reached. After 10 min of solvent evaporation, PhaF was injected with a Hamilton syringe into the subphase (PBS buffer) beneath the polymer monolayer at a protein final concentration of 0.18 μM. The increase of surface pressure was recorded as Δπ(t), until a stable surface pressure was reached, and the microscopic modifications

were traced by BAM. The effect of the composition of the monolayer on the adsorption kinetics of PhaF was demonstrated through the injection of PhaF under PLGA monolayers (Mn: 8370 g/mol; lactide content 68 % by weight (Schöne et al., 2015)) at an initial π of 10 mN/m, following the protocol described for PHOHHx. For all the experiments, the same volume injected was extracted from the subphase to avoid a volume-dependent change in π. To discard artifact results from the injection protocol, we performed a control experiment where blank solution (PBS) was injected (data not shown).

6.3.4. Brewster angle microscopy (BAM)

BAM allows a non-invasive imaging for studying thin films, or Langmuir monolayers, on liquid surfaces. It utilizes the reflection-free condition that occurs when p-polarized light is guided towards an A-W interface at a specific incident angle, called de Brewster angle. BAM measurements of pure and mixed films were carried out at the A-W interface using a Langmuir trough equipped with an Ellipsometer Accurion Nanofilm EP3 (EP3, Accurion, Gottingen, Germany). The instrument was equipped with 658-nm class IIIB laser source and a high performance CCD camera (1392 × 1040 pixel). Images were taken simultaneously during the π–A isotherm experiments with a resolution limit of 1 μm.

6.3.5. Infrared measurements of PhaF in solution

Measurement of the protein vibration spectrum in solution was carried out by Infrared (IR) spectroscopy by attenuated total reflection (ATR-IR) using a FT-IR Tensor 27 system with an ATR crystal (Bruker Optik GmbH, Ettlingen Germany). Drops with 3 different concentrations of the protein in PBS (0.1, 0.5 and 1.3 mg/ml) were placed on the ATR crystal and the liquid was pressed on the crystal with a hollow pistil. Spectra were obtained at ambient temperature in the spectral range of 1200-1800 cm^{-1} at a resolution of 2 cm^{-1}. An average of 64 cycles were used to increase signal to noise ratio. Spectra analysis was performed with OPUS software (version 7.5, Bruker Optik GmbH, Ettlingen Germany). The spectrum of the pure protein in solution (PBS) was obtained by subtracting the 0.1 mg/mL spectrum from the 1.3 mg/mL spectrum. By this procedure, most of the signal from proteins adsorbing to the ATR crystal is removed.

6.3.6. *In situ* infrared measurements

PM-IRRAS was used to determine the molecular conformation and orientation of the films. A polarization-modulation (PM) technique, PM-IRRAS, was applied to remove

the vibrational and rotational bands of water. The IRRAS set up consisted of a KSV NIMA PM-IRRAS spectrometer coupled to a Langmuir trough where the IR-beam was focused onto the A-W surface. FTIR spectra were acquired from 800 to 4000 cm^{-1} using s- and p-polarized light at an angle of incidence of 74°. Typically, 2500 scans were averaged. The differential reflectivity spectrum S is calculated from the collected difference (ΔR) and sum spectra (ΣR) of the detected intensities of the p- and s- polarized light as:

$$S = \frac{\Delta R}{\Sigma R} = \frac{R_S - R_p}{R_S + R_p}$$

To obtain the spectrum of the film adsorbing to the A-W interface, the sample spectrum is normalized with respect to the spectrum of the bare A-W interface S_0 with:

$$S_{film} = \frac{S - S_0}{S_0}$$

In the experiments with spread polymer films, these were compressed to a desired area per molecule, the barriers were then stopped and the IRRA spectra were recorded. In the adsorption experiments, the acquisition of the IRRA spectra started directly after the injection of the protein into the subphase. The PM-IRRAS measurements were performed twice. The biggest measurement error in IRRA spectra processing is normally obtained from the absorption-signal to baseline-noise ratio, resulting in false signal interpretation. To solve this problem, 3 background spectra were recorded and subtracted from the sample spectrum independently and only signals detected in all spectra were considered.

6.3.7. Langmuir-Schaefer films

The transfer of monolayers and mixed-films from the A-W interface onto solid substrates was carried out by horizontally touching the film with the substrate, a technique analogous to the Langmuir-Schaefer (LS) method (Bhuvanesh et al., 2017). LS-films of PhaF and PHOHHx transferred to silicon wafers were used for optical microscopy and atomic force microscopy (AFM) imaging. For IRRAS measurements, LS-films of PhaF were transferred to gold coated glass slides (Arrandee, Werther, Germany).

6.3.8. Atomic force microscopy (AFM)

AFM was carried out with a JPK Nanowizzard 4 in tapping mode. Cantilevers with a nominal spring constant of 40 N/m and a nominal tip radius of 8 nm were used.

IV. RESULTS AND DISCUSSION

1. Characterization of the oligomerization of *P. putida* phasins and identification of the role of coiled-coils in the establishment of PhaF and PhaI complexes

The results included in this section and the corresponding methodology have been accepted and published in BBA-general subjects (Elsevier) Citation: Tarazona NA, Maestro B, Revelles O, Sanz JM and Prieto MA (2018). "Role of leucine zipper-like motifs in the oligomerization of *Pseudomonas putida* phasins." Biochim Biophys Acta Gen Subj. Doi: 10.1016/j.bbagen.2018.11.002. Tarazona NA designed and performed the experiments and wrote the paper. Maestro B, Revelles O, and Sanz JM contributed to data analysis and to the final version of the manuscript. Prieto MA designed the experiments, supervised the findings of this work and the writing of the paper.

1.1. Prediction of coiled-coils regions among phasins PhaF and PhaI

1.1.1. Prediction and comparison of the secondary structure of phasins

Phasins from *P. putida* KT2440 share considerable sequence similarity (57 % similarity, 35 % identity) (Figure 11A). As members of the same family they may share some structural features, such as a previously reported preponderant α-helix composition, intrinsic disorder and coiled-coil regions (Maestro et al., 2013; Mezzina and Pettinari, 2016). In previous work, we also suggested a propensity for phasin associations, most likely via coiled-coiled interactions (Maestro et al., 2013). Due to the lack of suitable crystals of PhaF and PhaI, we used sequence analysis methods to gather information about the secondary structure of PhaI, and to compare it to the published PhaF structural model (Maestro et al., 2013). Although errors of structure estimation are possible, secondary structure prediction procedures have reached an accuracy (about 84 %) that is close to the theoretical limit (~88 %) (Yang et al., 2018).

All methods used in this study (the PHD, Jpred and MLRC) predicted an α-helix to be the predominant secondary structure of PhaI (~80 %), consisting of 2 helices -a long, uninterrupted α-helix from K9 to R109, and a shorter one from K115 to A136- (Figure 11B). This is remarkably similar to the PhaF N-terminal which comprises a long α-helix (S13–R105) followed by a shorter helix including residues R111–G133, and is in agreement with previous predictions for other phasins (which show a secondary structure composed of around 90 % α-helix) (Neumann et al., 2008; Mezzina et al., 2014).

Intrinsically disordered regions within PhaI were investigated using the PONDR predictors from the Disprot Database of Protein Disorder. With an average probability of about 50 %, PONDR-FIT predicted the region between Q73-L92 to be disordered (Figure 11C). Interestingly, a longer region (K46-L107) was found to be highly disordered by PONDR-VLXT (maximum probability of 0.92). This method additionally predicted regions that undergo a disorder-to-order transition upon binding to their targets (MoRFs), suggesting that PhaI disorder increases from 32 to 61 % in the unbound state. According to both predictors, the PhaI disordered stretches are similarly located to those of the PhaF N-terminal (Figure 11C).

1.1.2. Sequence, length and organization of PhaF and PhaI coiled-coils: identification of a leucine zipper-like motif

Coiled-coil predictions made by the COILS and MARCOIL methods showed 2 regions of PhaI with a high propensity for coiled-coils (Figure 12). Note that the results of both methods are very similar.

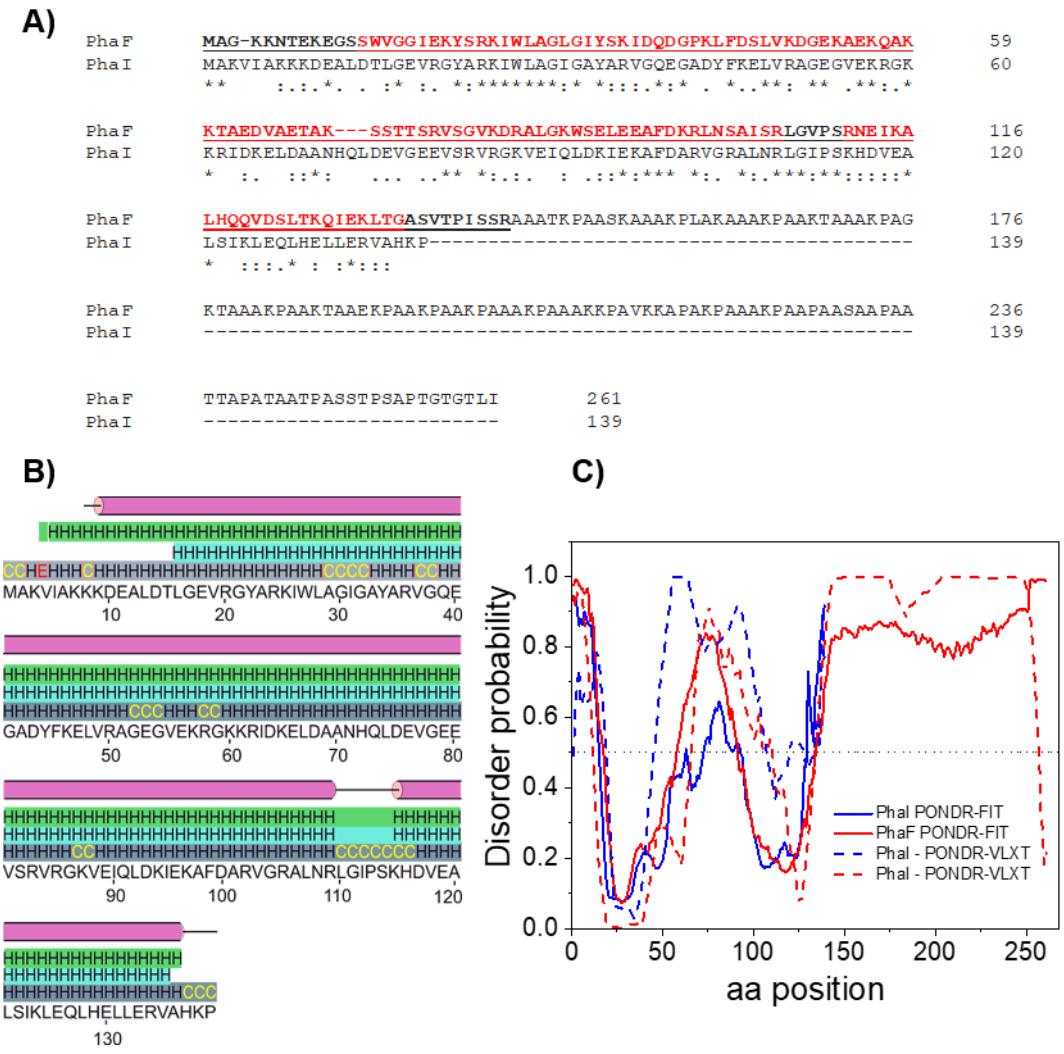

Figure 11. *In silico* analysis of phasins: A) Clustal alignment of PhaI and PhaF. PhaF α-helices are highlighted in red. The amino acid sequence of the PhaF N-terminal (BioF) is underlined. **B)** Secondary structure prediction of PhaI by the PHD (green), Jpred (blue) and MLRC (grey) tools. H = α-helix; E = extended β-strand; C = random coil; blank = other secondary structure (e.g., loop). Consensus helices predicted by at least 2 methods are represented via pink cylinders (helix 1 from K9 to R109, and helix 2 from K115 to A136). **C)** Protein disorder prediction for PhaI (blue), and comparison to disordered regions of phasin PhaF (red), using the PONDR-FIT (full line) and PONDR-VLXT (dashed line) predictors.

According to the COILS procedure, the first coiled-coil motif (CCM1) would extend over 46 amino acids between E56 and A101 and be located within the first α-helix; the second coiled-coil (CCM2) would comprise residues H116 to A136 within the short α-helix (Figure 12A). Interestingly, CCM2 shares characteristics with the coiled-coil stretch of PhaF (Maestro et al., 2013), encompassing residues R111 to A134, before since both lie in similar positions in the protein (Figure 12B) and show a predominance of leucine or valine

at heptad position *d* (Figure 12C).

In the PhaF coiled-coil, all *d* positions are occupied by leucine residues; it was therefore proposed to act as a leucine zipper-like motif for PhaF oligomerization (hereafter ZIPF). Although one of the *d* positions of the PhaI CCM2 is occupied by a valine, it was hypothesized that this region might play a role similar to that of the ZIPF motif in PhaI oligomerization (with this new motif hereafter termed ZIPI). Even though CCM1 was predicted to be a coiled-coil with strong probability, the length of this region, the lack of leucine residues at position *d*, and its predicted high degree of disorder in the absence of a target (Figure 11C), suggest CCM1 to have a different role in PhaI than that of ZIPI.

It is worth to mention that we did not found any significant similarities between the ZIPI or ZIPF motifs and $PhaP_{Ah}$, either in amino acid sequence or length, suggesting that phasins from different families use distinct mechanisms to acquire a coiled-coil-mediated oligomerization.

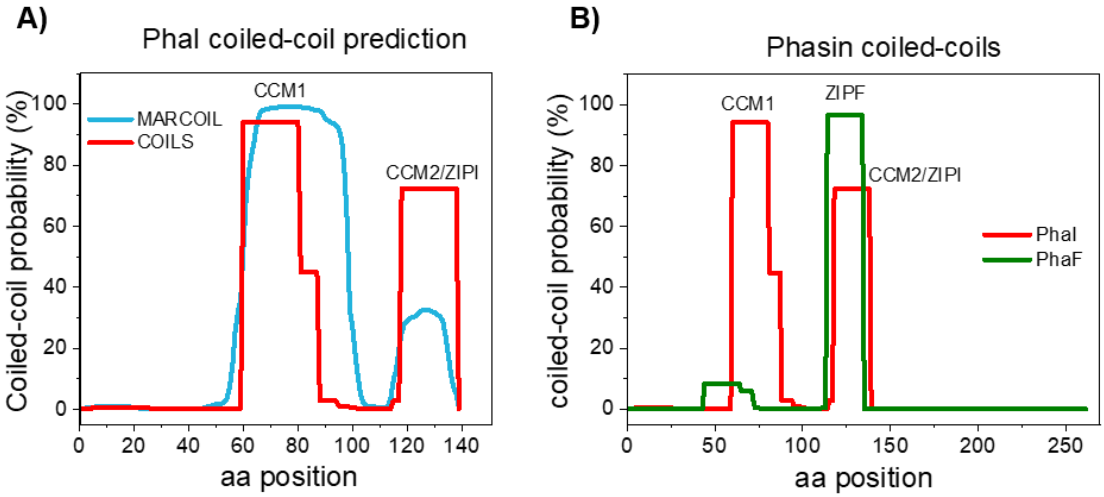

C)

```
PhaF    45   DSLVKDGEKAEKQAKKTAE---DVAETAKSSTTSRVSGVKDRALGKWSELEEAFDKRLNS 101
               LV+ GE  EK+ KK  +    D A          VS V+ +   +  ++E+AFD R+
PhaI    46   KELVRAGEGVEKRGKKRIDKELDAANHQLDEVGEEVSRVRGKVEIQLDKIEKAFDARVGR 105
heptad:           defgabcdefgabcdefgabcdefgabcdefgabcdefgabcdefg
```

CCM1

```
PhaF   102   SAISRLGVPSRNEIKALHQQVDSLTKQIEKLTGA  134
               A++RLG+PS+++++AL  +++ L + +E++
PhaI   106   RALNRLGIPSKHDVEALSIKLEQLHELLERVAHKP 139
heptad:           efgabcdefgabcdefgabcdefg
```

ZIPF/ZIPI

Figure 12. Prediction of coiled-coil motifs (CCM). A) MARCOIL prediction of coiled-coils for PhaI (blue), and COILS prediction (red) (21-residue window size). **B)** Comparison of the COILS outputs for PhaI (red) and PhaF (green). **C)** Amino acid sequence of the predicted coiled-coils (highlighted), and best heptad phase for CCM1, CCM2/ZIPI and ZIPF. Residues at the *a* and *d* positions are highlighted in red.

To predict the most probable oligomeric state of phasin coiled-coils, the LOGICOIL algorithm was used, with a coiled-coil output set at a threshold of 10 % (Figure 13A). The LOGICOIL score for the long CCM1 of PhaI (1.51) showed a clear preference for a tetramer state when compared to the second most probable conformation (antiparallel dimer: 1.01). However, this score showed no clear-cut prediction for the mode of ZIPI oligomerization, although there is a slightly higher propensity to the homo-trimer (1.02) vs. homo-tetramer (0.99) or homo-dimer (0.97). In any case, this aspect needs to be further investigated. DrawCoil software was used to create a helical wheel diagram for the postulated oligomers in order to visualize the interface formed by the ZIPI oligomers (Figure 13B). This revealed non-polar residues at positions *a* (V118, L125, L132) and *d* (L121, L128, V135).

A)

	Predicted state (raw scores)			
	Anti*	**Para****	**Trimer**	**Tetramer**
CCM1	1.00	0.94	0.81	1.51
CCM2/ZIPI	1.01	0.97	1.02	0.99

B)

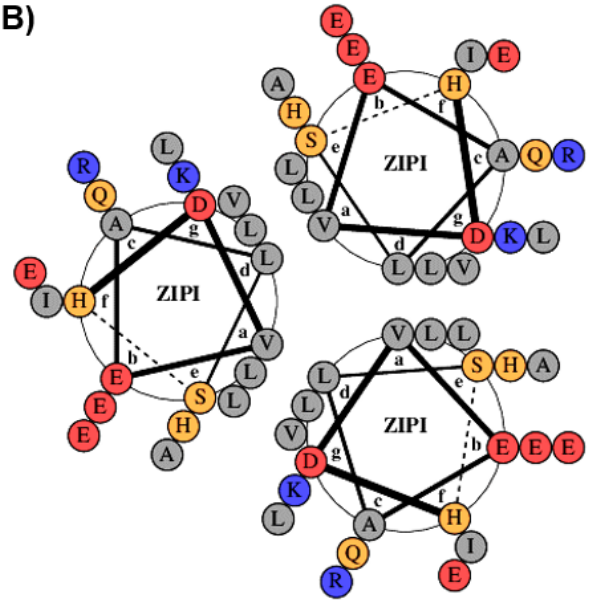

Figure 13. Oligomeric conformation prediction of PhaI. **A)** Multi-state coiled-coil oligomeric state prediction by LOGICOIL using a Marcoil threshold value of 10. Most probably state is written in red. *Antipaparallel dimer, **parallel dimer. **B)** Helical-wheel diagram (DrawCoil) of ZIPI trimer. Residues interior are colored by type; grey circles denote hydrophobic amino acids. The helical wheel plots for ZIPI trimer shows non-polar residues at *a* (V118, L125, L132) and *d* positions (L121, L128, V135) forming the oligomer interface.

1.2. Study of the *in vitro* and *in vivo* oligomerization of PhaF and PhaI

1.2.1. The interaction between PhaF and PhaI, as revealed by Biolayer interferometry

The structural similarity of PhaF and PhaI and the presence of coiled-coil regions with similar heptad repeats and location, revealed by *in silico* analyses, suggested the existence of protein complexes between these phasins. Experimental evidence for these interactions was sought by examining PhaF-PhaI *in vitro* oligomerization via biolayer interferometry (BLItz®, ForteBio Inc., USA) (Figure 14). The latter is an optical analytical technique that monitors in real time the interaction between 2 different molecules with the first one (termed the ligand or bait) immobilized on a biosensor surface, and the other (the analyte or interacting partner) maintained in solution (Sultana and Lee, 2001).

The density of the ligand on the surface of the biosensor was optimised by testing different concentrations of His_6-PhaF (0, 0.6, 1.2, 2.4, 4.8, 5 μM) following steps i, ii and iii (Figure 14A, B). For PhaF-PhaI binding experiments, purified His_6-PhaF (ligand) was immobilized at concentration of 4.8 μM on the biosensor to obtain a high density on its surface and to ensure an acceptable signal-to-noise readout. Since all attempts to purify PhaI failed given its tendency to form self-aggregates even at low concentration, the soluble fraction of *E. coli* BL21(DE3) [pETI] homogenate, containing overexpressed recombinant PhaI was used as the analyte solution. No background signal was obtained when using *E. coli* soluble fraction as a control (data not shown); a change in signal could therefore only arise through the binding of PhaI.

Although no binding constants could be calculated due to the lack of purified PhaI and the absence of information on its oligomerization state in the soluble fraction, the results show that PhaI interacts with PhaF, inducing a wavelength shift, i.e., when PhaI binds to PhaF the surface of the biosensor tip becomes increasingly thicker with increasing concentrations of the soluble fraction (Figure 14C). The nonlinear binding of PhaI to PhaF could be attributed to a molecular crowding effect induced by the presence of other proteins in the soluble fraction obtained from the homogenate.

1.2.2. PhaF and PhaI homo- and hetero-oligomers are confirmed by an *in vivo* two-hybrid system

The BACTH system was used to confirm the ability of *P. putida* KT2440 phasins to form PhaF-PhaI hetero-oligomers, and to test their homo-oligomerization *in vivo* (Karimova et al., 2000). The system is based on the reconstitution of adenylate cyclase (Cya) activity in an *Escherichia coli cya* deficient strain as explained in Figure 8.

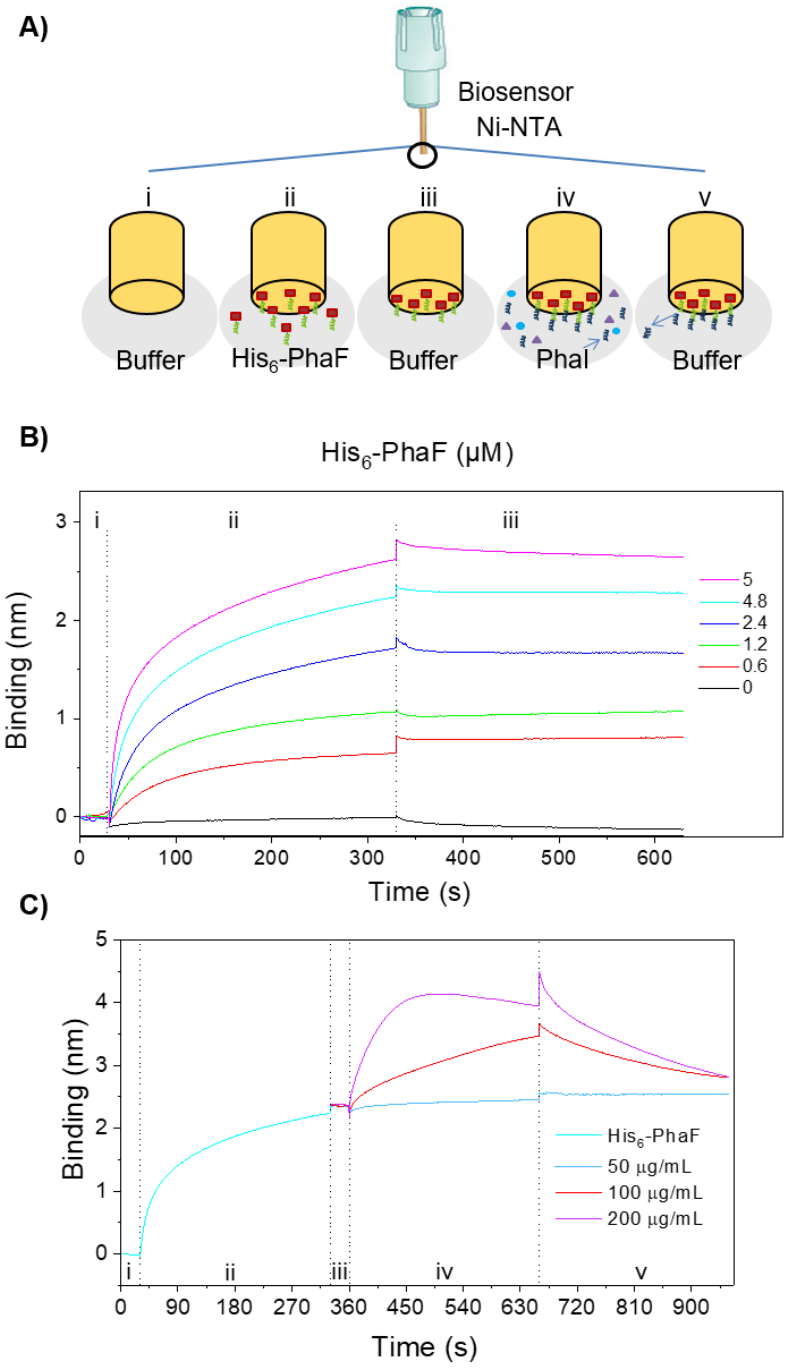

Figure 14. ***In vitro*** **interaction between PhaF and PhaI. A)** Illustration of the steps in the biolayer interferometry assay involving His_6-PhaF and PhaI on a Ni-NTA biosensor. Segments designations: (i) initial buffer background; (ii) association of His_6-PhaF with the biosensor; (iii) baseline prior to association (buffer alone); (iv) association of PhaI with immobilized His_6-PhaF, and (v) dissociation from the biosensor of non-interacting analyte molecules. **B)** Sensorgram of the optimization of His_6-PhaF loading onto Ni-NTA biosensors at several concentrations (0, 0.6, 1.2, 2.4, 4.8 and 5 μM). **C)** Sensorgram showing the response (wavelength shift, nm) to the interaction between His_6-PhaF and PhaI at different concentrations: 50 (blue) 100 (red) and 200 μg/mL (magenta) (examined in *E. coli* BL21(DE3) [pETI] soluble fraction).

When the complementary fragments T18 and T25 of *B. pertussis* Cya are fused to proteins that interact, hetero-dimerization of the chimeric proteins re-establishes the Cya^+ phenotype, and the functional complementation of the enzyme is measured via β-gal activity in liquid culture. As shown in Figure 15, BTH101 bacteria that co-expressed the T18-PhaF and T25-PhaF fusions showed levels of β-gal activity 20 times those of bacteria harbouring control plasmids (1218 U/mg CDW vs. 56 U/mg CDW). This indicates that PhaF oligomerization occurs *in vivo* in agreement with previously reported *in vitro* results (Maestro et al., 2013), and demonstrates that interaction of *Pseudomonas* phasins is testable using the BACTH system. A significant β-gal activity signal was also seen for the interaction between T18-PhaI and T25-PhaI (2480 U/mg CDW), providing the first experimental evidence of PhaI dimerization.

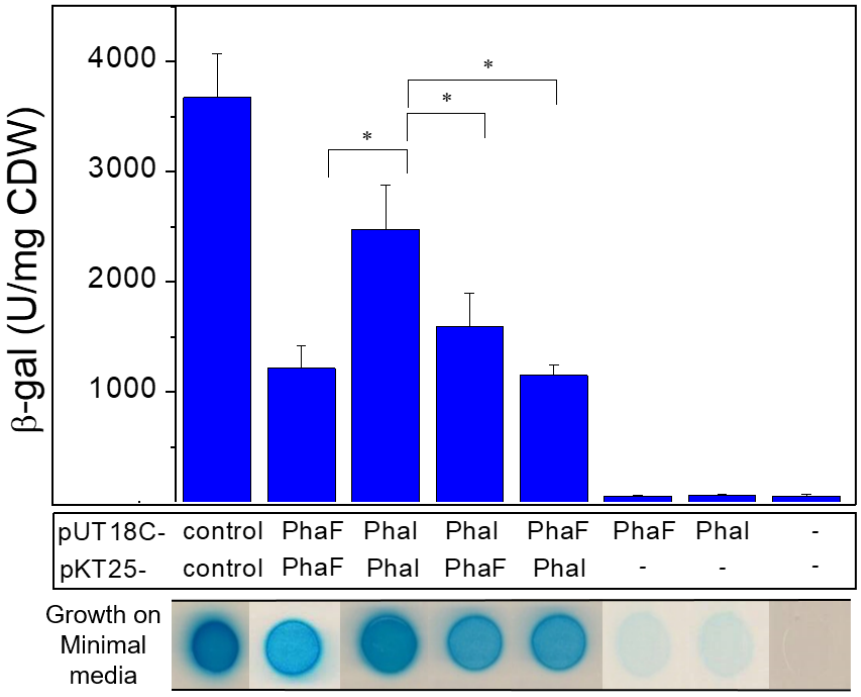

Figure 15. BACTH assays of phasin PhaF and PhaI oligomerization. β-gal activity (Miller Units per mg of cell dry weight, U/mg CDW) of BTH101 co-transformed with the indicated plasmids expressing PhaI or PhaF fused to the complementary fragments T18 and T25. The reported values correspond to the mean for 3 clones tested for each interaction. Control indicates plasmids containing a DNA sequence coding for a leucine zipper motif (Gcn4 leucine zipper). The symbol "-" indicates negative control vectors. Statistically significant differences between the samples (p value < 0.05) are indicated with "*". Bottom: growth of BTH101 *cya* cells carrying fusion plasmids in M63+Maltose plates supplemented with IPTG and X-gal. *cya* bacteria are unable to ferment lactose or maltose, therefore the growth of the strains on M63-maltose agar depends on functional interactions between proteins fused to T18 and T25 fragments.

The specificity of the results was confirmed by the fact that the proteins expressed independently from plasmids pUT18C-*phaF* or pUT18C-*phaI* did not lead to significant β -gal activity, nor to growth on M63-maltose agar when tested with the complementary negative controls (empty pKT25 plasmids) (Figure 15). Finally, the β-gal activity of cells co-expressing either T18-PhaI and T25-PhaF or T18-PhaF and T25-PhaI were 20-30 times (1600 and 1150 U/mg CDW) those of negative controls (56 U/mg CDW) but only a third of those recorded for the positive control. These results confirm the PhaF-PhaI interaction detected *in vitro* and support the idea that GAPs could form a network-like layer on the surface of the PHA granule, driven by homo- and hetero-oligomerization.

1.3. Identification of a leucine zipper-like motif involved in the oligomerization of PhaF and PhaI

To determine whether the deletion of the predicted ZIPI coiled-coil has an impact on the observed oligomerization of phasins, a truncated version of the *phaI* gene was fused to the C-terminal of T18. The T18-PhaI$^{\Delta ZIPI}$ chimeric protein lacked residues H116 to A136, corresponding to the ZIPI motif. Plasmid pUT18C-*phaI*$^{\Delta ZIPI}$ was co-transformed with pKT25-*phaF* or pKT25-*phaI* in *E. coli* BTH101 to test the complementation efficiencies using the β-gal test as described above. The inability of the transformants carrying T25-PhaF and T18-PhaI$^{\Delta ZIPI}$ fusions to restore the Cya+ phenotype, as shown by the negative β-gal result (50 U/mg CDW), confirmed the ZIPI motif to be essential for the interaction of PhaI with PhaF (Figure 16).

Possible defects in protein expression were ruled out since the T18-PhaI$^{\Delta ZIP}$ fusion protein was detected with a monoclonal antibody (CyaA 3D1) directed against the T18 fragment (Figure 17B). Additionally, the homo-oligomerization efficiency of the wild-type T25-PhaI and its truncated version T18-PhaI$^{\Delta ZIPI}$ was almost 13 times less (196 U/mg CDW) than that recorded for the interaction between the wild-type monomers (2480 U/ mg CDW), suggesting that ZIPI is crucial for PhaI homo-dimerization *in vivo* and that is the main oligomerization motif of PhaI.

1.4. Determination of the stability of the hydrophobic core of the leucine zipper-like motif

To check the importance in PPIs of the hydrophobic residues within the predicted leucine zipper-like motif of PhaI, 4 variants of ZIPI were constructed using site-directed mutagenesis. The 3 residues L121, L128 and V135 occupying the *d* positions of the heptad repeat were substituted by alanine residues in different combinations, as shown in Figure 17A. Modifications were designed to selectively destabilize the hydrophobic core of the oligomer without affecting the overall α-helical structure of the coiled-coil, thus avoiding protein instability and degradation (Robichon et al., 2011).

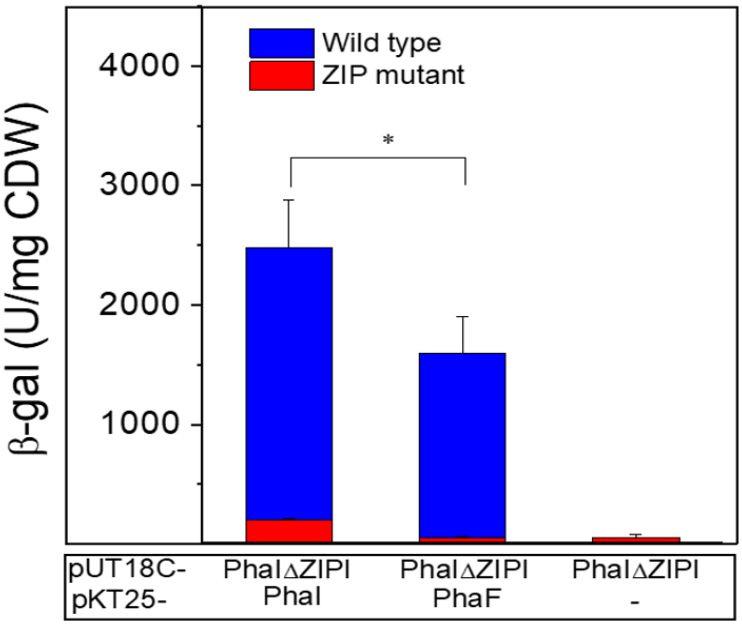

Figure 16. BACTH assay of PhaI$^{\Delta ZIPI}$ compared to wild-type PhaI. β-gal activity (/mg CDW) of BTH101 co-transformed with the indicated plasmids expressing PhaI$^{\Delta ZIPI}$, PhaI or PhaF fused to the complementary fragments T18 and T25. Values correspond to the mean for 3 clones tested for each interaction. "-" refers to the negative control vectors. Statistically significant differences between the samples (p value < 0.05) are indicated with "*".

Western blot analyses using anti-T18 monoclonal antibody showed that all PhaI variants were produced at the same level as that of the wild-type protein (Figure 17B), indicating that any defect in oligomerization was not due to a diminished expression of the variants of PhaI.

The ZIPI mutants were cloned into pUT18C plasmid yielding pUT18C-*phaI*^{V135A}, pUT18C-*phaI*^{L128A,V135A}, pUT18C-*phaI*^{L128A} and pUT18C-*phaI*^{L121A,L128A,V135A}. Each of the constructs was co-transformed with pKT25-*phaF* and pKT25-*phaI* vectors in BTH101 to test the ability of these mutants to form oligomers.

β-gal activity tests for the interaction between native PhaI and ZIP mutants revealed no significant difference between wild-type PhaI and PhaI^{V135A} or PhaI^{L128A} (in which only 1 of the leucine residues was substituted by alanine) (Figure 17C). However, the mutation of either 2 or 3 residues in the coiled-coil of PhaI^{L128A,V135A} and PhaI^{L121A,L128A,V135A} reduced 4-fold the strength of the interaction with wild-type PhaI. These results indicate that the homo-oligomerization interface of PhaI is stabilized by the presence of at least 2 voluminous hydrophobic residues at positions *a* and *d* in ZIPI, in agreement with the results of previous studies (Lau et al., 1984; Truebestein and Leonard, 2016).

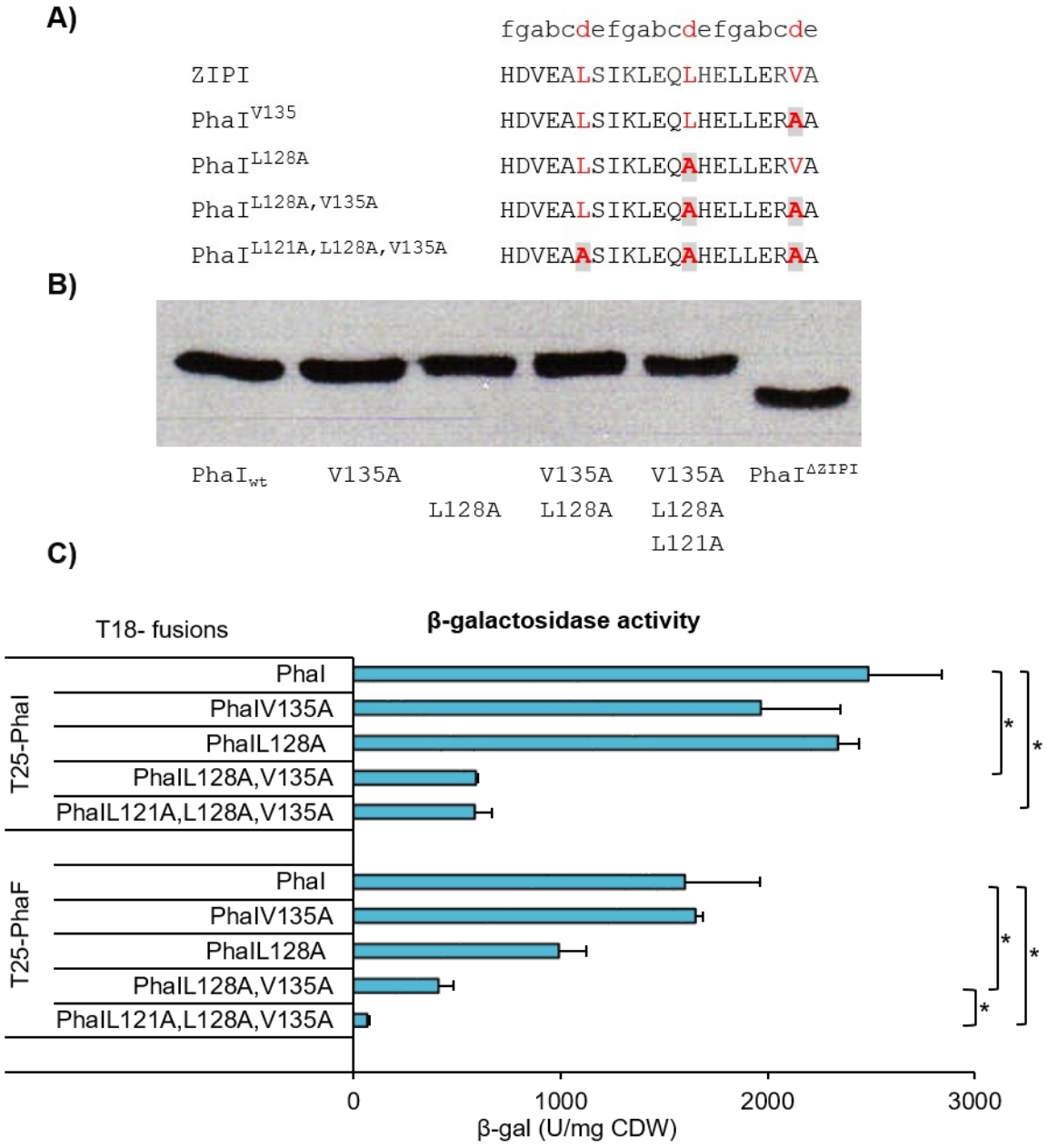

Figure 17. A) Amino acid sequence of ZIPI variants. Residues at *d* positions are highlighted in red. Alanine substitutions are in grey. **B)** Western blot analysis of pUT18C-PhaI variants using and antibody directed against T18. The residues substituted by alanine in each construction are shown. **C)** β-gal tests for the interaction between PhaI variants and native PhaF and PhaI. Amino acid substitutions are shown for every mutant. Statistically significant differences between the samples (p value < 0.05) are indicated with "*".

The interaction of PhaF with the PhaI variant forms (PhaI^{V135A} and PhaI^{L128A}) showed no significant differences compared to the wild-type PhaI. However, when the second and third *d* positions, L128 and V135, were modified in PhaI^{L128A,V135A}, the complementation efficiency decreased by around 75 %. As expected, when the 3 hydrophobic residues of ZIPI were substituted by alanines in PhaI^{L121A,L128A,V135A}, virtually no interaction was seen between both phasins according to the negative β-gal results (68 U/mg CDW). These results suggest that the PhaF-PhaI interface is more sensitive to hydrophobicity alterations than the interface formed between PhaI oligomers. Interestingly, these data are similar to those obtained for the interaction between PhaF and the PhaI C-terminal deletion variant, in which the entire ZIPI was removed (50 U/mg CDW) (Figure 16). This suggests that the *d* residues in the ZIPI heptad repeat contribute decisively to the hydrophobic core of the PhaI-PhaF hetero-oligomer.

As a proof-of-concept, the ZIPI motif (21 residues) was cloned into pUT18C plasmid, yielding pUT18C-*ZIPI*, and its interaction with pKT25-*phaF* and pKT25-*phaI* was tested as explained above. We observed that the T18-ZIPI fusion was not folding correctly, since inclusion granules were observed in the cell cytoplasm at the microscopic level, and the protein was recovered mostly in the pellet fraction after centrifugation of the cell homogenate (data not shown). Nonetheless, the β-gal activity of the co-transformants was significantly higher than the negative controls, 340 U/mg CDW) and 590 U/mg CDW, for PhaI-ZIPI and PhaF-ZIPI interaction, respectively. These results suggest that this motif have potential to be used for phasins oligomerization, however the production of the chimeric protein needs to be improved.

2. A comprehensive analysis of phasin PhaF potential interacting partners using "omic" techniques

The results included in this section and the corresponding methodology are being prepared for submission to Environmental Microbiology (Wiley Online Library). Authors: Tarazona NA, Hernández-Arriaga AM, Kniewel R and Prieto MA (2018). Tarazona NA designed and performed the experiments, with support from Hernández-Arriaga AM, and wrote the paper. Kniewel contributed to data analysis and to the final version of the manuscript. Prieto MA designed the experiments, supervised the findings of this work and the writing of the paper.

2.1. Isolation and identification of PhaF putative interacting partners

PhaF is one of the most abundant proteins on the surface of PHA granules, which occupy almost the entire cytoplasm of *P. putida* cells, and have been proven to play important roles in several cellular processes. These observations suggest that interactions occur between this protein and other cellular components during PHA biogenesis. To test this hypothesis, we performed an *in vitro* interaction/pull-down experiment combined with MS, as explained in Figure 9. In brief, recombinant His_6-PhaF was used as a "bait" to capture potential interacting proteins produced during mcl-PHA accumulation (PHOHHx) in *P. putida* KT2440. To this end, the next successive steps were followed: i) the incubation of 100 μg of purified His_6-PhaF with the soluble fraction of *P. putida* KT2440 homogenate (assay concentration: 1 mg of total protein content), ii) binding of His_6-PhaF and interacting proteins to a Ni-Sepharose column, iii) washing away nonspecific proteins, iv) elution of the bound proteins, and v) analysis by SDS-PAGE and MS.

To identify non-specific interacting proteins, *P. putida* KT2440 soluble fraction-alone was passed through a clean Ni-Sepharose column and processed in the same manner as the sample (Figure 18C, Lane 3). Proteins identify in this preparation by MS were deemed to be background and were removed from the final dataset.

To optimize the recovery of PhaF interacting partners, the following particulars were considered for the preparation of the *P. putida* KT2440 soluble fraction (obtained after the centrifugation of the homogenate). First, considering the reported non-specific binding of PhaF to DNA through its C-terminal domain (Galán et al., 2011), the homogenate was treated with DNase (Figure 18A) and the soluble fraction was separated by centrifugation (Figure 18A). This would enhance the specificity of the interacting proteins identified by MS. Second, due to the formation PhaF homo-oligomers, as demonstrated in the previous section, it is likely that recombinant His_6-PhaF interacts with native PhaF located at the surface of the PHA granules. This could neglect the identification of non-PHA related interacting proteins. Additionally, PHA granules would clog the Ni-Sepharose column used for the separation of His_6-PhaF complexes. Therefore, the PHA granule fraction was also subtracted from the homogenate by centrifugation at 18,000 *g*. However, we cannot exclude the presence of some GAPs that may be present in the isolated soluble fraction. The DNA- and PHA-free soluble fraction used in this study is shown in Figure 18A (lane 4).

Based on the results of the previous section demonstrating the interaction of phasins PhaF and PhaI, we performed an anti-PhaI western blot to see if PhaF captured PhaI in the conditions used for the pull-down as a means to validate the assay. Western blot analysis, using an antiserum generated by SDS-PAGE-separated PhaI material as the antigen, showed a single band with a molecular weight of nearly 17 kDa, confirming PhaI

as a PhaF interacting partner and hence the suitability of the experimental design (Figure 18B). Despite PHA-free soluble fractions were used as the source of interacting proteins, the presence of PhaI in the Western blot can be expected for two reasons: i) PhaI is also one of the most abundant proteins produced during PHA accumulating conditions, and ii) the interaction between PhaF and PhaI was proven to be highly specific, which means that PhaF would recruit even small amounts of PhaI detached from the PHA granules during sample preparation.

For MS analyses, the polyacrylamide gel containing the His_6-PhaF co-eluted protein fraction (Figure 18C, Lines 1 and 2) and the fraction containing proteins non-specifically bound to the column alone (Figure 18C, Lane 3) was run approximately 1 cm, cut, subjected to trypsin digestion and analyzed by MS, as explained in Materials and Methods. For these experiments, 3 biological replicates (S1, S2 and S3) were performed.

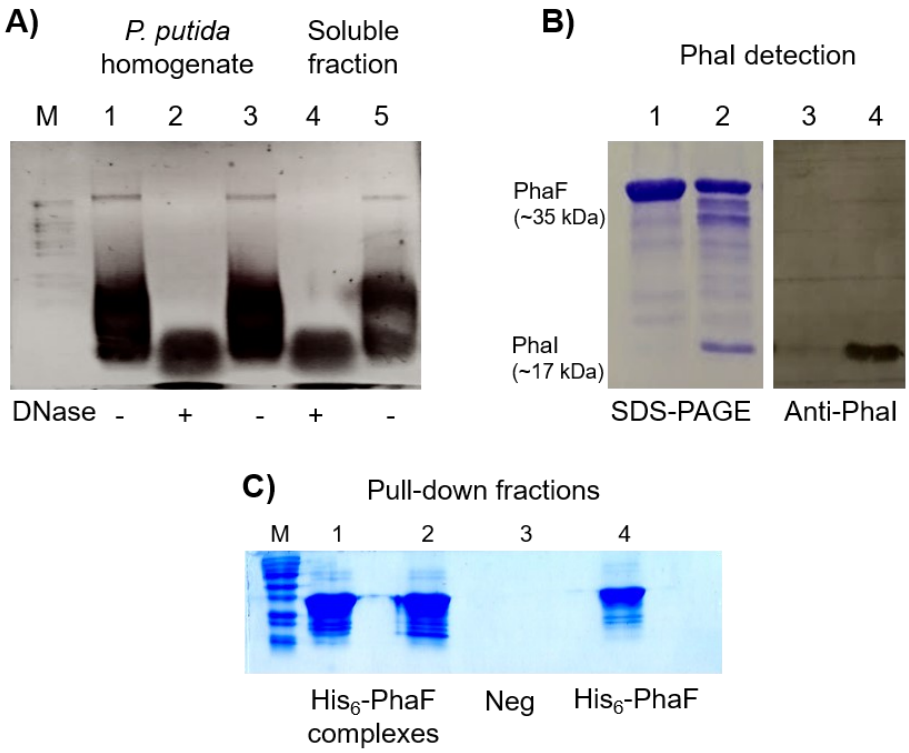

Figure 18. Samples for PhaF pull-down A) 0.7 % Agarose gel electrophoresis of *P. putida* KT2440 soluble fractions. Lanes: M -molecular weight size marker; 1 - homogenate; 2, 3 - homogenate after 20 min incubation with (+) or without (-) DNase; 4, 5 – soluble fraction separated by centrifugation) from the homogenate in lane 2 and 3, respectively. **B)** 12.5 % SDS-PAGE (lanes 1 and 2) and Western blotting (lanes 3 and 4) of pull-down eluted fractions. Western blot was performed with anti-PhaI rabbit polyclonal antibody. Lanes: 1, 3 - His_6-PhaF; and 2, 4 - His_6-PhaF + soluble fraction of *P. putida* KT2440. C) Coomassie Colloidal staining of pull-down eluted fractions for MS analyses. Lanes: M - molecular weight marker; 1, 2 - His_6-PhaF + soluble fraction (S1 and S2 biological replicates); 3 - negative control: for testing non-specific bound of the soluble fraction to the column; and 4 - only His_6-PhaF.

By MS analyses, 7 proteins were identified to bind non-specifically in the column alone (Neg) and were considered as background (data not shown). However, none of these proteins was present in any of the 3 samples analyzed. This could be attributed to the high concentration of His_6-PhaF in the samples binding specifically to the metal ions in the column, displacing possible weak interactions of other proteins with the column.

The outcome of proteomic analyses of the 3 biological replicates, number of proteins captured by His_6-PhaF, is shown as a Venn diagram in Figure 19. Samples S1 and S2 identified almost the same number of proteins, 27 and 26, respectively; where 9 of these proteins are common in both samples. In the case of S3, an increase in the number of proteins identified is observed. From these, 12 and 14 proteins were also identified in S1 and S2, respectively. The increase in the number of proteins identified in S3 could be explained by a higher concentration of the bait in the sample, as can be seen in Table 5. However, around 62 % of the proteins in S3 were identified only with 1 peptide spectrum match (PSM), which represents the total number of identified peptide spectra matched for the protein. Therefore, these proteins are likely false positives dragged by the high presence of the bait in the sample.

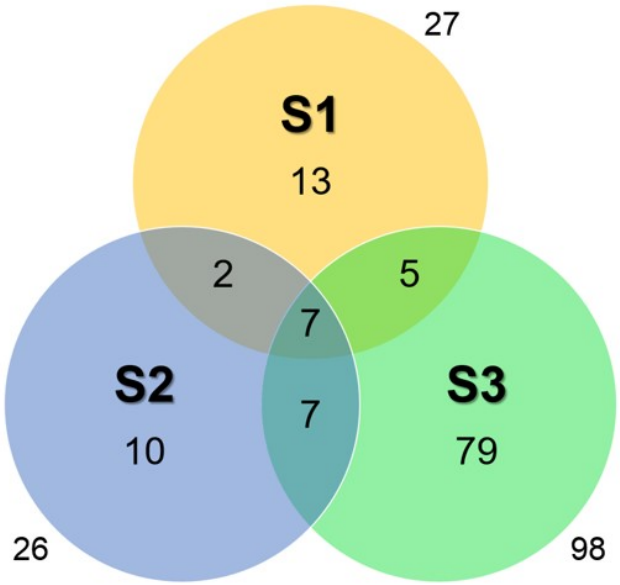

Figure 19. Venn diagram of MS datasets. Number of proteins identified in the pull-down experiment using His_6-PhaF as bait. S1, S2 and S3 represent biological replicates.. The total number of proteins identified in S1, S2 and S3 were 27, 26 and 98, respectively. PhaF is included in the 7 common proteins.

When the detection of more than 1 PSM is considered as the threshold for individual samples, the number of proteins identified in S3 with high confidence is 30. If only proteins identified in all the 3 replicates were considered, the pull-down experiments

suggest 6 potential PhaF interacting proteins (Figure 19, Table 5). The Pearson´s r correlation coefficients for the MS datasets for PSM number in the 3 samples (6 interacting partners plus PhaF) were calculated as 0.999 for S1-S2, S1-S3 and S2-S3.

In decreasing number of PSMs averaged across 3 replicates, the proteins captured by PhaF were: Phasin PhaI (58 PSMs), ATP synthase subunit beta (21 PSMs), TetR-like transcriptional regulator PhaD (18 PSMs), tRNA methyltransferase TrmJ (17 PSMs), putative electron transfer flavoprotein-ubiquinone oxidoreductase (16 PSMs) and outer membrane protein OprF (11 PSMs). The highest PSM value corresponds to PhaF (3082), likely due to the presence of high quantities of bait protein and its self-oligomerization.

Table 5. Proteins associated with PhaF identified by MALDI-TOF MS

		Score[a]			Coverage[b] %			# Peptides[c]			# PSM[d]		
UniProt	**Protein**	**S1**	**S2**	**S3**	**S1**	**S2**	**S3**	**S1**	**S2**	**S3**	**S1**	**S2**	**S3**
Q88D21	Phasin PhaF	2919	2929	4013	90	92	93	39	37	41	913	921	1248
Q88D20	Phasin PhaI	78	73	65	70	68	50	14	11	10	22	20	16
Q88D22	Transcriptional regulator, TetR family, PhaD	26	10	24	42	19	14	5	3	2	9	3	6
Q88PL1	tRNA (cytidine/uridine-2'-O-)-methyltransferase, TrmJ	18	16	31	17	17	22	3	3	3	6	5	6
Q88F95	Electron transfer flavoprotein, putative	12	3	38	5	4	19	2	1	8	4	1	11
Q88BX4	ATP synthase subunit beta	7	8	73	7	7	43	2	2	12	2	2	17
Q88L46	Outer membrane protein, OprF	4	6	36	6	8	29	1	2	5	1	2	8

[a]sum of the ion scores of all peptides that were identified for each protein

[b]percentage of the protein sequence covered by identified peptides

[c]number of distinct peptide sequences identified in the protein

[d]number of Peptide Spectrum Matches, indicating the total number of identified peptide spectra matched for the protein

2.2. Proteomic analysis of PHA carbonosomes

A proteomic analysis of isolated *P. putida* KT2440 PHA granules, consisting of PHOHHx, was carried out to obtain an approximation of the proteins associated to these structures *in vivo*. PHA granules were isolated from PHA-accumulating culture homogenates treated with DNase using different centrifugation separation methods, glycerol and sucrose gradients, (see Material and Methods section). The glycerol (or sucrose) fraction containing native PHA granules was washed and processed for MS analyses (Figure 20). PHA granules-associated proteins were separated by 15 % SDS-PAGE (run approximately 1 cm). The gel section containing the whole protein fraction was cut-off into 2 vertical slices and subjected to tryptic digestion as explained before. In total, 3 samples were processed consisting of 2 granule fractions (biological replicates)

resulted from the glycerol gradient, G1 and G2, and 1 sample derived from the sucrose gradient, SU1. It is worth to mention that SU1 granule fraction was isolated from a *P. putida* KT2440 homogenate that was not treated with DNase (Figure 18A, lane 5).

Previous publications have stated that a high number of proteins found in the PHA granule proteomes of other microorganisms arise from experimental artefacts during their isolation (Sznajder et al., 2015; Narancic et al., 2018). In fact, a doubtful number of proteins are isolated complexed to the granules using either of the methodologies employed in this thesis. In search of a fitter identification of PHA granule-associated proteins, the following workflow was used. First, a threshold of 2 PSMs was set for individual samples. When applied, about 200 proteins were identified in G1 and G2 PHA granule fractions (glycerol gradient), with a Pearson´s r correlation coefficient of 0.81. Meanwhile 373 proteins were found in SU1 fraction, obtained from a sucrose gradient (Figure 20C). When comparing the methodologies applied to isolate the granules (G1 vs. SU1 or G2 vs. SU1), the Pearson´s r correlation coefficient decreased to ~0.4.

From these results, we could conclude that the difference observed in the number of proteins isolated is more likely due to the removal of DNA from G1 and G2 samples. Therefore, DNase treatment should be applied when the isolation of PHA granules is aimed to avoid false positives. For the second step of the workflow analysis, the proteins detected by MS in all the 3 samples were selected as positive identifications, resulting in 97 putative granule-associated proteins (Figure 20).

To increase the stringency of the analysis, in the third step, only the proteins that were identified by at least 2 different peptides were accepted, yielding the 78 proteins listed on Table 6. Some of the most abundant proteins listed in this table have been already reported to be associated with PHA granules in pseudomonads. These include the phasins PhaF and PhaI, the synthases $PhaC1_{Pp}$ and $PhaC2_{Pp}$ and the acyl CoA synthase FadD1 (Q88EB7). FadD1 play a central role in mobilization of PHA, as it converts the 3-hydroxycarboxylic acid monomers, obtained by PhaZ-mediated degradation of PHA, to 3-hydroxyacyl-CoA (3HA-CoA). The latter can be further recycled by the cells (Ruth et al., 2008).

Remarkably, other fatty acid metabolism-related proteins including FabG (Q88QB3), FadE (Q88LN6), FadL (Q88M85) and a putative acyl-CoA dehydrogenase (Q88QW6) were also identified. The association of FabG (3-ketoacyl-acyl ACP reductase) with PHA granules is of special interest. This enzyme was shown to convert 3-ketoacyl-CoA into 3HA-CoA monomers, in *E. coli* recombinant strain, that are incorporated into PHA polymers by recombinant PhaC (Ren et al., 2000). However, the association of this proteins with PHA granules needs to be further validated.

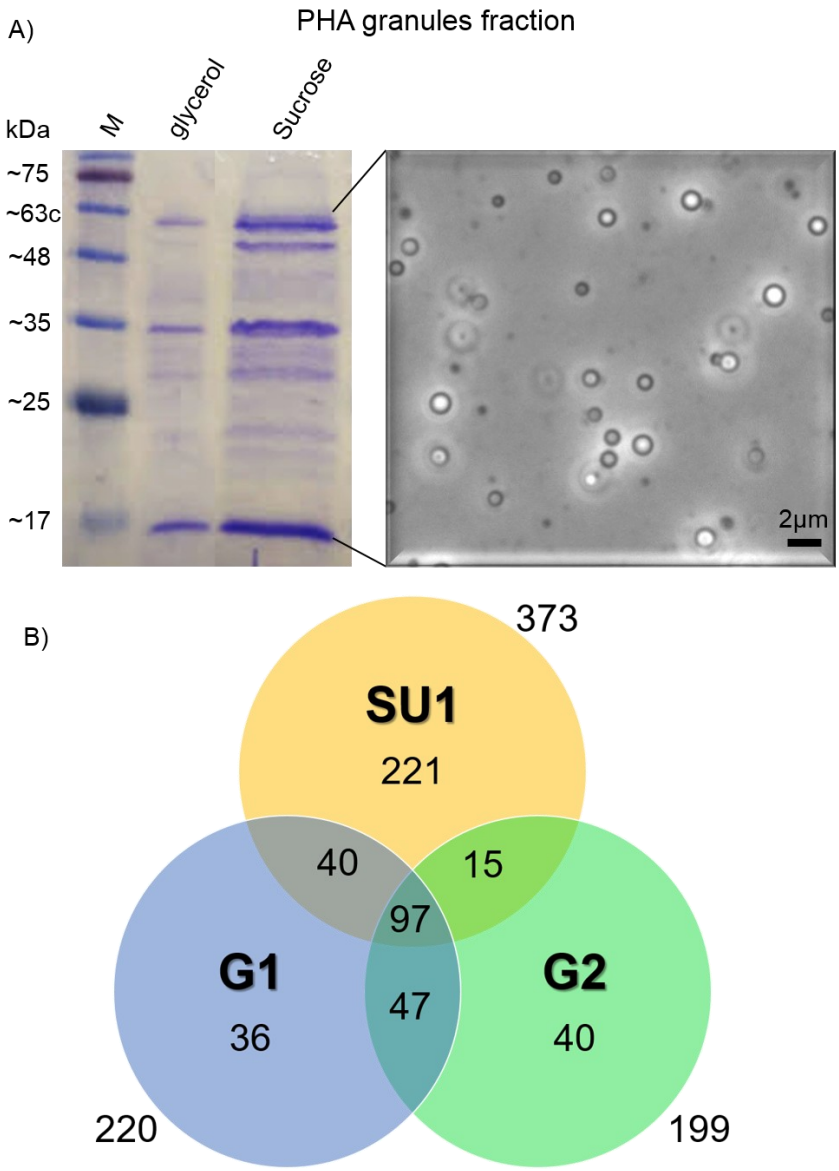

Figure 20. A) 12.5% SDS-PAGE of *P. putida* KT2440 granules using 2 different isolation methodologies and optical microscopy images of the isolated granules. M-Molecular weight size marker (BLUeye Prestained Protein ladder, GeneDireX, Inc.). **B)** Venn diagram of MS datasets for the number of proteins identified in the granule fraction isolated using a glycerol gradient (G1 and G2) or a sucrose gradient (SU1). The total number of proteins identified in SU1, G1 and G2 were 373, 220 and 199, respectively.

The remaining 2 proteins of the *pha* cluster, the depolymerase $PhaZ_{Pp}$ and the transcriptional regulator PhaD, were not found when the restrictions were applied to the proteomic analysis. For instance, only 1 PSM and 1 peptide from PhaD was detected in the glycerol gradient sample G2; and $PhaZ_{Pp}$ was found in only 2 of the 3 samples analyzed (2 PSMs and 1 peptide in G1; plus 4 PSMs and 3 peptides in SU1). However, we cannot ignore

the fact that the production of these proteins during PHA accumulation is quite low (de Eugenio et al., 2007; de Eugenio et al., 2010).

Although the procedure for PHA granule isolation and the bioinformatics analyses were quite stringent, several proteins without obvious involvement in PHA metabolism were found associated with the granules. They mostly included abundant cellular constituents classified as ATPase subunits, ribosome-associated proteins, cell periphery and outer membrane proteins, and protein folding-associated proteins or chaperons. Therefore, they are likely present as the result of contamination from other subcellular compartments as has been reported before for the isolation of PHA and other intracellular structures such as magnetosomes (Grünberg et al., 2004). However, the detection of GroL (Q88N55), Tig (Q88KJ1) and DnaK (Q88DU2) on the surface of the granule is not entirely surprising, since the expression of some chaperone proteins was found to increase under nitrogen-limited growth in *P. putida* (Poblete-Castro et al., 2012). Interestingly, these proteins have also been detected in PHA granules of phasin mutant strains and non-natural PHA-producers where they are proposed to have similar function as phasins, e.g. enhancing protein folding (Han et al., 2006; Pötter et al., 2004). A bioinformatics analysis of known protein interactions carried out with the STRING database (Szklarczyk et al., 2017) showed that ribosome-associated proteins form complexes with the chaperone proteins mentioned above (data not shown).

When comparing the granule proteome to the pull-down results from section 2.1, we found that 4 putative PhaF partners were detected using both isolation approaches (blue highlighted proteins in Table 6). The presence of PhaI was expected, since it is a well-described GAP and its interaction with PhaF was demonstrated in Results section 1.

Table 6. Proteins associated with PHA granules identified by MALDI-TOF MS.

UniProt	Protein/gen annotation	# Peptides			# PSM		
		G1	G2	SU1	G1	G2	SU1
Q88D21	**Phasin PhaF GN=PP_5007**	**7**	**8**	**17**	**14**	**42**	**83**
Q88L46	Outer membrane protein OprF GN=oprF	13	13	10	32	46	23
Q88D25	**PHA polymerase C1 GN=phaA**	**8**	**9**	**22**	**10**	**16**	**58**
Q88D20	**Phasin PhaI GN=PP_5008**	**3**	**3**	**16**	**4**	**8**	**60**
Q88EB7	**Long-chain-fatty-acid-CoA ligase GN=fadD1**	**8**	**9**	**18**	**17**	**20**	**31**
Q88EE6	Agglutination protein GN=tolC	16	15	9	24	33	10
Q88NM2	Outer membrane protein H1 GN=oprH	5	3	7	7	47	9
Q88NK1	Porin D GN=oprD	12	13	7	21	29	9
Q88D23	**PHA polymerase C2 GN=phaC**	**4**	**3**	**19**	**7**	**8**	**39**
Q88F95	Electron transfer flavoprotein-ubiquinone oxidoreductase, putative GN=PP_4203	9	7	17	11	11	29
Q88QN7	Elongation factor Tu-B GN=tufB	6	2	17	6	3	31
Q88PT3	Uncharacterized protein GN=PP_0765	6	9	4	10	20	8
P0A138	Peptidoglycan-associated lipoprotein GN=pal	5	4	3	11	21	4
Q88BX2	ATP synthase subunit alpha GN=atpA	10	4	8	13	13	9
Q88DM2	D-alanyl-D-alanine carboxypeptidase GN=dacA	5	3	8	13	6	14
Q88MX4	Glucose dehydrogenase (Pyrroloquinoline-quinone) GN=gcd	6	5	5	14	14	5

Continuation Table 6. Proteins associated with PHA granules identified by MALDI-TOF MS.

UniProt	Protein/gen annotation	# Peptides			# PSM		
		G1	G2	SU1	G1	G2	SU1
Q88NT3	OmpA family protein GN=PP_1121	3	4	5	5	18	10
Q88LE1	Uncharacterized protein GN=PP_1993	8	6	6	10	10	12
Q88I56	Uncharacterized protein GN=PP_3145	4	4	6	7	15	9
Q88LN6	**Acyl-CoA dehydrogenase FadE GN=PP_1893**	**8**	**5**	**7**	**12**	**11**	**8**
Q88DD5	HflK protein GN=hflK	7	7	4	13	12	4
Q88ES5	Flagellin GN=fliC	8	5	6	11	11	7
Q88QB3	**3-oxoacyl-(Acyl-carrier-protein) reductase FabG GN=PP_0581**	**3**	**3**	**16**	**3**	**3**	**22**
Q88R66	Outer membrane protein OprE3 GN=oprQ	7	6	5	8	14	6
Q88N76	Undecaprenyl-PP-MurNAc-pentapeptide-UDPGlcNAc GlcNAc transferase GN=murG	2	2	13	2	6	19
Q88Q70	NADH dehydrogenase GN=ndh PE=4 SV=1 - [Q88Q70_PSEPK]	2	3	12	2	6	18
Q88BX0	ATP synthase subunit b GN=atpF	5	5	3	6	15	4
Q88FI0	Isocitrate lyase GN=aceA	7	4	2	9	13	3
Q88M85	**Long-chain fatty acid transporter FadL GN=PP_1689**	**7**	**5**	**4**	**11**	**8**	**6**
Q88NS3	Outer membrane lipoprotein, putative GN=PP_1131	4	3	5	6	10	9
Q88RL3	Lipoprotein, putative GN=PP_0116	6	4	3	9	13	3
Q88DN0	LPS-assembly lipoprotein LptE GN=lptE	7	6	5	9	9	6
Q88QL8	30S ribosomal protein S5 GN=rpsE	6	4	4	9	11	4
Q88R09	Sarcosine oxidase, alpha subunit GN=soxA	4	5	9	6	6	12
Q88CP1	Cadmium translocating P-type ATPase GN=cadA-2	5	4	2	10	11	2
P0C071	outer membrane protein MepC OS=*P.* putida GN=mepC	7	4	5	9	7	6
Q88BX4	ATP synthase subunit beta GN=atpD	6	3	12	7	3	12
Q88M60	Peptidyl-prolyl cis-trans isomerase GN=fklB-2	3	2	9	3	2	16
O52470	Cell division protein FtsA OS=*P.* putida GN=ftsA	3	3	8	5	4	11
Q88N90	Lipoprotein, putative GN=PP_1322	5	5	4	7	9	4
Q88PU7	Probable malate:quinone oxidoreductase 1 GN=mqo1	3	2	7	3	3	13
Q88IS4	Probable malate:quinone oxidoreductase 3 GN=mqo3	3	3	8	3	5	10
Q88QN5	50S ribosomal protein L3 GN=rplC	5	4	6	5	4	9
Q88RE2	HemY protein GN=hemY	7	3	3	8	6	4
Q88CK6	Efflux membrane fusion protein, RND family GN=PP_5174	3	5	8	3	6	8
Q88QI8	Outer membrane protein OprG GN=oprG	4	5	2	5	10	2
Q88QL2	30S ribosomal protein S4 GN=rpsD	3	2	7	5	2	10
P0A140	Membrane protein insertase YidC GN=yidC	3	4	6	4	5	7
Q88E27	Carbon starvation protein CstA GN=cstA	3	3	4	3	8	5
Q88PU5	Lipoprotein, putative GN=PP_0753	5	2	6	5	3	8
Q88DU2	Chaperone protein DnaK GN=dnaK	2	2	6	2	2	11
Q88GZ6	Quinate dehydrogenase (Pyrroloquinoline-quinone), putative GN=PP_3569	4	3	3	4	8	3
Q88I66	Glycosyl transferase, putative GN=PP_3135	2	2	10	2	2	11
Q88QN9	30S ribosomal protein S7 GN=rpsG	2	3	8	2	4	9
Q88R99	Porin E GN=oprE	5	3	3	7	3	5
P59374	30S ribosomal protein S11 GN=rpsK	3	4	3	3	8	3
Q59692	Cell division protein FtsZ GN=ftsZ	4	2	4	5	5	4
Q88CH5	Membrane fusion protein GN=PP_5206	5	2	3	5	6	3
Q88MI0	30S ribosomal protein S2 GN=rpsB	2	2	5	2	3	9
Q88N55	60 kDa chaperonin GN=groL	3	2	7	3	3	8

Continuation Table 6. Proteins associated with PHA granules identified by MALDI-TOF MS.

UniProt	Protein/gen annotation	# Peptides			# PSM		
		G1	G2	SU1	G1	G2	SU1
Q88QW6	**Acyl-CoA dehydrogenase, putative GN=PP_0368**	**3**	**3**	**4**	**5**	**4**	**5**
Q88KF1	Aconitate hydratase B GN=acnB	3	3	5	4	4	5
Q88KJ1	Trigger factor GN=tig	3	3	5	3	5	5
Q88M23	Uncharacterized protein GN=PP_1752	3	2	3	7	2	4
Q88PB7	Rod shape-determining protein MreB GN=mreB	4	2	5	4	4	5
Q88QN8	Elongation factor G 1 GN=fusA	3	2	7	3	3	7
Q88EE4	Aerotaxis receptor, putative GN=PP_4521	4	2	3	4	5	3
Q88N96	30S ribosomal protein S9 GN=rpsI	3	2	3	4	5	3
Q88C30	Uncharacterized protein GN=PP_5353	2	2	3	2	6	3
Q88DA4	Outer membrane efflux protein GN=PP_4923	2	4	2	2	6	3
Q88MR7	OmpA family protein GN=PP_1502	3	2	4	4	2	5
Q88FA7	Succinate dehydrogenase flavoprotein subunit GN=sdhA	6	2	2	6	2	2
Q88NH1	Lipoprotein, putative GN=PP_1238	2	2	3	2	5	3
O52248	Toluene efflux pump membrane transporter TtgB GN=ttgB	2	2	3	2	2	5
Q88E96	Uncharacterized protein GN=PP_4570	2	2	5	2	2	5
Q88QD0	Uncharacterized protein GN=PP_0564	3	2	4	3	2	4
Q88CK5	HlyD family secretion protein GN=PP_5175	2	2	3	2	2	4
Q88KP1	Methyl-accepting chemotaxis transducer	2	2	2	3	2	3

2.3. Subcellular localization of PhaF interacting partners, PhaD and PhaI

We were intrigued by the observation that PhaD was identified as interacting with PhaF in the pull-down experiment but not identified in the PHA granule proteome. To confirm these observations and better investigate the *in vivo* localization of PhaD, the pSEVA238-GFP vector was used to construct PhaD-GFP and PhaI-GFP C-terminal fusions (Table 3). For *in vivo* localization studies, *P. putida* KT2440 cells carrying the plasmids pSEVA238-DG (PhaD-GFP fusion) and pSEVA238-IG (PhaI-GFP fusion) were cultured in LB medium overnight and were transferred to a final OD_{600} 0.3 into M63 0.1 N medium containing 15 mM octanoic acid for PHA production. The fluorescence of the GFP fusions was analyzed after 2 h induction with 0.5 mM 3-methylbenzoate. A co-localization of PhaD-GFP with PHA granules was not observed. In contrast, the PhaI-GFP control showed distinct granular spots consistent with co-localization with PHA granules (Figure 21). This result supports the PHA granule proteome data, indicating that the PhaD transcriptional regulator is not located at the surface of the granules produced by *P. putida* KT2440.

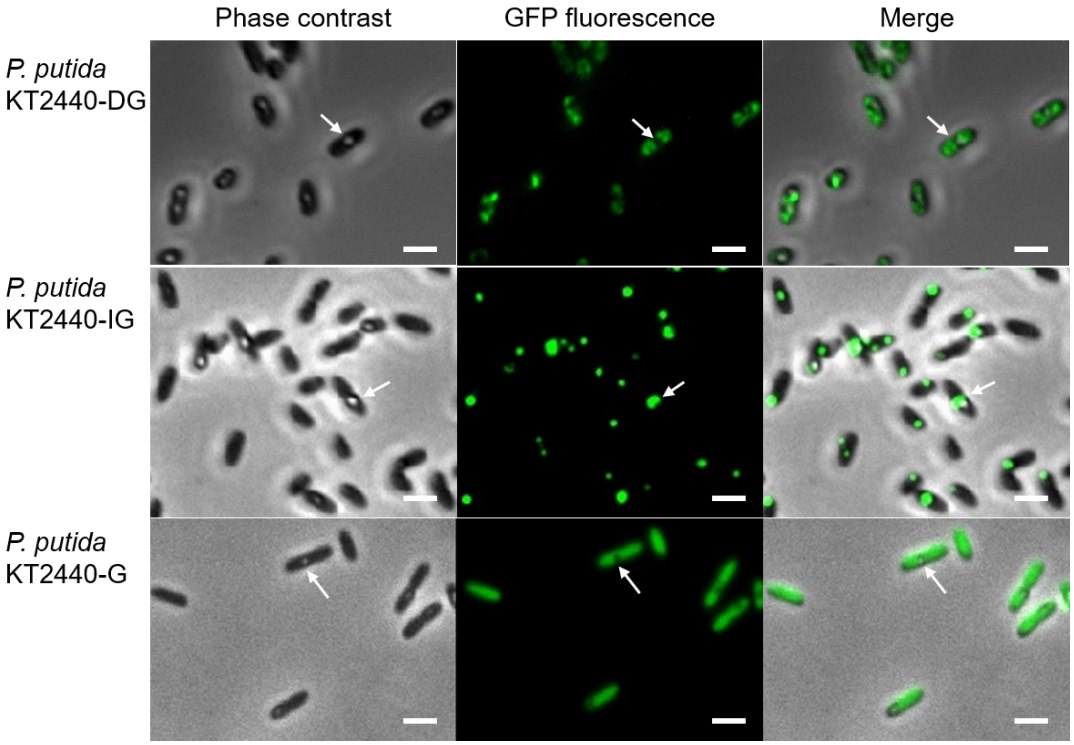

Figure 21. Fluorescent microscopy images of *P. putida* KT2440 expressing GFP fusion proteins. *P. putida* KT2440 cells carrying the plasmids pSEVA238-DG (PhaD-GFP fusion), pSEVA238-IG (PhaI-GFP fusion), and pSEVA238-G (GFP negative control). Fluorescence was recorded using GFP filter (488 nm). White bars represent 2 μm. White arrows show PHA granules.

2.4. Detection of PhaF and PhaD interaction by bacterial two-hybrid analysis

From the pull-down results, we concluded that PhaF not only interacts with PhaI, as previously demonstrated, but potentially also interacts with PhaD. To confirm the *in vivo* physical interaction between PhaF and PhaD, we used the BACTH system explained in the previous section. Plasmids were constructed as explained in Materials and Methods, section 5.2 and are listed in Table 3. For example, the plasmid pUT18C-*phaF* produces PhaF fused at its N-terminal with the T18 Cya fragment (T18-PhaF fusion). *E. coli* co-expressing the plasmids carrying T18-PhaD and T25-PhaF fusions showed levels of β-gal activity more than 20 times the negative control plasmids (1460 U/mg CDW vs. 52 U/mg CDW, Figure 22). This value is similar to the β-gal results to detect homo-oligomerization of T18-PhaF and T25-PhaF (1218 U/mg CDW) or the interaction of T18-PhaI and T25-PhaF (1600 U/mg CDW), indicating that an interaction between PhaF and PhaD occurs *in vivo* and it is unlikely to be mediated by other *P. putida* proteins.

The interaction of PhaF with the synthase $PhaC1_{Pp}$ was also tested to determine if the absence of $PhaC1_{Pp}$ from the pull-down assay MS results (Table 5) was due to the lack of the protein in the soluble fraction or to a non-existing interaction between PhaF and $PhaC1_{Pp}$. No β-gal activity was detected from the interaction between T18-PhaC1 and T25-PhaF (44 U/mg CDW), providing additional experimental evidence of the lack of interaction between these 2 GAPs. The specificity of the results was confirmed by the fact that PhaF produced from plasmid pKT25-*phaF* did not lead to significant β-gal activity when tested with the complementary empty plasmid pKT25 (52 U/mg CDW). As was demonstrated for other PHA synthases, we also confirmed that $PhaC1_{Pp}$ forms dimers when tested by the BACTH assay (1727 U/mg CDW), verifying the correct expression and folding of $PhaC1_{Pp}$.

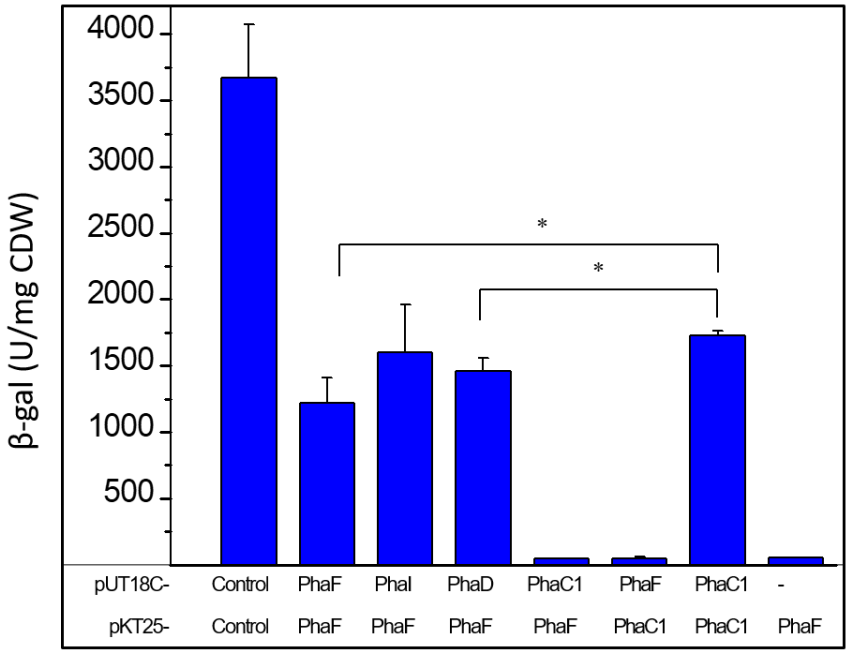

Figure 22. PhaF and PhaD interact by BACTH assay. β-gal activities (Miller Units per mg of cell dry weight, U/mg CDW) of *E. coli* BTH101 cells co-transformed with different combinations of the complementary plasmids pUT18C and pUT25, producing PhaF, PhaI, PhaD or PhaC1. The reported values correspond to the average obtained from 3 transformant clones tested for each interaction. Control corresponds to the plasmids containing a DNA sequence coding for a leucine zipper motif (GCN4) as a positive interaction control. The symbol "-" corresponds to the negative control pUT18C empty vector. Statistically significant differences between the samples (p value < 0.05) are marked with "*".

2.5. Determination of the ability of the PhaF-PhaD complex to interact with DNA

It is well recognized that PhaD protein acts as a transcriptional regulator of the *phaIF* operon as it binds to the upstream promoter region of *phaI* (P_I) activating the transcription of *phaI* and *phaF* genes (de Eugenio et al., 2010) (Figure 4B). Based on this information we performed mobility shift assays using a 230 bp DNA fragment containing the promoter region of *phaI* carrying the putative PhaD-binding motif and purified proteins PhaD-His_6, His_6-PhaF independently or a previously formed PhaD-PhaF complex (Figure 23). Binding of the proteins to the DNA was performed as described in Materials and Methods.

Free DNA was separated from complexed DNA by electrophoresis on native polyacrylamide gels. A single retarded DNA band was detected when the DNA was incubated in the presence of increasing concentrations of PhaD (complex C1 in Figure 23A), corresponding to a specific PhaD-DNA complex. DNA was partially complexed when 0.6 μM of the protein was used and was fully complexed by using 8 μM of PhaD protein. The binding of PhaF to the DNA also showed a super-shifted band, when using 0.4 μM of the protein. DNA was completely complexed at 8 μM of protein concentration. Although lower concentrations of PhaF were needed to completely complexed the DNA sugesting a stronger binding affinity of PhaF, it was shown that the PhaF also associates to a 170 bp DNA fragment of the coding region of the *glpK* gene, used as a negative control for binding specificity (Figure 23B). This non-specific binding of PhaF to DNA was demonstrated previously (Galán et al., 2011). Under the same binding conditions, PhaD failed to associate with the *glpK* DNA, indicating specificity of PhaD for the DNA containg P_I promoter region (Figure 23B).

Simultaneous addition of PhaD and PhaF (preincubated together for 15 min) to the specific DNA lead a retarded DNA band (complex C2) that migrates at different position on the gel that the ones observed when complexed with the proteins individually (Figure 23A). These results indicate that both PhaD and PhaF are able to bind to this DNA simultaneously. The results suggest that the specific recognition of the P_I promoter region by PhaF could be mediated by PhaD, However, the molecular bases of this interaction and the exact role of this interaction in the function of the PHA regulator, needs to be further investigated.

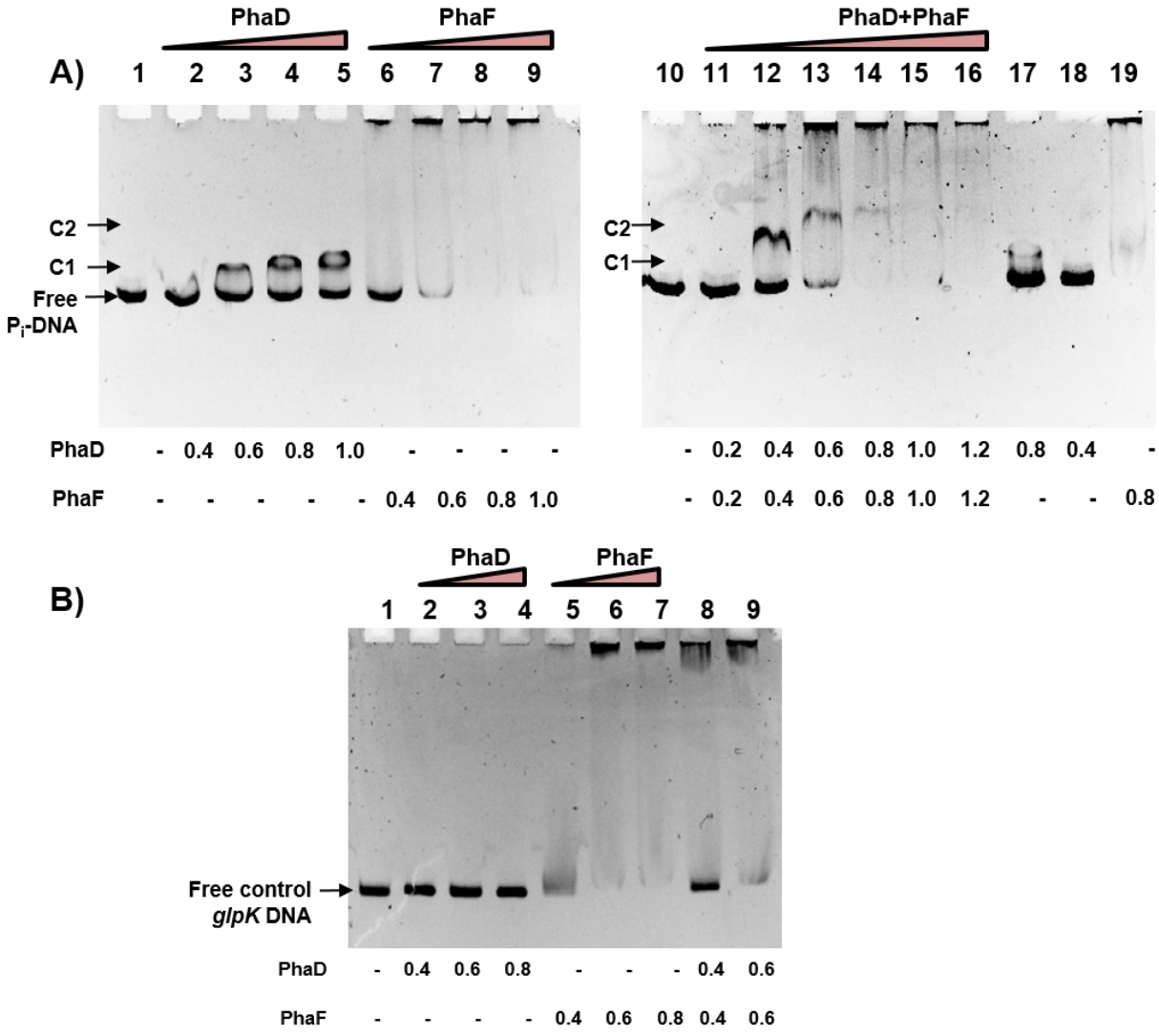

Figure 23. Electrophoretic Mobility Shift Assay (EMSA) of *phaI* promoter DNA probe (P_I) in the presence of PhaD and PhaF. A) P_I -DNA was incubated with varying concentrations (μM) of PhaD-His$_6$ (lanes 2-5 and 17-18); His$_6$-PhaF (lines 6-9 and 19); or equimolar concentrations of His$_6$-PhaF and PhaD-His$_6$ (lanes 11-16). **B)** DNA probe of *glpK* as a non-specific control, incubated with PhaD-His$_6$ (lines 2-4); His$_6$-PhaF (lanes 5-7); or PhaD and PhaF together (lanes 8-9).

3. Molecular insights into the interaction of PhaF with natural and synthetic polyester interfaces, towards the upgrading of PhaF as coating material

Most of the results included in this section and the corresponding methodology have been submitted to Biomacromolecules (ACS Publications) with the following title: Molecular insights into the physical adsorption of amphiphilic protein PhaF onto copolyester surfaces. Authors: Tarazona NA, Machatschek R, Schulz B, Prieto MA, and Lendlein A. Tarazona NA designed and performed the experiments and wrote the paper with support from Machatschek R. Schulz B designed the experiments, contributed to data analysis and to the final version of the manuscript. Prieto MA and Lendlein A designed the experiments, and supervised the findings of this work and the writing of the paper. The section 3.1 was published as part of a collaboration paper. in Langmuir (ACS Publications). Citation: Mato A, Tarazona NA, Hidalgo A, Cruz A, Jiménez M, Pérez-Gil J, and Prieto MA(2019). "Interfacial activity of Phasin PhaF from *Pseudomonas putida* KT2440 at hydrophobic–hydrophilic biointerfaces." Langmuir 35(3): 678-686.

3.1. *In vitro* binding of PhaF to casted films of its natural substrate PHA

To get a first insight into PhaF binding abilities towards PHA *in vitro,* we prepared supported films of PHA produced by *P. putida* KT2440 by solvent casting using chloroform. Cast PHOHHx films (0.1 mg) were homogeneous and showed a thickness of approximately 0.8 μm (Figure 24).

The film stability was tested by adding 100μL of Tris-HCl buffer into the self-made chamber. As the water penetrated the film, the polymer was partially removed from the glass surface and hydrophobic domains were formed as seen by the patchy fluorescence pattern in Figure 24A. When the film was incubated with buffer containing 1μM of Alexa 647-labeled His_6-PhaF, similar domains were observed and images showed that PhaF perfectly surrounded the borders of the patchy polymer while Nile Red was bound uniformly to the total surface area of the PHA (Figure 24B). This pattern suggests PhaF high affinity for the polymer. His_6-PhaF non-specific binding to silica (coverslip) was detected, probably due to electrostatic interactions (Figure 24B, image on the right); however, fundamental differences in the binding time and the formation of patches was observed.

3.2. Study of the surface behavior of pure PhaF Langmuir monolayers at the air-water interface as a first approach to characterize PhaF conformation and stability

3.2.1. Surface behavior of pure PhaF monolayers

One of the most remarkable features of PhaF is its surface activity, induced by the segregation of polar residues from the hydrophobic ones on both sides of its N-terminal α-helix (Maestro et al., 2013). The maximum surface pressure (π_{max}) of increasing amounts of His_6-PhaF in different chemical environments, its saturating concentration at the A-W interface and the effect of spreading (Langmuir monolayer) or injecting (adsorption Gibbs monolayer) the protein at the aqueous solution is presented in Figure 25.

When PhaF was spread in increments at the A-W interface, it showed greater surface activity on PBS than on water, reaching a maximum π of ~22 mN/m. This could be explained by the high ionic strength of PBS (salting out effect) (Yano et al., 2011; Zhang, 2012) or by its pH being closer to the isoelectric point of PhaF at pH = 10 , which favors proteins surface activity (Dee et al., 2003).

Upon spreading low concentrations of protein on the surface (Langmuir), a rather high increase of the surface pressure was observed, confirming PhaF as a highly surface active protein. A pseudo-plateau was observed at π = 16-17 mN/m, probably due to a reorientation of the molecules at the interface (see structural characterization below).

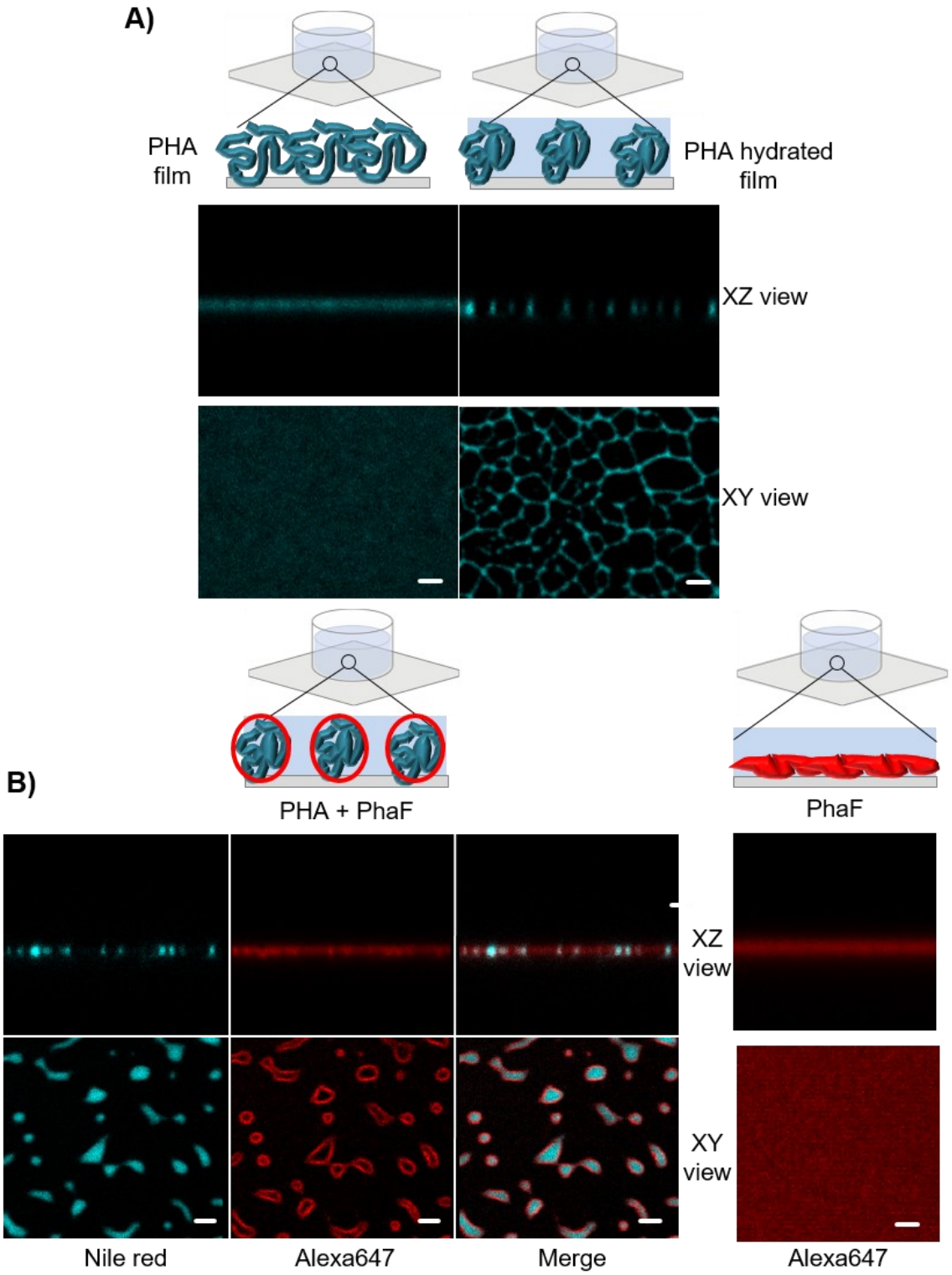

Figure 24. Binding of PhaF to PHOHHx supported layers. **A)** Vertical (XZ) and horizontal (XY) confocal images showing PHOHHx supported layers stained with Nile Red, without (left image) or with (right image) addition of 50 mM Tris-HCl pH 7.5 and 300 mM NaCl. **B)** Vertical (XZ) and horizontal (XY) confocal images showing the distribution of Alexa 647-labeled His_6-PhaF (Red) on PHA films (Blue) after 5 min or in the bare glass substrate (right) after 15 min. Scale bar = 2 μm.

Since direct spreading of the protein at the A-W interface can be considered as a rather harsh method that might cause conformational changes, Gibbs layer formation upon injecting of the protein into the subphase was evaluated as an alternative method to produce PhaF monolayers. Therefore, increasing amounts of His_6-PhaF were injected into PBS and were allowed to reach a stable surface pressure. The minimum concentration required to observe an increase of the surface pressure for Gibbs layers was higher by a factor of 10 when comparing to spreading of the protein solution at the A-W interface (0.10 vs. 0.01 µM), suggesting that the adsorption of the protein at the interface during spreading was irreversible. Interestingly, Gibbs layers did not show a plateau at ~16 mN/m.

Regardless of the formation mechanism, an equilibrium was established at ~22 mN/m and a protein concentration 0.16-0.18 µM was sufficient to reach a saturation of the surface. This equilibrium is comparable to our previous observation under dynamic conditions (stirring the subphase) (Mato et al., 2018).

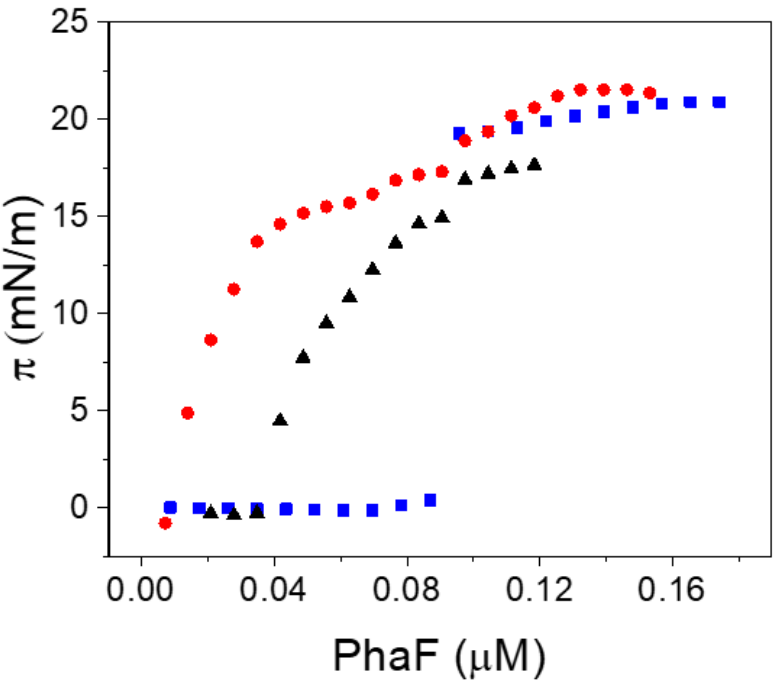

Figure 25. Surface-activity of PhaF as a function of protein concentration. Each point in the curves corresponds to the maximal value of the surface pressure (π) reached after protein addition. PhaF spread on *MilliQ* water, pH 5.5 (triangles) or PBS, pH 7.4 (circles). Protein injected into PBS subphase (squares). All presented isotherm data correspond to individual experiment data reproducible with a random measurement error of ~5 % concerning the surface pressure for the independently repeated experiments.

3.2.2. Phase behavior and morphology of PhaF monolayers

A comparative study of spread and adsorbed monolayers of PhaF at the A-W interface was performed with π-A isotherms and π-t adsorption kinetics. These measurements were combined with *in situ* BAM and PM-IRRAS to study morphological and structural features of the monolayers (Figure 26). During the compression of the PhaF Langmuir monolayer (π-A isotherm) a steady increase of the surface pressure starting from 1 mN/m with C_s^{-1} of 60 mN/m was observed (Figure 26A). Distinct transition points, which appeared as 2 minimum values in the Cs^{-1} isotherm, were detected between ~16 mN/m and 22 mN/m. This gradual slope or "accordion" configuration may be an effect of repulsive forces along compression, conformational changes or mechanical distortion as it has been reported for other proteins (Toimil et al., 2012; Liu et al., 2017).

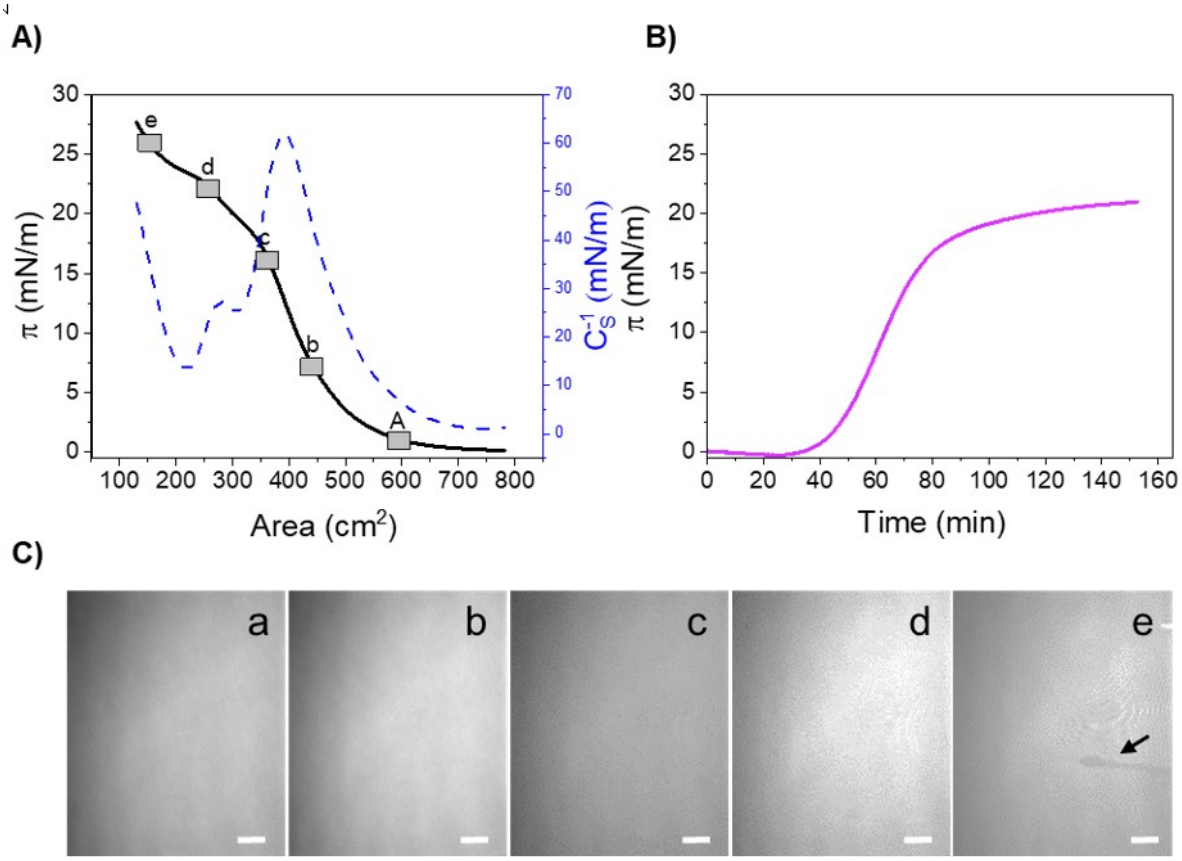

Figure 26. PhaF monolayers at the air-water (PBS) interface. A) Surface pressure-area isotherm (π-A, solid line) and compressibility modulus (Cs^{-1}, dotted line) of His_6-PhaF (0.013 µM) spread on PBS. **B)** Surface adsorption isotherm of PhaF (0.18 µM) in a surface-area/volume ratio of 0.8 cm^{-1}. All presented isotherm data correspond to individual experiment data reproducible with a random measurement error of ~5 % concerning the surface pressure for the independently repeated experiments. **C)** BAM images of PhaF monolayer at different surface pressures (A-E in π-A curve). Scale bar = 50 µM.

Based in our observations from the IRRAS spectrum (see below), the first minimum is attributed to a PhaF reorientation at the A-W interface. We noted that the maximum surface pressure that can be obtained via adsorption from the subphase is about 22 mN/m (Figure 25 and 26B), which is identified with a densely covered interface. Therefore, the second transition around this surface pressure indicates collapse or multilayer formation. BAM images of the Langmuir monolayer are shown in Figure 26C. Despite the pseudo-plateau in the isotherm, only a homogeneous phase with no sudden change in intensity was present during compression up to 22 mN/m, at the resolution scale of the microscope (1 μm).

The morphology of films at higher π was almost identical, except for the formation of some structures "folds" with different brightness (arrow in image E). The adsorption of PhaF at the A-W interface (π-t isotherm) was studied following the increase in surface pressure after injection of a single protein portion (0.18 μM) without any external mechanical force (Figure 26B). Adsorption of PhaF comprised a considerable lag time, followed by a sudden increase in π after 30 min (gas phase to liquid phase transition) and a gradual saturation of the interface at a maximal surface pressure of 21 ± 1 mN/m. No changes in morphology were observed in BAM, forming homogeneous layers similar to A-D in Figure 26C. It is worth to mention that the adsorption isotherm of PhaF was identical at 21 ºC and 37 ºC (Figure 27). Our results indicate that despite the methodology use for PhaF monolayer formation, 22 mN/m is the maximum surface pressure to which PhaF may be compressed before it becomes unstable.

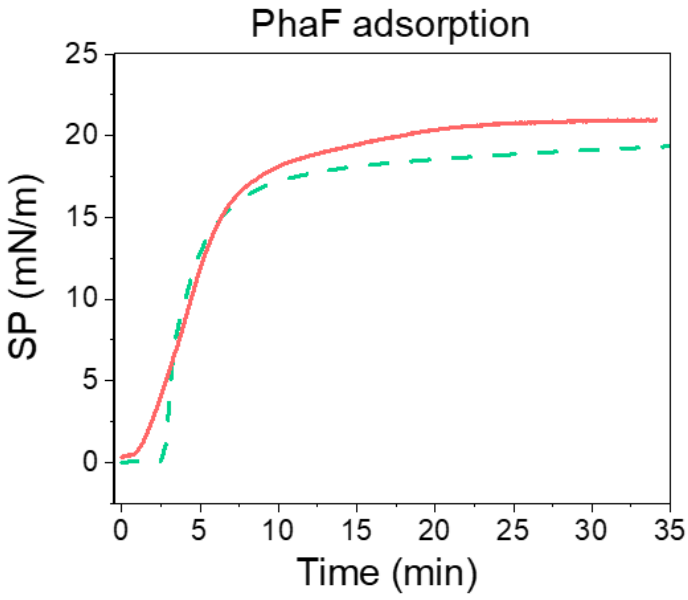

Figure 27. Surface adsorption isotherm of PhaF at 21 ºC (dash line) and 37 ºC (solid line). Surface area/volume ratio = 1.4 cm^{-1}.

3.2.3. Conformation and orientation of PhaF at different environments

Since the adsorption of protein monolayers at the A-W interface could also lead to conformational changes, the infrared spectrum of His_6-PhaF was measured in solution in order to get the conformation of the protein in its native environment (Figure 28A). The spectrum in Figure 28A shows that the amide I and the amide II bands of the protein are centered at 1650 cm^{-1} and 1546 cm^{-1} (with shoulder at 1520 cm^{-1}), respectively. The amide I band at 1650 cm^{-1} in PBS buffer is typical for alpha-helical structure, but can also contain contributions from random coil sections that have a similar amide I band position as alpha helices (1644 cm^{-1}) (Castano et al., 2002). This result agrees very well with the expected high α-helical content of PhaF (Maestro et al., 2013). The peak intensity ratio is unexpected, since the ratio of amide I to amide II for α-helical proteins in solution is about 2 (Venyaminov and Kalnin, 1990). Here, the amide II peak may overlap with vibrations from carboxylic acid side groups in the range from 1550 to 1580 cm^{-1}(Barth, 2000). Furthermore, the spectrum was recorded on an ATR crystal which leads to an overestimation of amide II intensity relative to amide I (Wilcox et al., 2016).

In situ PM-IRRAS spectra of His_6-PhaF monolayers show similar trends for layers prepared via adsorption from solution (Figure 28B,C) and via compression (Figure 28D). At lower surface pressures (Figure 28B), the main component of amide I is at 1650 cm^{-1}, in agreement with the alpha helical conformation found in solution, which also agrees with the amide II bands at 1515 to 1550 cm^{-1} (Goormaghtigh et al., 1994). At higher surface pressures (Figure 28C), a shoulder of increasing intensity at about 1670 cm^{-1} (a) is observed for the amide I band. This shoulder could be attributed to an increasing degree of dehydration of the α-helices, which is supported by a vibration of the carboxylic acid side-groups at 1715 cm^{-1}(b). Since deprotonation is expected in PBS, the side-groups have to be at least partly exposed to air. A shoulder at 1630 cm^{-1} (c) in the amide I band of spread monolayers (Figure 28D) indicates the presence of a small content of beta sheets, supporting that injecting is a more gentle method of producing monolayers than spreading.

The ratio of amide I to amide II intensity can be used to determine the orientation of the helices at the air-water interface (Castano et al., 1999). Up to a surface pressure of 12 mN/m, the ratio is about 1, indicating a tilt angle of about 45° with the surface normal, i.e. a random organization. Between 12mN/m and 23 mN/m, the ratio is much bigger than 1, suggesting that the helix axis are more or less parallel to the air-water interface.

Finally, at 30 mN/m, the ratio approaches unity again, suggesting a random orientation. Since BAM suggests the layer collapses around 25 mN/m, this result was expected.

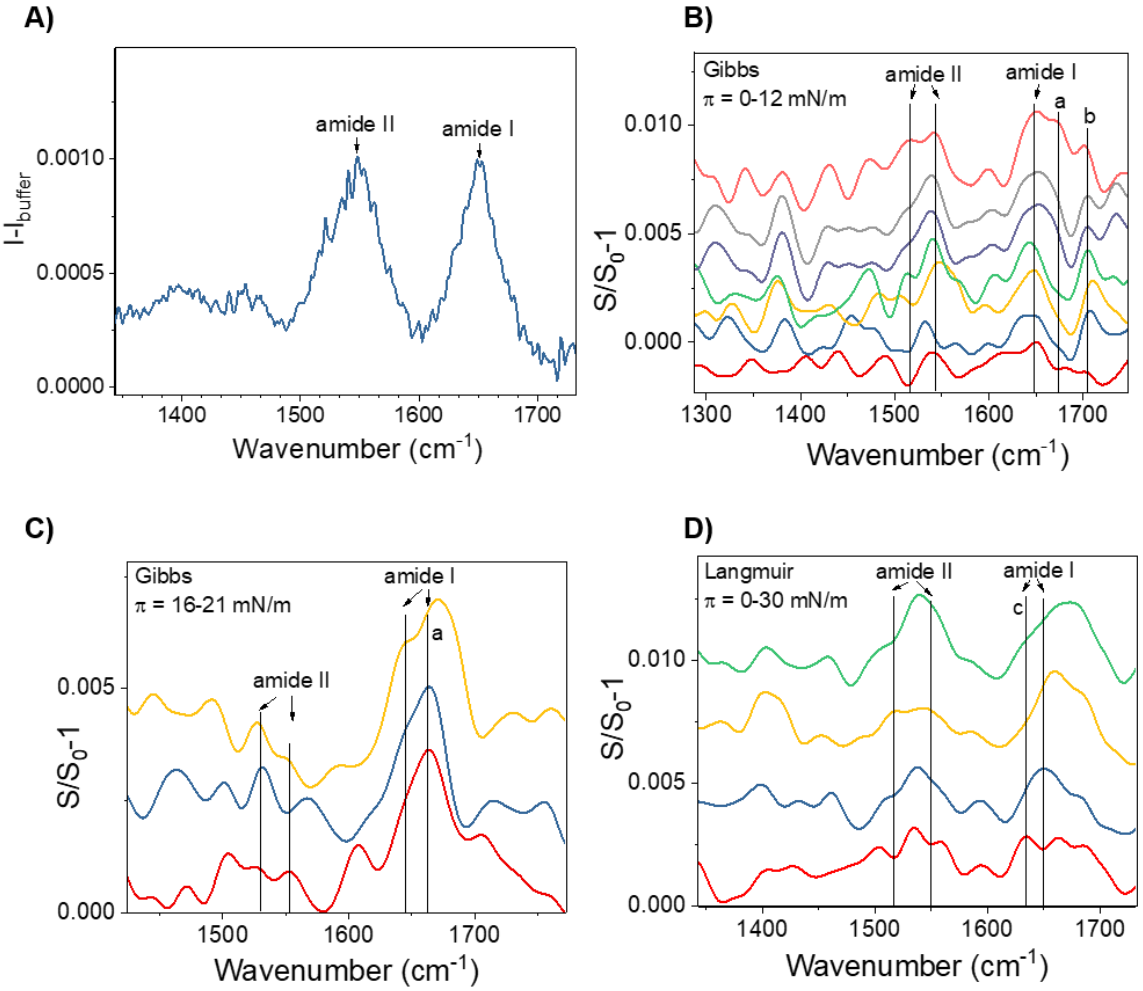

Figure 28. A) IR spectrum of His$_6$-PhaF in PBS buffer. B) PM-IRRAS spectra of PhaF at the A-W interface (Gibbs monolayers). From bottom to top: background spectrum, π = 0, π = 1, π = 2, π = 5, π = 8, and π = 12 mN/m. Vertical lines a, b = carboxylic acid side-groups vibration. **C)** PM-IRRAS spectra of PhaF Gibbs monolayers at higher π. From bottom to top: π = 16, π = 18, and π = 21 mN/m. Vertical line a = carboxylic acid side-groups vibration. **D)** PM-IRRAS spectra of PhaF at the A-W interface (Langmuir monolayers). From top to bottom: π = 0, π = 12.5, π = 23, and π = 30 mN/m. Vertical line c = peak at 1630 cm^{-1} assigned to β-sheets. Spectra of the replicate measurements agreed qualitatively.

3.3. Adsorption of PhaF onto PHA Langmuir monolayers as mimicking of the protein native environment

Although phasins production and location are strictly associated with the PHA granules in bacteria, these proteins have been proven to bind to different hydrophobic substrates *in vivo* and *in vitro* (Hänisch et al., 2006; Dong et al., 2010). The use of the Langmuir technique as a model system to study PhaF-polymer interaction was

benchmarked by injecting His_6-PhaF in the subphase (PBS buffer) of preformed PHOHHx monolayers as described in Materials and Methods. This system was further extended to PLGA monolayers as a less hydrophobic substrate.

To identify the ideal packing density of PHOHHx for these experiments, the π-A isotherm for PHOHHx on PBS at 20 ± 1 °C was first analyzed (Figure 29A). The sudden steep increase of the surface pressure is typical for polymers for which the A-W interface is a bad or theta solvent (Maestro et al., 2011). Collapse of the monolayer is observed at π = 15.7 mN/m and 21 ± 1 $Å^2$ by a plateau with almost no upturn in the surface pressure even up to a MMA of 5 $Å^2$. Although the phases of PHA monolayer systems are not well characterized, the horizontal plateau observed at small molecular areas is similar to that referenced for poly(3-*R*-hydroxyundecenoate) (Jagoda et al., 2011),

BAM images of PHOHHx films in Figure 29C show that the surface is uniform for high MMA (a); however, at very low surface pressure (π = 0 mN/m), PHOHHx films exhibit dark regions of water covered by gaseous phase together with gray zones (b). These domains vanish during the monolayer compression and very small bright globular domains of roughly uniform size appear forming a mixed phase (c). An increase in number of the globular structures is observed when the film collapses at π = 15.7 mN/m (d). These observations lead to the conclusion that at the collapse pressure of 15.7 mN/m, further reduction of the MMA results in chains being squeezed out of the interface. This happens locally, leading to the micron sized globular structures observed in BAM. The small lateral size of these reversibly formed globular domains allows for their fast dissolution upon expansion of the layer, indicated by the low surface pressure-area hysteresis during compression-expansion cycles (Figure 30A). Optical microscopy (Figure 30B) and AFM (Figure 30C) of PHOHHx films transferred to silicon wafers confirmed the model of having isolated 3-dimensional globuli embedded in a monolayer.

The absorption of PhaF to a highly packed film of PHOHHx (π = 12 mN/m) was monitored by means of increase in the system surface pressure at constant areas (Δπ(t)) (Figure 29B). It has been previously demonstrated for lipid-protein systems, that molecules penetrating lipid monolayers increase their surface pressure; while the surface pressure should essentially stay almost unchanged when proteins stay below the surface (e.g. interacting with lipid headgroups) (Kanintronkul et al., 2005; Blume and Kerth, 2013). Upon injection of the protein beneath the PHOHHx film, the π of the interface increased from π = 12 mN/m to ~ 16 mN/m, owing the area occupied by PhaF molecules. After this point, the isotherm exhibited a semi-plateau or “bend” that was absent when the protein adsorbed to the A-W interface. This bend is consistent with the maximum surface pressure reached by pure PHOHHx monolayers after compression (Figure 29A) and may be linked to the PHOHHx monolayer collapse (Dynarowicz-Łątka and Kita, 1999, Garg et al., 2017). Further insertion of PhaF increased the surface pressure slowly, until a

maximum π = ~22 mN/m was reached. In order to verify the influence of PhaF on the morphology of the PHOHHx monolayer, BAM images were recorded at different stages of protein adsorption (Figure 29C). At surface pressures below the polymer collapse, the BAM images of PhaF adsorbing to PHOHHx are nearly similar to the ones of the pure polymer (i, ii), However, a phase-separation was observed above the bend, consisting of patches (bright thick stripes) of one component distributed between another (iii, iv, v).

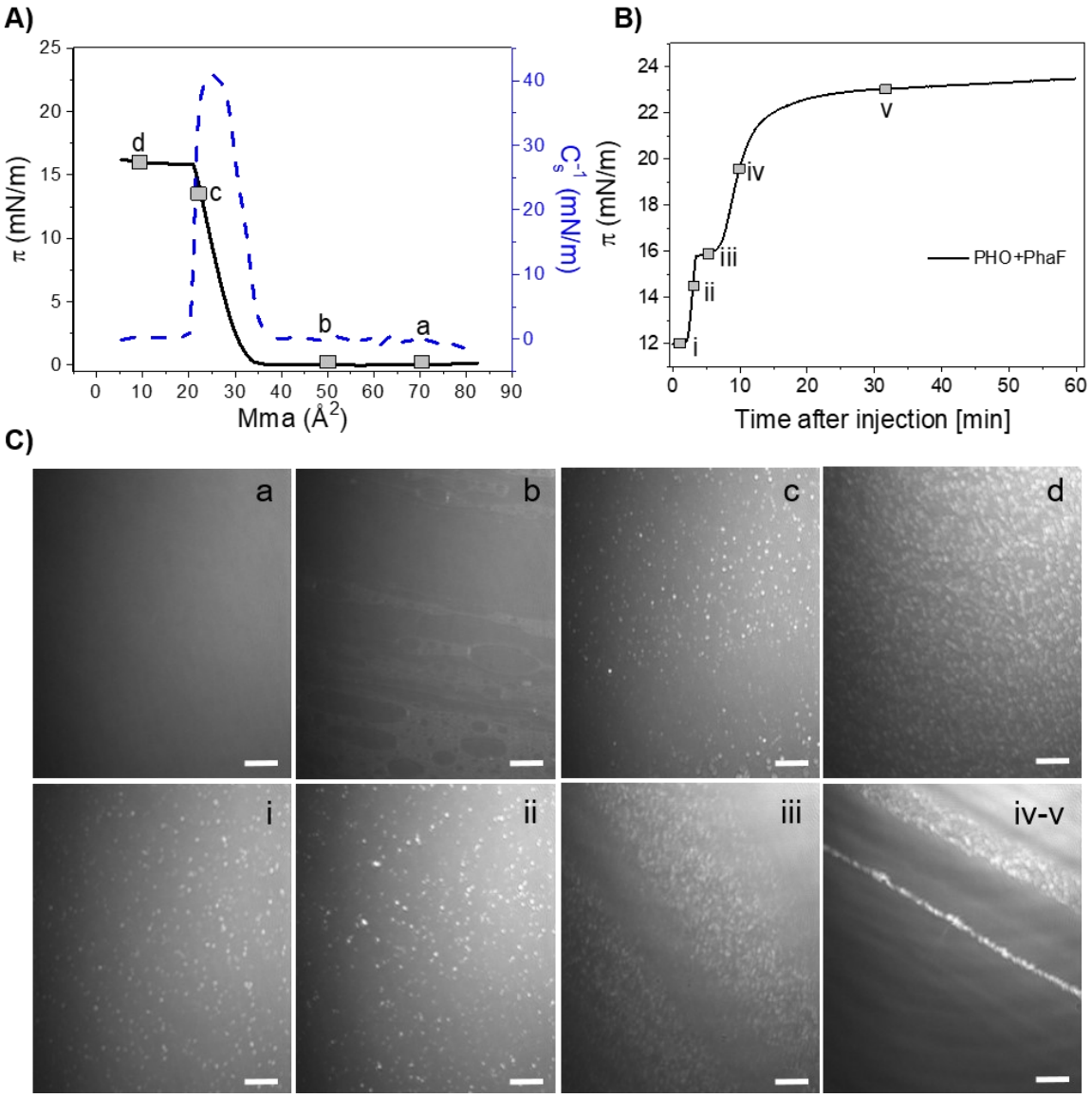

Figure 29. A) Isotherm of surface pressure (π) versus mean molecular area per monomer unit of PHOHHx (MMA). **B)** Adsorption of His_6-PhaF into preformed PHOHHx monolayer at 12 mN/m. **C)** BAM images of PHOHHx at the A-W interface (a-d) or after PhaF injection under the polymer monolayer (i-v). Scale bar = 50 µM. Each experiment was performed twice. All presented isotherm data correspond to individual experiment data reproducible with a random measurement error of ~5 % concerning the surface pressure or the MMA values for the independently repeated experiments.

We conclude that the PhaF molecules reduce the available surface area for the PHOHHx chains, and the polymer is squeezed out of the layer when its collapse surface pressure is reached.

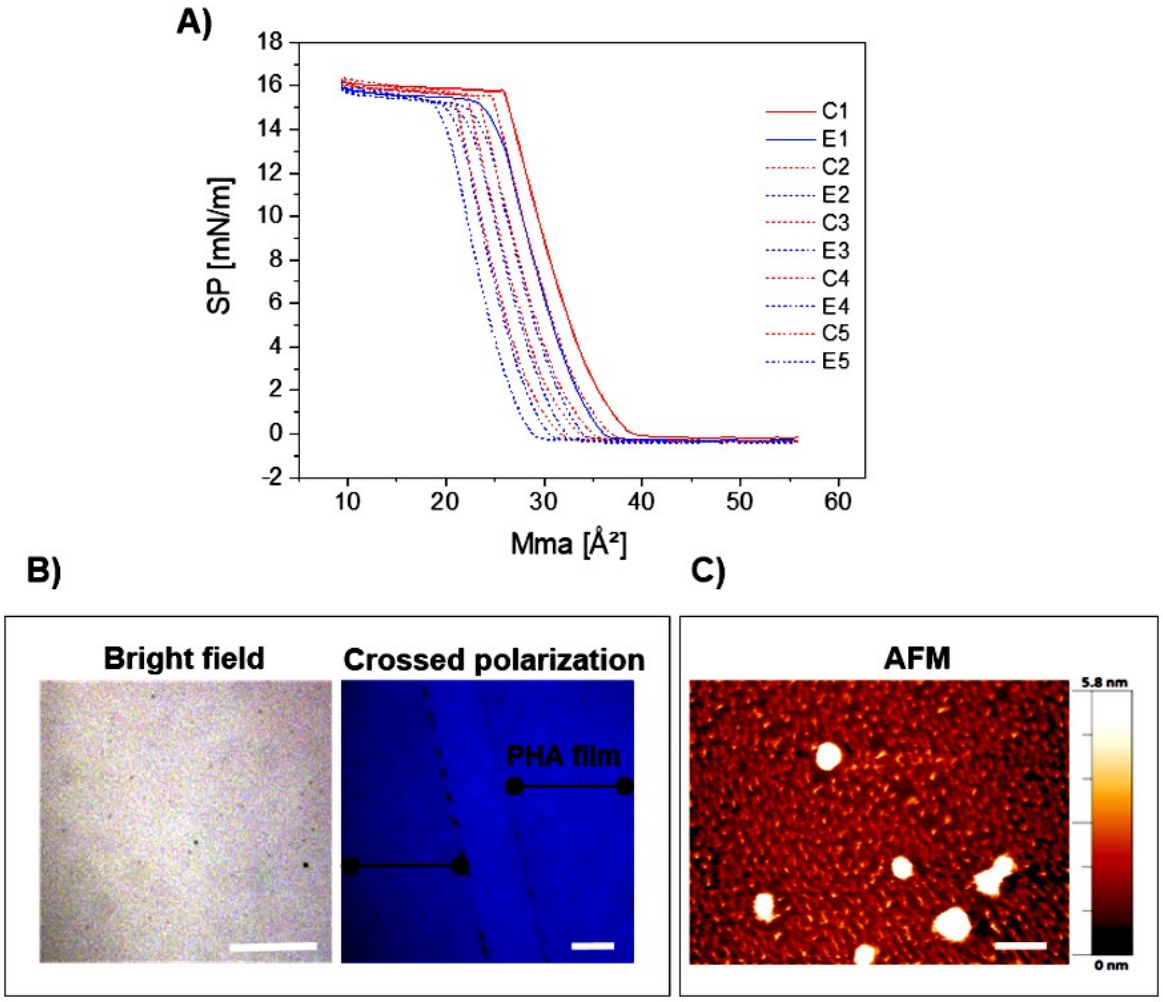

Figure 30. A) compression-expansion Isotherm of PHOHHx. Surface pressure (π) versus MMA per monomer unit of PHOHHx. **B)** Optical microscopy (bright field and crossed polarization) of PHOHHx LS-films on silicon wafer transferred at 7.5 mN/m. Scale bar = 25 μM. C) AFM images of PHOHHx LS-films silicon wafer transferred at 7.5 mN/m. Scale bar = 120 nm.

3.3.1. Adsorption of PhaF onto synthetic polyester monolayers

To address the effect of the substrate hydrophobicity on the adsorption of PhaF, the same concentration of protein was injected under preformed PLGA (Mn: 8370 g/mol; lactide content 68 % by weight) monolayers at an initial π = 10 mN/m. The comparison of the 3 scenarios for protein absorption (A-W, PHOHHx-water and PLGA-water) is shown in Figure 31. All the experiments were carried out in the same vessel, considering that

PhaF velocity of adsorption might be diffusion limited. As seen in Figure 31, the kinetics of PhaF adsorption was markedly affected by the monolayer composition. However, the π(t) curves cannot be translated directly into surface adsorption velocity curves. When PhaF inserts into preformed polymer films, the interface is already densely covered, and the insertion of additional molecules leads to an immediate increase of the surface pressure.

In contrast, for the bare A-W interface, a certain threshold surface concentration needs to be reached to observe an increase in the surface pressure, indicated by a lag time. Nevertheless, by comparing the slope of the π(t) curve for PHOHHx at t = 0 and the bare A-W interface for t = 40 min (where a preformed PhaF layer exists), we find that the surface pressure increases at least as fast for preformed PHOHHx layers as for preformed PhaF layers. This holds true up to the collapse surface pressure of the polymer at 15.7 mN/m. Then, further insertion requires the displacement of PHOHHx chains into the third dimension, which slows down the insertion. On the other hand, the more hydrophilic polymer PLGA, for which the A-W interface is a good solvent, shows distinctly slower increase of the surface pressure than both PHOHHx and the bare A-W interface, suggesting that PhaF molecules can barely penetrate the film. Furthermore, monolayers of PLGA-PhaF did not show the "bend" observed for PHOHHx-PhaF, confirming that its origin is the collapse of the PHOHHx monolayer.

When increasing concentrations of PLGA were spread on the bare A-W interface, a pressure-induced aggregation (network-like structures) is observed by BAM at π > 11 (Figure 31B), consistent with previous reports of PLGA Langmuir monolayers (Schöne et al., 2015). Although PhaF increases the surface pressure of the PLGA system, the smooth surface observed upon injection of the protein (Figure 31B) implies that the presence of PhaF does not induce conformational changes in the polymer. This morphology was maintained up to ~20 mN/m. As pointed above, this could be an effect of the penetration of only few protein molecules into the PLGA monolayer, which causes lower mobility of the polymer chains compared to the increment of PLGA molecules on the interface.

These results indicate that the protein determines the maximum surface pressure of protein-polymer films, as the surface pressure of the mixed films is the same as the PhaF equilibrium pressure. The injection of the blank solution into the subphase did not alter the initial pressure, neglecting a possible disruption of the monolayer (data not shown).

3.3.2. Structure and orientation of PhaF in mixed protein-polymer layers

At the air water interface, the ester carbonyl bond of pure PHOHHx that is expected at 1741 cm^{-1}, does not give rise to a PM-IRRAS signal (Figure 32A). This is attributed to the random walk of the polymer chains and the flexibility of the ester bond allowing for rotation around the COC bond, resulting in random orientation of the carbonyl groups.

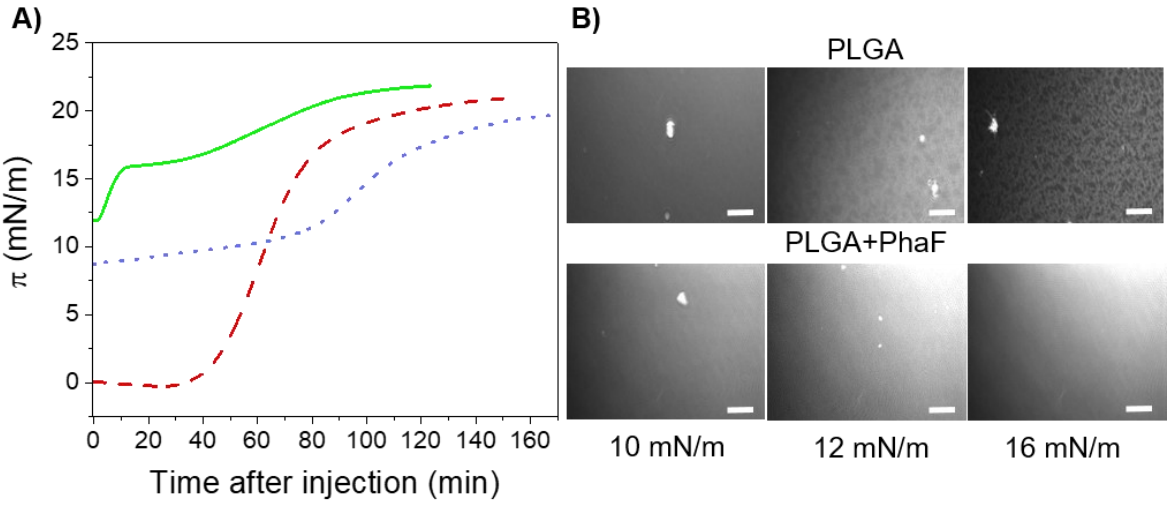

Figure 31. His_6-PhaF adsorption at hydrophobic/hydrophilic interfaces. **A)** The $\Delta\pi(t)$ graph shows the increase of surface pressure after protein injection at the A-W (dashed line), PHOHHx-water (solid line) and PLGA-water (dotted line) interface. Each experiment was performed twice. Data correspond to individual experiments reproducible with a random error of ~5 % concerning the surface pressure for the independently repeated experiments. **B)** BAM images of PLGA and PLGA-PhaF mixed layers. Scale bar = 50 µM

Hydrogen bonding between carbonyl oxygen atoms and water molecules could lead to an orientation of the ester bonds, but the layer is not expected to contain any solvent in the concentrated regime, which is realized for $\pi > 2.4$ mN/m.

In contrast to water, PhaF was clearly able to enter the concentrated PHOHHx monolayer, as indicated by the peak at 1740 cm^{-1} (a) in Figure 32B. This absorption band is caused by the carbonyl bonds of the ester groups of PHOHHx. Thus, the interaction with PhaF causes a reorientation of the PHOHHx molecules, indicated by a preferentially parallel orientation of the carbonyl C=O bond with respect to the A-W interface. It has to be emphasized that this reorganization is not caused by reduction of the available area per repeat unit due to competitive adsorption of the proteins, since additional compression of the pure PHOHHx film to 16.3 mN/m and 13 $Å^2$ per repeat unit (Figure 32A) did not lead to a preferential orientation of the carbonyl bonds. The presence of PhaF in the layer is demonstrated by the amide I peak at 1656 cm^{-1} in conjunction with a weak and broad amide II signal between 1500 and 1550 cm^{-1}. The intensity ratio suggests that the helices are oriented essentially parallel to the A-W or polymer-water interface (Castano et al., 1999). The peak at 1575 cm^{-1} (b) is attributed to the vibrations of deprotonated carboxylate groups in the protein. When going from 19 mN/m to 21 mN/m, this peak intensity decreases, while a shoulder appears at about 1715 cm^{-1}.

We suggest that this shift in intensity is caused by the protonation of acidic side-groups, which indicates that the protein molecules become less hydrated at 21 mN/m. Another strong peak at 1680 cm^{-1} should not be misread, since it can be caused by faulty removal of the water bending absorption as frequently observed when working with PM-IRRAS.

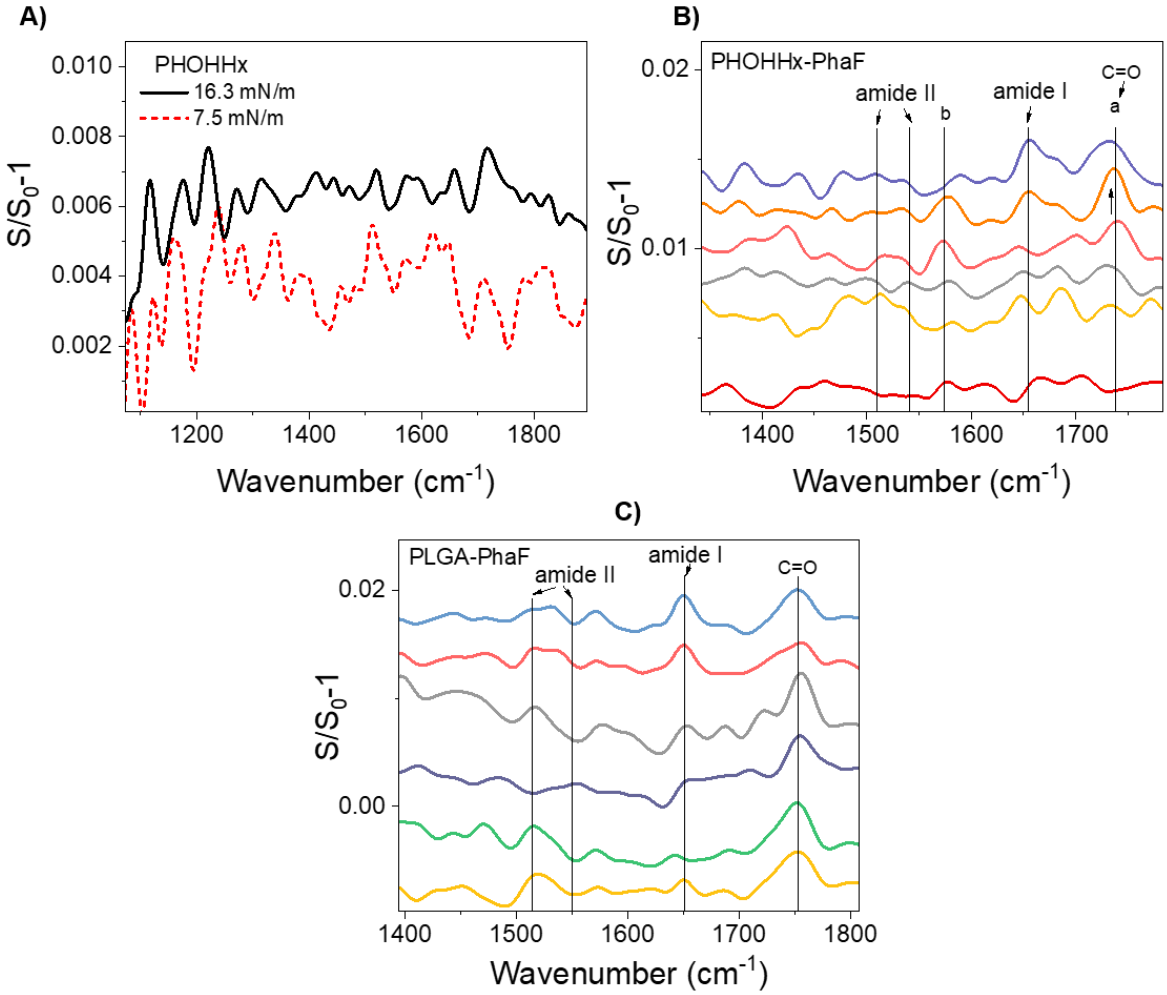

Figure 32. A) PM-IRRAS spectra of PHOHHx at 7.5 and 16.3 mN/m. **B)** PM-IRRAS spectra of His_6-PhaF adsorption to the PHOHHx preformed monolayer. From bottom to top: PHOHHx background, π = 12, π = 14.5, π = 16, π = 19, and π = 21 mN/m. Vertical lines a = carbonyl bonds of PHA ester groups and b = deprotonated carboxylate groups. **C)** Spectra of PhaF adsorption to the PLGA monolayer. From bottom to top: PLGA background, π = 9.4, π = 10.2, π = 13, π = 19, and π = 19.7 mN/m. C=O peak = carbonyl bonds of PLGA ester groups. Spectra of the replicate measurements agreed qualitatively.

When comparing the PM-IRRAS spectra of PhaF absorbing to PHOHHx and PLGA, we found similar peak positions. At the final surface pressure of the PLGA-PhaF mixed layer (Figure 32C), the position of amide I and amide II is at 1650 cm^{-1} and 1510 to 1550 cm^{-1}, respectively, indicating alpha helical conformation. In analogy to PHOHHx, the intensity ratio suggests that the main axis of the helices are oriented parallel to the A-W or air-polymer interface. In contrast to PHOHHx, the PLGA molecules exhibit a preferentially parallel alignment of their carbonyl bonds with respect to the A-W interface as demonstrated by the carbonyl stretching band at 1750 cm^{-1} in the absence of PhaF. This can be explained by hydrogen bonding between carbonyl oxygen and water. Since the polymer is in good solvent conditions the films contain a lot of water (Schöne et al., 2015). The intensity of this carbonyl vibration does not change when the protein adsorbs. Interestingly, discernible amide vibrations are only observed at surface pressures above 19 mN/m, indicating that only few protein molecules are causing the rise in surface pressure.

Overall, our PM-IRRAS measurements confirm the importance of polymer hydration in determining protein adsorption to polymer materials, a finding that is also summarized in the "Whiteside rules" (Wei et al., 2014). The more hydrophilic PLGA strong interactions with water hinder the insertion of PhaF and stabilizes its conformation while the more hydrophobic PHOHHx, which contains no water, adapts its conformation to the presence of the protein.

3.4. Stability of PhaF films on solid substrates and elevated temperature

Since we suggest PhaF as a prospective coating to make hydrophobic polymer materials more biocompatible by increasing their hydrophilicity, its stability upon transfer to solid substrates and at physiological temperature needs to be ascertained. Hence, the secondary structure of proteins assembled at the A-W interface to form a Gibbs layer and then transferred to solid gold substrates, was investigated via PM-IRRAS (Figure 33).

Both monolayers transferred at 18 mN/m, have a rather similar spectrum in the 1500-1800 cm^{-1} region. The position of the amide I band is shifted to higher wavenumbers when compared to PhaF in solution (Figure 33A). However, the only secondary structure that relates to amide I vibrations at 1665 cm^{-1} is loops or β-turns and long polypeptides do not assume an all β-turn structure (Goormaghtigh et al., 1994). Therefore, this shift is not related to a change in protein conformation, but indicates dehydration of the α-helices (Lórenz-Fonfría et al., 2015) expected at the air-gold interface. In addition, the amide II peaks at 1527 and 1549 cm^{-1} support the assumption of a predominantly α-helical structure (Venyaminov and Kalnin, 1990).

The shoulder at 1718 cm^{-1} is attributed to the carbonyl vibration of the carboxylic acid side-groups, which are protonated in air. The amide I to amide II ratio is about 2,

which corresponds well with the ratio of the molecular absorption coefficients in water (Venyaminov and Kalnin, 1990). That means that the angle between the surface normal and both amide II and amide I vibration dipole moments has to be equal, since only the component parallel to the surface normal leads to absorption on a metallic surface substrate. Since the angle between the helix axis and amide I dipole moment is about 30° whereas the angle between the helix axis and the amide II dipole moment is 90°, the angle between surface normal and helix axis should be around 60°, i.e. the helices lie almost flat.

In the C-H stretching region, 2800-3100 cm^{-1} (side-chain related adsorption bands), the intensity of the peaks varies between both temperatures (Figure 33B). A marked decrease of the CH_2 vibration peaks (2927 and 2858 cm^{-1}, assigned to assymetric CH_2 and symmetric CH_2 vibrations, respectively) was observed at 37 °C, suggesting less parallel orientation of the side-chains with respect to the gold-air interface. However, the strong peak at 2962 cm^{-1} (assymetric CH_3 vibration), which has a transition moment that is known to be parallel to the long axis of the side-chain indicates that PhaF forms alpha helices that are oriented preferably parallel to the interface and stable at the gold-air interface up to temperatures of 37 °C.

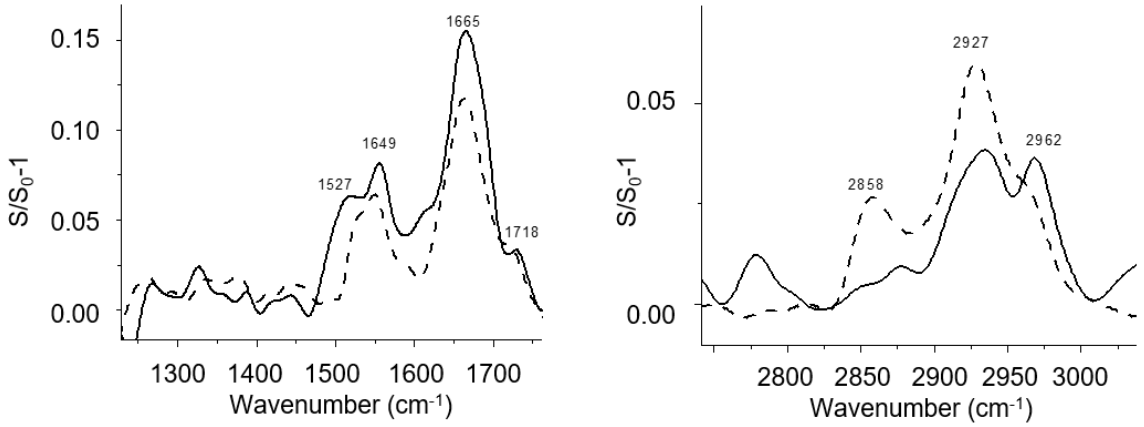

Figure 33. PM-IRRAS of Gibbs molonalyers of His_6-PhaF transferred to gold substrates at 21 °C (dashed lines) or at 37 °C (solid lines).

3.4.1. Morphology of pure PhaF films on solid surfaces investigated by AFM

Optical microspcopy of LS-films of PhaF (transferred to a silicon wafer at 21 mN/m) showed the presence of a smooth and homogeneous film on the micrometer scale (Figure 34A). AFM was used to characterize the topography and roughness of the protein film on the nanometer scale. AFM images of LS-films of PhaF transferred to silicon wafers at 21 mN/m revealed the presence of a smooth film with occasional packing defects

(Figure 34B) The thickness of the monolayer was measured by scratching with a tweezer and analyzing the height histogram (Figure. 34B).

The thickness is in excellent agreement of the diameter of an alpha helix (1-2 nm), confirming the result from PM-IRRAS that the helices are oriented parallel to the A-W interface at 21 mN/m. AFM does not suggest an in-plane ordering or supramolecular organization of the helices.

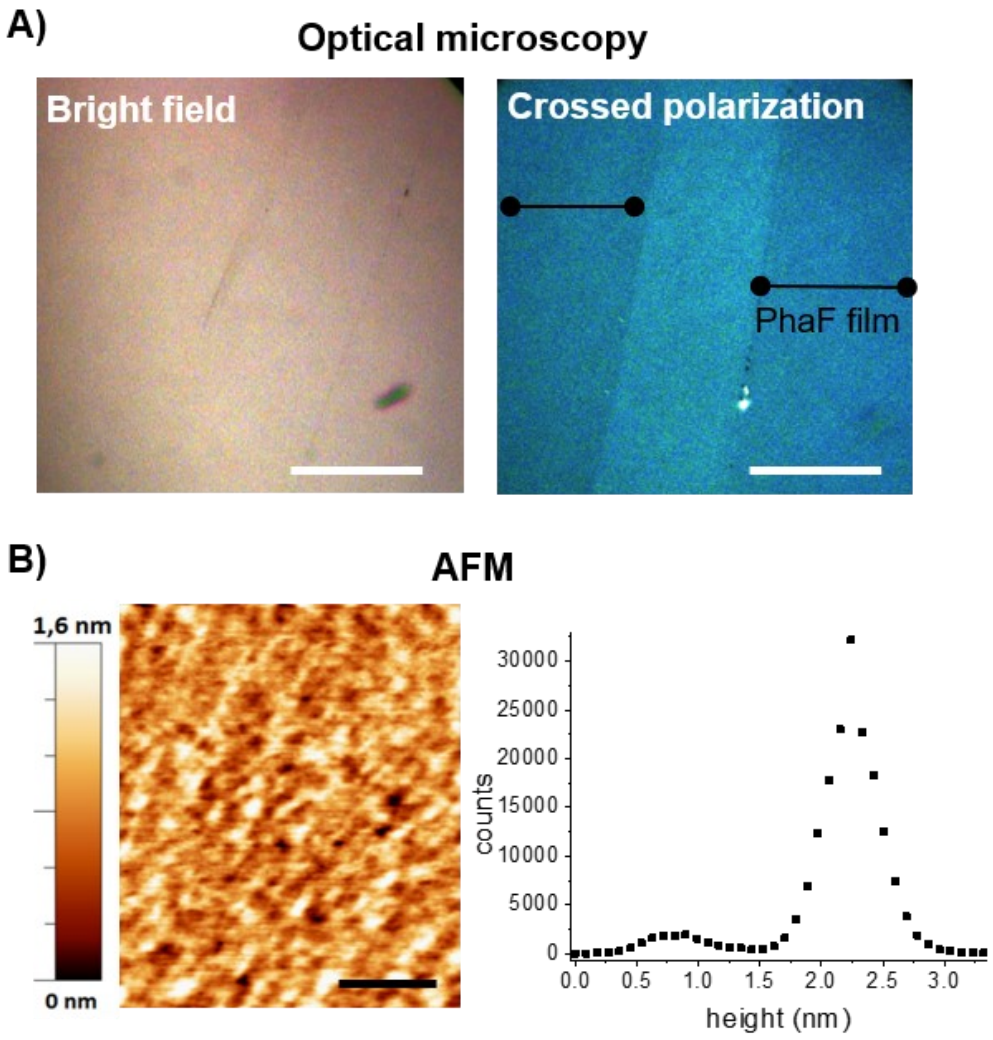

Figure 34. A) Optical microscopy of scratched His_6-PhaF LS-Films on silicon wafer, transferred at 21mN/m. White scale bar = 50 µm. **B)** AFM image of His_6-PhaF LS-film transferred to a silicon wafer at 21 mN/m, and AFM Histogram of scratched film. Black scale bar = 800 nm.

V. INTEGRATED DISCUSSION

Despite the long list of PHA-related studies, the complex organization of carbonosomes as supramolecular structures, and their surface composition, remain incompletely understood. Many bacterial species have phasins with crucial roles in the accumulation of PHA. Involved in simultaneous protein-protein and protein-PHA interactions, phasins are multifaceted proteins. Indeed, it is very likely that phasins form more than one functionally important complex with different PHA-related proteins, allowing them to perform their different roles. Some members of the phasin family have even been suggested to interact with DNA or cytoskeletal elements in the formation of PHA granules. The first two chapters of this thesis were directed towards the study of protein-protein interactions involving phasins and the possible effect of these interactions on the accumulation of PHA. The third part of this work engaged in almost unexplored aspects of phasins physical adsorption to PHA, namely, the molecular conformation of both species during the interaction process and the control of the conditions to preserve a stable PHA-PhaF complex. This section was prompted by the growing interest in the design of bioinstructive materials using PHA-phasin platforms in biomedicine, and proposes an innovative system via which to study the interaction of phasins with polymers, i.e., by mimicking the PHA-phasin interface. This could be used to assess the stability of phasins at different interfaces for the design of new materials.

1. The formation of stable phasin-phasin homo- and hetero-oligomers in *Pseudomonas* is mediated by coiled-coil motifs, the sequences and structures of which resemble leucine zipper-like motifs

The bacterial phasin superfamily contains numerous phylogenetically distinct families. Some of their members have roles in the physical stabilization of PHA granules, the control of the number and size of these granules, their segregation into daughter cells, and their mobilization (Mezzina and Pettinari, 2016; Maestro and Sanz, 2017). The molecular basis for their diversity has remained elusive owing to a lack of knowledge regarding phasin structure. The first insights in this respect were obtained by low-resolution structural studies involving the making of *in silico* predictions. Over time, studies on PhaP from *R. eutropha* ($PhaP_{Re}$) (Neumann et al., 2008), PhaP from *Azotobacter* sp.FA8 ($PhaP_{Az}$) (Mezzina et al., 2014), PhaF from *P. putida* (Maestro et al., 2013), PhaP from *A. hydrophila* ($PhaP_{Ah}$) (Zhao et al., 2006) and PhaP from *Synechocystis* sp. PCC 6803 ($PhaP_{Sp}$) (Hauf et al., 2015); revealed these proteins to have structural similarities. For instance: i) most phasins have a high percentage of their amino acids in an α-helical conformation; ii) they change their secondary conformation

in the presence of a hydrophobic support or molecule mimicking the PHA surface (such as sodium oleate); iii) they contain disordered regions, investing them with a conformationally flexible nature; iv) all phasins form oligomers in solution, mainly trimers and tetramers; and v) these proteins have coiled-coil amino acid sequences in their primary structure that might be involved in oligomerization events.

Coiled-coil mediated oligomerization was first suggested by Maestro et al. (2013) (Maestro et al., 2013). The structural characterization of PhaF revealed it to be a leucine zipper-like sequence (coiled-coil) that followed on from the protein's N-terminal (PHA binding domain) (Figure 6). It was also shown that PhaF forms tetramers in solution, supporting the idea of coiled-coil-mediated oligomerization. Recently, Zhao et al. (2016) reported the crystal structure of $PhaP_{Ah}$ to be a tetramer with 8 α-helices each showing a coiled-coil structure (Zhao et al., 2016). Each monomer had a hydrophobic and a hydrophilic surface (amphipathic helix); this is common to most phasins, investing them with surfactant properties (among others) (Mato et al., 2018).

The present study extends these observations by providing the full characterization of the leucine-zipper motif of *P. putida* KT2440 phasins. The use of sequence analysis methods to identify functionally important residues in macromolecules is a well established strategy. Such methods can, for example, identify protein–protein binding sites (Yang et al., 2016). This work was started using secondary and tertiary structure prediction tools to identify coiled-coil regions potentially involved in the oligomerization of phasins PhaF and PhaI.

A canonical coiled-coil protein motif is formed from a heptad repeat - *abcdefg* - in which hydrophobic amino acids at positions *a* and *d* are conserved. This allows them to appear on the same side of the helix (which has 3.6 amino acids per turn). The hydrophobic face produced is the driving force behind the formation of the coiled-coil (Mason and Arndt, 2004). As a result, helices deriving from such repeating sequences are amphipathic, with both hydrophobic and polar faces. The association of 2 to 5 helices via their hydrophobic faces drives coiled-coil formation (Truebestein and Leonard, 2016). The prevalence of these regions suggests that they may help meet some of the fundamental requirements for phasin function, though in a manner not yet understood.

During the present work, a coiled-coil sequence was identified in PhaI that resembles a leucine zipper-like motif (ZIPI), and which is essential for PhaI homo- and hetero-oligomerization (Figure 12). Despite the absence of any significant homology among phasins, the heptad repeat of ZIPI is highly conserved in the phasins of members of *Pseudomonas*. In all 58 species, Leu residues (L121 and L128 in ZIPI) occupy the first two *d* positions of this region, while the third *d* position may be Leu, Val or Ile (V135 in ZIPI) (data not shown). In the present work, these residues were shown to stabilize the PhaI-PhaI and PhaF-PhaI oligomers, confirming the oligomerization of these phasins

through coiled-coils. It should be remembered that while coiled-coils are widespread in phasins, the amino acid sequences within this motif differ from family to family. For instance, no significant similarities were found between the ZIPI or ZIPF motifs and the $PhaP_{Ah}$ coiled-coil, either in their amino acid sequences or in their length. This suggests that phasins from different families use different mechanisms to achieve coiled-coil-mediated oligomerization.

Preliminary observations on the biological importance of this motif in the function of PhaI, obtained via fluorescence microscopic observations of PhaI-GFP, $PhaI^{\Delta ZIPI}$-GFP, and $PhaI^{L121A,L128A,V135A}$-GFP fusions, showed a localization of the fusion proteins on the surface of the granules with moderate diffusion to the cytoplasm. This results suggest that although the oligomerization process is not obligatory for the binding of the protein to the PHA granules, it restricts the optimal binding of PhaI to the granule surface (work in progress). This might be explained by pre-existing intra-chain hydrogen bonds in alpha helical proteins stabilizing phasin monomers, allowing them to interact with the PHA without the need for the intervention of other proteins. However, further evidence is needed to corroborate these observations since the presence of PhaI-GFP fusions in the granule fraction could be due to the formation of inclusion bodies.

Based on the present results, and those of other authors, the binding of phasins to PHA seems to be driven by a non-specific interaction involving the amphipathic α-helix, such that the hydrophobic side of the helix faces the polymer while the hydrophilic side is exposed to the solvent (Maestro et al., 2013). They also reveal important structural and functional roles for phasin coiled-coils, and might be helpful in elucidating the mechanisms behind the stability and dynamics of phasin complexes. The important role of the coiled-coil structures in these phasins could afford us a better understanding of the potential formation of a network-like structure on the granule surface. Finally, the presence of this motif might be considered in the design of novel variants of PHA-binding affinity tags, based on PhaF or PhaI, for the immobilization of recombinant proteins on PHA-based materials.

Previous ultracentrifugation experiments showed 70% of PhaF to be in a tetrameric state (Maestro et al., 2013). The computational predictions for the oligomeric states of PhaF and PhaI made in the present study, however, show no clear preference for a specific oligomeric species. When the known rules for hydrophobic cores (pairwise associations at the *d*–*a* positions) (Harbury et al., 1993; Vincent et al., 2013) are taken into account and applied in the LOGICOIL algorithm, the PhaF and PhaI homo- and hetero-oligomerization mediated by the coiled-coils identified in the present work would favour the formation of parallel trimers. The latter rules state that: II (isoleucine at position *d* and *a*) is a well-established trimer-favouring pairwise interaction, as is LL (leucine at position *d* and *a*); LV (leucine at position *d* and valine at position *a*) is a dimer

-favouring combination; and IL (isoleucine at position *d* and leucine at position *a*) favours tetrameric conformations (Harbury et al., 1993). However, all attempts by our group to purify PhaI for ultracentrifugation and circular dichroism studies have failed, and the true oligomerization state cannot yet, therefore, be reliably concluded. Moreover, when taking into account i) the propensity for disorder of PhaI and PhaF, in which the influence of external and environmental conditions trigger transitions between disordered and ordered states, and ii) the distinct roles assigned to these proteins, it cannot be ruled out that phasins have more than one functionally important oligomeric species, and that may change from one into another.

A broader topic worthy of discussion is the impact of the 2 homologous phasins on PHA metabolism. In previous studies made by our group on the independent effect of PhaF and PhaI mutations in *P. putida* (Dinjaski and Prieto, 2013), the double mutant *phaFI* showed a strong reduction in PHA accumulation when growing in octanoic acid (7% compared to 63% CDW reached in the parental strain), a clear demonstration of a negative impact on fitness. The *phaF* deletion strain also showed reduced PHA accumulation (33% CDW) as well as defective segregation, generating two different cell populations (Figure 7). Though, the granules coalesce in a single large granule (which does seem to occur in other microorganisms lacking phasins (Wieczorek et al., 1995)), very likely due to the presence of PhaI. However, the phenotype associated with the deletion of *phaI* could not be properly addressed since the mutation of *phaI* also caused a polar mutation in the *phaIF* operon, inhibiting *phaF* expression. In fact, the *phaI* disrupted strain produced 7.5-fold less PhaF than did the wild-type strain. This deletion and the reduction of *phaF* expression had a bigger impact on PHA accumulation than *phaF* deletion (21 % CDW). Interestingly, the expression of BioF (the N-terminal of PhaF, which shares 57 % similarity with PhaI) was able to recover PHA production in the *phaI* deletion strain to the level of the *phaF* mutant, suggesting that, in terms of PHA accumulation, BioF can replace PhaI but not PhaF. Although it remains unknown if this is an effect of phasin dosage, these findings suggest that these proteins work in harmony and are essential for optimal PHA synthesis and accumulation.

Of further interest, in the strain *Herbaspirillum seropedicae* SmR1 the production of phasins $PhaP1_{Hs}$ and $PhaP2_{Hs}$ has been associated with a backup expression mechanism (phasin compensation); $PhaP1_{Hs}$ is the major phasin expressed in PHA-accumulating conditions, and *phaP2* increases its expression up to 6-fold upon the deletion of *phaP1* (Alves et al., 2016). However, this has never been observed by our group in the *phaF* deletion mutant since the expression of *phaI* was reduced 1-2 fold (data not shown), indicating that another mechanism may be operating in *Pseudomonas* or that PhaF may be involved in the regulation of the expression of genes from the *pha* cluster. This is further discussed in the next chapter.

2. Protein-protein interactions involving PhaF and the transcriptional regulator PhaD allow new hypotheses to be constructed regarding the roles of PhaF in the system regulating PHA metabolism

Despite the strong sequence similarity between PhaF and PhaI, our group has long recorded that the deletion of *phaF* has a notable impact on overall cell physiology, resulting in a less fit phenotype (discussed above). This is most likely a consequence of the presence of the C-terminal in PhaF that binds DNA. It has been reported that, while PhaF, plays a structural role, it also enhances the expression of *phaC1* and *phaI* and drives the organization and segregation of PHA during cell division (Prieto et al., 1999; Galán et al., 2011; Dinjaski and Prieto, 2013). The presence of high concentrations of PhaF at the granule surface, and the abundance of these granules in the cytoplasm, together suggest that PhaF interacts with other cell components and/or participates in extensive networks of protein–protein interactions, very likely obeying specific cell signals. The present work attempted to gain a deeper insight into the PHA regulatory system in *P. putida* KT2440 and the involvement of PhaF in it.

One of the peculiarities of PhaF is its modular organization into a PHA granule-binding domain (located at the N-terminal) and an AKP-rich histone-like DNA-binding domain (located at the C-terminal). It has been proposed that the “needle array” organization of PHA granules in *P. putida* involves the formation of a complex between the PHA granules, PhaF (C-terminal domain) and the nucleoid. However, similar arrangements of supramolecular structures such as magnetosomes suggest that other mechanisms may participate in such systems. The chain-alignment of magnetosomes, which enable magnetotactic bacteria to sense the geomagnetic field, is controlled by these structures' interactions with actin-like proteins such as MamK (Barber-Zucker and Zarivach, 2017). In search of similar mechanisms governing PHA granule arrangement, it was in our group previosly hypothesized that cytoskeletal proteins such as tubulin-homologous FtsZ or the actin-like protein MreB might mediate the localization of granules through direct or indirect interactions with PhaF (Galán et al., 2011). However, despite much effort to show a direct association between PhaF and cell division proteins or actin-like proteins, no evidence for this was found (data not shown). Nevertheless, the involvement of such factors in a complex controlling the organization and distribution of PHA granules, cannot yet be ruled out.

A holistic approach was followed in the present work in the hope of identifying the PhaF protein's interacting cytoplasmic partners, allowing a “systems view” of the

unknown components of the complex. In recent years, the pull-down technique has become an invaluable tool for the study of protein functions via protein-protein interactions. Combining this technique with a high throughput identification technology, known and unknown interactions between PhaF and the proteins present in its native environment were detected under PHA-producing growth conditions. Indeed, 6 proteins were detected as potential interacting partners. Although DNA- and PHA-free soluble fractions were used as the source of interacting proteins, PhaI (recognized as a GAP) was the most abundant protein captured by PhaF. This might be explained by the fact that the interaction between these proteins is highly specific, with PhaF recruiting even small amounts of soluble PhaI.

In silico analyses of other PhaF-interacting proteins, including ATP synthase subunit beta, flavoprotein-ubiquinone oxidoreductase (a putative electron transfer protein), and the outer membrane protein OprF, provided little information about any putative interaction with PhaF or their abundance in the PHA granule proteome. In fact, none of these proteins has a phasin motif or coiled-coil regions that might relate them to PHA binding proteins.

The most interesting finding made during these analyses was the presumed interaction of PhaF and the regulatory protein PhaD. PhaD is a member of the TetR family of regulators (de Eugenio et al., 2010), a large and important family of one-component signal transduction systems in bacteria in which a single polypeptide contains both a sensory domain and a DNA-binding domain. These proteins possess a conserved helix-turn-helix (HTH) signature at the N-terminal of the DNA-binding domain as well as a ligand-binding domain (LBD) at the C-terminal (Cuthbertson and Nodwell, 2013). They commonly act as repressors and interact with specific DNA targets to prevent or abolish transcription in the absence of an effector. In contrast, the binding of the ligand to the LBD induces structural changes, driving the dissociation of the repressor from the target DNA and the subsequent transcription of the TetR-regulated genes. A well known exception to the repressible regulation of gene expression observed in most TetR regulators is that involving DhaS, which is an activator of dihydroxyacetone (Dha) kinase required for glycerol catabolism in *Lacotococcus lactis* (Christen et al., 2006). It forms a complex with DhaQ (coactivator), and in the presence of Dha can then activate the transcription of the *L. lactis dha* operon. EMSA studies, DNase I footprinting analyses, and *lacZ* reporter fusion experiments have confirmed that PhaD is also an activator of the expression of the *pha* operons via its binding to the *phaI* and *phaC1* promoter regions (P_I *and* P_{C1} respectively) of the *pha* cluster in *P. putida* KT2440. Like DhaS, PhaD binds to operator sequences (OPRc1 and OPRi) partially overlapping the corresponding promoter boxes (Christen et al., 2006; de Eugenio et al., 2010).

In a *phaD* mutant strain, the transcription of *phaC1* and of the *phaC1ZC2D* operon

was significantly reduced when growing on octanoic acid (de Eugenio et al., 2010). The expression levels were similar to those seen when wild-type cells were cultured in glucose, suggesting that PhaD controls the carbon source-dependence of the transcription profile of this operon, and implying that the system might be induced by either octanoate or some octanoate-derived metabolite. In addition, PHA accumulation in the mutant strain was undoubtedly affected, though not abolished (18 % CDW vs. 70 % in the wild-type strain). However the influence of PhaD on *phaC1* regulation remains unclear due to the involvement of other global transcriptional regulators such as Crc (De la Rosa et al., 2014).

What is clear is that phasin expression is regulated by PhaD. In fact, *phaI* mRNA is completely absent in the *phaD* mutant strain, and the *phaF* gene only very weakly expressed. In addition, no PhaI or PhaF phasins were detected in the PHA granules when *P. putida* KT2440 *phaD* mutant was cultured under PHA production conditions (de Eugenio et al., 2010). Taking these results into consideration, and the absence of PhaD in the PHA granules (checked by *in vivo* localization of the PhaD-GFP fusion protein), it might be hypothesized that the complex formed between PhaD and PhaF is likely involved in the system controlling phasin expression.

The first evidence that PhaF is involved in regulating the expression of genes from the *pha* cluster was provided by Prieto et al. (1999) (concluded from work on the strain *P. putida* GP01). PhaF was proposed able to bind to both DNA, thus exerting a transcriptional regulatory effect, and to PHA granules, working as a protein ligand recruiting PhaF from the cytoplasm, thus preventing the regulatory function of this phasin (Prieto et al., 1999). PhaF was proposed to be a transcriptional repressor, though this was later rebutted by Galan et al. (2011). Via transcriptomic experiments performed with *P. putida* KT2442, the latter authors determined a role for PhaF as a transcriptional activator of the *pha* cluster. Their transcriptomic results also revealed the whole transcriptome to be altered in a PhaF deletion mutant, suggesting a role for PhaF as a global transcriptional regulator. Its effect on the transcriptome profile might be due to either specific or non-specific DNA-binding of the PhaF protein to the nucleoid, or to a lack of control over PHA synthesis and segregation.

Nonetheless, it seems likely that PhaF is involved in "hybrid regulation system" combining 2 mechanisms: i) non-specific binding to DNA and to PHA granules, and ii) specific regulation of *pha* cluster genes via its interaction with PhaD. Although there is no conclusive evidence for the regulation of the *pha* cluster by protein-protein interactions, the interaction between PhaF and PhaD shown in the present work *in vivo*, plus the results of the accompanying EMSA experiments (Figures 22 and 23), support this idea.

Similar regulatory mechanisms involving phasins have been reported in scl-PHB-accumulating bacteria, e.g., in *R. eutropha* H16, *Paracoccus denitrificans* and

H. seropedicae (Maehara et al., 2001; Maehara et al., 2002; Pötter et al., 2002; York et al., 2002; Yamada et al., 2007; Yamada et al., 2013; Alves et al., 2016). In *R. eutropha* H16, the expression of *phaP1* seems to be controlled at the transcriptional level by $PhaR_{Re}$, which acts as a repressor of transcription. $PhaR_{Re}$ can attach to 4 different ligands in *R. eutropha*, including the promoter regions of *phaP1*, *phaP3* and *phaR* and the surface of PHB granules. Under cultivation conditions inappropriate for PHA formation, or in mutants faulty for PHA accumulation, $PhaR_{Re}$ attaches to the *phaP* promoter region, repressing transcription. When PHA is synthesized, the $PhaR_{Re}$ repressor is sequestered from the DNA by the PHA granules, and phasin transcription is initiated. $PhaR_{Re}$ thus couples PHB synthesis with phasin expression (York et al., 2002). Whether there are other components in such regulatory systems that interact with $PhaR_{Re}$ and PHB granules is unknown, but none has ever been identified.

The deduced amino acid sequence of PhaF showed no similarity to that of PhaR, and no evidence was found that PhaF acts as a repressor of phasins on its own; its deletion in *P. putida* reduced the transcription of *phaI*. In addition, PhaD, which is not associated with PHA granules, positively affects PHA synthesis and PhaI production in mcl-PHA producing *Pseudomonas* species (de Eugenio et al., 2010). Together, these observations suggest that the regulatory system of mcl-PHA synthesis is more complicated than that of scl-PHA synthesis. Based on the present results, plus the fact that PhaF guarantees proper levels of phasin expression (thus avoiding the perturbation of PHA synthesis and granule formation), it might be concluded that PhaF and PhaD act in harmony to control the expression of the *pha* genes. Research is presently underway at our laboratory to determine whether PhaF is a transcription coactivator of PhaD.

3. Towards the improvement of phasin-coated materials. Development of a methodology for studying PhaF interactions with polymers by mimicking its natural environment.

Interest in polymeric materials of natural origin that can outperform synthetic polymers, and which might have applications in medical devices, drug delivery, and tissue-engineering (Koller, 2018), has placed bacterial PHA under the spotlight. However, limitations such as the intrinsic hydrophobicity of PHA currently prevent any competition with traditional synthetic plastics (Li et al., 2016). Much effort has gone into diversifying PHA through metabolic engineering (to make recombinant PHA-producing strains) or chemical modification (graft/block copolymerization and functionalization) (Hazer and Steinbüchel, 2007; Chanprateep, 2010; Tan et al., 2014; Li et al., 2016; Ferre-

Guell and Winterburn, 2018). Examples of such chemical modification include PHA-grafted with polyethylene glycol (PEG) chains (PHA-g-PEG). Such grafting increases the polymer's hydrophilicity, ensuring a low interface tension with blood and reducing protein adsorption and platelet adhesion - a requisite for materials used in blood-contacting devices (Chung et al., 2003).

A common approach to the modification of synthetic polymers is the formation of hybrid protein/peptide-polymer conjugates. The integration of the structural and functional properties of peptides/proteins and the versatility of polymers in such conjugates could allow for the modulation of target polymer conformational properties, nanostructural organization, and assembly behavior (Krishna and Kiick, 2010; Russell et al., 2018). Different methodologies for incorporating proteins into polymer scaffolds include protein immobilization on their surfaces via physical adsorption, and chemical, plasma or photochemical treatment (Katti et al., 2008). For tissue engineering applications, the immobilization of desired proteins onto scaffolds allows the surface properties of materials to be improved in terms of their biocompatibility and the control of cell-adhesion. Growth factors, therapeutic proteins, extracellular matrix proteins (or peptides with cell binding domains) have been immobilized on scaffolds of different composition such as PLA, PCL, and PLGA (Neff et al., 1998; Lin et al., 2006; Katti et al., 2008).

Although different ways of modifying PHA have been tried, functional modification by surface coating with proteins remains largely unexplored. To date, strategies based on PHA polymerases and phasins (as linker molecules) have mainly been reported. Using $PhaC_{Re}$ from *R. eutropha*, Rehm's group developed efficient covalent bonding methods for the functionalization of natural and artificial PHA granules. The final products had a variety of potential biotechnological and biomedical applications (Rehm et al., 2016). In addition, Chen's group recently reported the surface modification of PHA via phasin adsorption, overcoming non-specific protein adsorption and achieving the immobilization of signalling groups on the granule surface (see Table 1) (Dong et al., 2010; Xie et al., 2013). By coating different PHA with fusions bearing $PhaP_{Ah}$-cell binding motifs, e.g., RGD, they succeeded in promoting the attachment and proliferation of different cell lines *in vitro* (Dong et al., 2010; You et al., 2011; Xie et al., 2013).

While covalent bonding achieves potentially greater surface stability than physical adsorption, it suffers from limitations including the deactivation of the attached fusions by organic solvents, the ineffective removal of excess/unreacted reagents and cross-linkers, and unwanted modifications of the polymer surface (Katti et al., 2008; Tallawi et al., 2015). Physical adsorption, however, allows biomaterials to be easily functionalized by their simple immersion in a solution containing the biomolecules to attach to their surface via interactions involving van der Waal forces, electrostatic forces, hydrophobic

interactions and hydrogen bonds (Tallawi et al., 2015). This method therefore allows surface modifications to be made while maintaining the properties of the bulk polymer, the solvent-free procedure reducing any damage (Park et al., 2005; Tallawi et al., 2015).

Phasin-based functionalization should allow for a new generation of bioinstructive materials that provide cell-interacting motifs able to influence cell behavior, but there is still a scarcity of information regarding the robustness and stability of phasins at hydrophilic/hydrophobic interfaces. Neither is a great deal known about their adsorption behavior, nor has the alteration of the molecular conformation of polymers and phasins during the functionalization process been addressed. The present work thus explored new strategies that might allow for a more controlled immobilization of phasins on PHA surfaces.

The first of the present experiments using PHA-supported films aimed to confirm the capacity of PhaF to bind to PHA *in vitro* in the absence of other possible components of PHA granules, such as phospholipids. The PHA used in this study was a semi-crystalline polymer, with a glass transition temperature of approximately -35°C. This made the casted films very likely to undergo dewetting processes, which seemed to be accelerated upon the addition of a buffer solution, as shown by the formation of isolated domains (Figure 24). However, when PhaF was added to the casted films, the protein perfectly surrounded the PHA domains, confirming their high affinity for the polymer surface.

Once PhaF-PHA binding was proven to occur, the Langmuir technique (one of the best known for investigating and understanding molecular interactions at interfaces) was used to gain deeper insight into the interaction between PhaF and PHA. In this technique, films are formed at the air-water interface with precise control of the distance between molecules and other experimental conditions (Giner-Casares et al., 2014; Schöne et al., 2017). It was hypothesized that this technique might be used with the same success to study the physical adsorption of proteins onto prospective biomaterial surfaces. When characterizing protein adsorption, the adsorption isotherm and adsorption and desorption kinetics are usually described, the presence of adsorbed proteins confirmed, and certain physical properties of the adsorbed protein layer, e.g., its thickness, typically reported (Hlady et al., 1999). However, given the hydrophobic nature of PHA, only a few studies have examined the formation of thin PHA films at air-water interface (Nobes et al., 1994; Lambeek et al., 1995; Jo et al., 2007; Jagoda et al., 2011). These studies mainly focused on the spreading behavior, stability, hysteresis and degradation kinetics of P3HB and its copolymers, which as bulk materials are brittle and have high melting points (Nobes et al., 1994; Lambeek et al., 1995; Jo et al., 2007).

In the present work, the adsorption of PhaF onto air-water interfaces was first addressed to evaluate and characterize the organization of self-assembling monolayers.

Using *in situ* spectroscopic techniques (infrared reflection-absorption spectroscopy [IRRAS]) and Brewster angle microscopy, PhaF was seen to form stable, robust monolayers with an almost flat orientation of its α-helix at the interface at both 21ºC and physiological temperatures. PhaF films were successfully transferred to solid substrates (gold and silicon wafers) using the Langmuir Schaefer technique, maintaining the PhaF α -helical conformation (Figures 33 and 34). Additionally, preliminary contact angle microscopy measurements showed that the protein reduced the hydrophobicity of silicon wafers (data not shown).

As revealed by AFM, the PhaF films were densely packed, covering almost all the surface of the solid substrates (Figure 34). This study is the first to provide evidence of the stability of PhaF at different interfaces and under different physicochemical conditions, and validates the use of phasin PhaF to prepare densely packed monolayer coatings for hydrophobic surfaces.

During the adsorption of the PhaF onto the PHA Langmuir thin films, the surface pressure (π) was increased, the Brewster angle changed in BAM microscopy, and the shift in the molecular arrangement of the polymer layer measured by PM-IRRAS. Stable mixed films of PHA and PhaF were obtained up to a π of ~16 mN/m. From that point, the excess of PhaF caused the formation of separate domains and the collapse of the polymer layer (Figure 29). The α-helix conformation of PhaF was also adopted at the air-water interface when adsorbing onto PHA, ensuring the best exposure of the hydrophobic residues to the polymer surface and revealing a suitable coating strategy for PHA-functionalized materials. This arrangement might explain the ability of PhaF to maximize its hydrophilic interactions in the aqueous environment, and optimise the hydrophobic forces in the polymer layer. In the prospective of the assumption made in this work, the surface of granules being formed merely by proteins, these results let us conclude that elevated concentrations of PhaF function as a surfactant, separating PHA into “granules” in hydrophilic environments as occurs in the bacterial cytoplasm. This role of PhaF was also demonstrated by Mato et al. (2018) by means of experiments using lipid monolayers (Mato et al., 2018).

Altering the surface properties of biomaterials to enable improved protein and cell interactions has largely relied on the implementation of chemical modifications; for the most part these have been investigated on a case-by-case basis (and have been challenging). The fact that phasins bind to different hydrophobic polymers through relatively non-specific interactions increases the number of polymer substrates that could be functionalized. In addition, the present results for the Δπ(t) of polyester films, and the PM-IRRAS spectra acquired following PhaF injection, highlight the importance of considering the hydrophobic nature of the polymer to be functionalized. More strongly attractive interactions induced between PhaF and PHA resulted in the insertion of a

much greater number of PhaF molecules.

In addition to serving as a concept-testing tool, the formation of PhaF-alone films using the Langmuir technique could be used as a method for manufacturing coated surfaces, transferring them onto different solid hydrophobic substrates while precisely controlling their thicknesses at the molecular level. Future work at our laboratory will focus on using PhaF fused to cell-interacting motifs, and to DNA molecules (via its C-terminal binding domain), to coat biomaterials for tissue engineering applications.

VI. CONCLUSIONS

1. Phasins PhaF and PhaI of the mcl-PHA-accumulating bacterium *P. putida* KT2440 were shown to interact *in vivo* and *in vitro*, supporting the hypothesis of phasin oligomers forming a network-like structure at the PHA granule surface.
2. A short leucine-zipper like motif, highly conserved in phasins from *Pseudomonas*, was identified as the main oligomerization motif of PhaF and PhaI.
3. Three critical hydrophobic amino acids were acknowledged responsible for the stabilization of PhaI and PhaF homo- and heterodimers.
4. A new PhaF-interacting protein, the PHA transcriptional regulator PhaD, was identified in a comprehensive proteomic study. These proteins formed oligomers *in vivo*, as verified in two-hybrid tests.
5. Analysis of the PHA granule proteome and the *in vivo* localization of the PhaD-GFP fusion protein showed that, unlike most of the proteins associated with the *pha* cluster, PhaD is not a granule-associated protein.
6. A potential role for the PhaF-PhaD interaction in the regulation of PHA transcription was revealed. This might represent a new regulatory system in *Pseudomonas*.
7. Combining the Langmuir technique with surface spectroscopy to study the interaction of phasins and polymers at different interfaces allowed phasin intracellular environments - where a hydrophilic/hydrophobic interface is formed at the surface of the PHA granule - to be mimicked.
8. PhaF was found capable of adsorbing onto PHA while maintaining its α-helical structure. The adsorption of this protein to different polymers was made possible through its hydrophobicity, rendering it with a greater affinity for hydrophobic polymers such as PHA.
9. A stable monomolecular film of PhaF was produced at an air-water interface at different temperatures, and was successfully transferred to solid substrates as a proof-of-concept of phasin-coated materials. The flat topography and scant roughness of the transferred protein, as measured by AFM, revealed the film on the top of the supports to be smooth.
10. This work provides new knowledge of the surface activity of PhaF, prompting the use of this protein as a suitable coating for hydrophobic polymers.

VII. REFERENCES

Alves, L. P. S., C. S. Teixeira, E. F. Tirapelle, L. Donatti, M. Z. Tadra-Sfeir, M. B. R. Steffens, E. M. de Souza, F. de Oliveira Pedrosa, L. S. Chubatsu and M. Müller-Santos (2016). "Backup expression of the PhaP2 phasin compensates for *phaP1* deletion in *Herbaspirillum seropedicae*, maintaining fitness and PHB accumulation." Frontiers in Microbiology **7**(739).

Arias, S., M. Bassas-Galia, G. Molinari and K. N. Timmis (2013). "Tight coupling of polymerization and depolymerization of polyhydroxyalkanoates ensures efficient management of carbon resources in *Pseudomonas putida*." Microbial Biotechnology **6** (5): 551-563.

Ayub, N. D., P. M. Tribelli and N. I. López (2009). "Polyhydroxyalkanoates are essential for maintenance of redox state in the Antarctic bacterium *Pseudomonas* sp. 14-3 during low temperature adaptation." Extremophiles **13**(1): 59-66.

Bäckström, B. T., J. A. Brockelbank and B. H. Rehm (2007). "Recombinant *Escherichia coli* produces tailor-made biopolyester granules for applications in fluorescence activated cell sorting: functional display of the mouse interleukin-2 and myelin oligodendrocyte glycoprotein." BMC Biotechnology **7**(1): 3.

Balk, M., M. Behl, J. Yang, Q. Li, C. Wischke, Y. Feng and A. Lendlein (2017). "Design of polycationic micelles by self-assembly of polyethyleneimine functionalized oligo[(ε-caprolactone)-co-glycolide] ABA block copolymers." Polymers for Advanced Technologies **28**(10): 1278-1284.

Banki, M. R., T. U. Gerngross and D. W. Wood (2005). "Novel and economical purification of recombinant proteins: Intein-mediated protein purification using in vivo polyhydroxybutyrate (PHB) matrix association." Protein Science **14**(6): 1387-1395.

Barber-Zucker, S. and R. Zarivach (2017). "A Look into the biochemistry of magnetosome biosynthesis in magnetotactic bacteria." ACS Chemical Biology **12**(1): 13-22.

Barnard, G. C., J. D. McCool, D. W. Wood and T. U. Gerngross (2005). "Integrated recombinant protein expression and purification platform based on *Ralstonia eutropha*." Applied and Environmental Microbiology **71**(10): 5735-5742.

Barth, A. (2000). "The infrared absorption of amino acid side chains." Progress in Biophysics and Molecular Biology **74**(3): 141-173.

Beeby, M., M. Cho, J. Stubbe and G. J. Jensen (2011). "Growth and localization of polyhydroxybutyrate granules in *Ralstonia eutropha*." Journal of Bacteriology: JB. 06125 -06111.

Bello-Gil, D., B. Maestro, J. Fonseca, N. Dinjaski, M. A. Prieto and J. M. Sanz (2017). "Poly-3-hydroxybutyrate functionalization with BioF-tagged recombinant

proteins." Applied and Environmental Microbiology: AEM. 02595-02517.

Bhuvanesh, T., S. Saretia, T. Roch, A. C. Schöne, F. O. Rottke, K. Kratz, W. Wang, N. Ma, B. Schulz and A. Lendlein (2017). "Langmuir–Schaefer films of fibronectin as designed biointerfaces for culturing stem cells." Polymers for Advanced Technologies **28** (10): 1305-1311.

Blume, A. and A. Kerth (2013). "Peptide and protein binding to lipid monolayers studied by FT-IRRA spectroscopy." Biochimica et Biophysica Acta (BBA) - Biomembranes **1828**(10): 2294-2305.

Bradford, M. M. (1976). "A rapid and sensitive method for the quantitation of microgram quantities of protein utilizing the principle of protein-dye binding." Analytical Biochemistry **72**(1-2): 248-254.

Bresan, S., A. Sznajder, W. Hauf, K. Forchhammer, D. Pfeiffer and D. Jendrossek (2016). "Polyhydroxyalkanoate (PHA) granules have no phospholipids." Science Reports **6**(26612).

Bryant, D. A. and Z. Liu (2013). Chapter Four - Green Bacteria: Insights into green bacterial evolution through genomic analyses. Advances in Botanical Research. J. T. Beatty, Academic Press. **66:** 99-150.

Castano, S., D. Blaudez, B. Desbat, J. Dufourcq and H. Wróblewski (2002). "Secondary structure of spiralin in solution, at the air/water interface, and in interaction with lipid monolayers." Biochimica et Biophysica Acta (BBA) - Biomembranes **1562**(1): 45-56.

Castano, S., B. Desbat, M. Laguerre and J. Dufourcq (1999). "Structure, orientation and affinity for interfaces and lipids of ideally amphipathic lytic LiKj(i=2j) peptides." Biochimica et Biophysica Acta (BBA) - Biomembranes **1416**(1): 176-194.

Chanprateep, S. (2010). "Current trends in biodegradable polyhydroxyalkanoates." Journal of Bioscience and Bioengineering **110**(6): 621-632.

Chen, S.-Y., Y.-W. Chien and Y.-P. Chao (2014). "In vivo immobilization of D-hydantoinase in *Escherichia coli*." Journal of Bioscience and Bioengineering **118**(1): 78-81.

Choi, K. H., A. Kumar and H. P. Schweizer (2006). "A 10-min method for preparation of highly electrocompetent *Pseudomonas aeruginosa* cells: application for DNA fragment transfer between chromosomes and plasmid transformation." Journal of Microbiological Methods **64**(3): 391-397.

Christen, S., A. Srinivas, P. Bähler, A. Zeller, D. Pridmore, C. Bieniossek, U. Baumann and B. Erni (2006). "Regulation of the *dha* operon of *Lactococcus lactis* a

deviation from the rule followed by the tetr family of transcription regulators." Journal of Biological Chemistry **281**(32): 23129-23137.

Chung, C. W., H. W. Kim, Y. B. Kim and Y. H. Rhee (2003). "Poly(ethylene glycol)-grafted poly(3-hydroxyundecenoate) networks for enhanced blood compatibility." International Journal of Biological Macromolecules **32**(1-2): 17-22.

Cole, C., J. D. Barber and G. J. Barton (2008). "The Jpred 3 secondary structure prediction server." Nucleic Acids Research **36**(Web Server issue): W197-W201.

Cristobo, I., M. J. Larriba, V. d. l. Ríos, F. García, A. Muñoz and J. I. Casal (2011). "Proteomic analysis of 1α,25-Dihydroxyvitamin D3 action on human colon cancer cells reveals a link to splicing regulation." Journal of Proteomics **75**(2): 384-397.

Cuthbertson, L. and J. R. Nodwell (2013). "The TetR family of regulators." Microbiology and Molecular Biology Reviews **77**(3): 440-475.

de Eugenio, L. I., B. Galán, I. F. Escapa, B. Maestro, J. M. Sanz, J. L. García and M. A. Prieto (2010). "The PhaD regulator controls the simultaneous expression of the *pha* genes involved in polyhydroxyalkanoate metabolism and turnover in *Pseudomonas putida* KT2442." Environmenta Microbiology **12**(6): 1591-1603.

de Eugenio, L. I., P. García, J. M. Luengo, J. M. Sanz, J. S. Roman, J. L. García and M. A. Prieto (2007). "Biochemical evidence that *phaZ* gene encodes a specific intracellular medium chain length polyhydroxyalkanoate depolymerase in *Pseudomonas putida* KT2442: characterization of a paradigmatic enzyme." Journal of Biological Chemistry **282**(7): 4951-4962.

Dee, K. C., D. A. Puleo and R. Bizios (2003). An introduction to tissue-biomaterial interactions, John Wiley & Sons.

Delorenzi, M. and T. Speed (2002). "An HMM model for coiled-coil domains and a comparison with PSSM-based predictions." Bioinformatics **18**(4): 617-625.

Dennis, D., C. Liebig, T. Holley, K. S. Thomas, A. Khosla, D. Wilson and B. Augustine (2003). "Preliminary analysis of polyhydroxyalkanoate inclusions using atomic force microscopy." FEMS Microbiology Letters **226**(1): 113-119.

Dinjaski, N., M. Fernandez-Gutierrez, S. Selvam, F. J. Parra-Ruiz, S. M. Lehman, J. San Roman, E. Garcáa, J. L. García, A. J. García and M. A. Prieto (2014). "PHACOS, a functionalized bacterial polyester with bactericidal activity against methicillin-resistant Staphylococcus aureus." Biomaterials **35**(1): 14-24.

Dinjaski, N. and M. A. Prieto (2013). "Swapping of phasin modules to optimize the in vivo immobilization of proteins to medium-chain-length polyhydroxyalkanoate granules in *Pseudomonas putida*." Biomacromolecules **14**(9): 3285-3293.

Dong, Y., P. Li, C. B. Chen, Z. H. Wang, P. Ma and G. Q. Chen (2010). "The improvement of fibroblast growth on hydrophobic biopolyesters by coating with polyhydroxyalkanoate granule binding protein PhaP fused with cell adhesion motif RGD." Biomaterials **31**(34): 8921-8930.

Driks, A. (2002). "Maximum shields: the assembly and function of the bacterial spore coat." Trends in Microbiology **10**(6): 251-254.

Drioli, E., C. A. Quist-Jensen and L. Giorno (2015). Molecular Weight Cutoff. Encyclopedia of Membranes, Springer**:** 1-2.

Dukhin, S., G. Kretzschmar and R. Miller (1995). Thermodynamics and macro-kinetics of adsorption, Elsevier: Amsterdam. **1:** 30-67.

Dynarowicz-Łątka, P. and K. Kita (1999). "Molecular interaction in mixed monolayers at the air/water interface." Advances in Colloid and Interface Science **79**(1): 1-17.

Erlendsson, L. S., M. Möller and L. Hederstedt (2004). "*Bacillus subtilis* StoA Is a Thiol-Disulfide Oxidoreductase Important for Spore Cortex Synthesis." Journal of Bacteriology **186**(18): 6230-6238.

Escapa, I. F., C. del Cerro, J. L. García and M. A. Prieto (2013). "The role of GlpR repressor in *Pseudomonas putida* KT2440 growth and PHA production from glycerol." Environmental Microbiol **15**(1): 93-110.

Escapa, I. F., J. L. García, B. Bühler, L. Blank and M. A. Prieto (2012). "The polyhydroxyalkanoate metabolism controls carbon and energy spillage in *Pseudomonas putida*." Environmental Microbiology **14**(4): 1049-1063.

Escapa, I. F., V. Morales, V. P. Martino, E. Pollet, L. Averous, J. L. García and M. A. Prieto (2011). "Disruption of beta-oxidation pathway in *Pseudomonas putida* KT2442 to produce new functionalized PHAs with thioester groups." Applied Microbiology and Biotechnology **89**(5): 1583-1598.

Ferre-Guell, A. and J. Winterburn (2018). "Biosynthesis and characterization of polyhydroxyalkanoates with controlled composition and microstructure." Biomacromolecules **19**(3): 996-1005.

Fonseca, P., F. de la Peña and M. A. Prieto (2014). "A role for the regulator PsrA in the polyhydroxyalkanoate metabolism of *Pseudomonas putida* KT2440." International Journal of Biological Macromolecules **71**: 14-20.

Franklin, F. C., M. Bagdasarian, M. M. Bagdasarian and K. N. Timmis (1981). "Molecular and functional analysis of the TOL plasmid pWWO from *Pseudomonas putida* and cloning of genes for the entire regulated aromatic ring meta cleavage pathway." Proceedings of the National Academy of Sciences (PNAS) **78**(12): 7458-7462.

Fuller, R. C., J. P. O'Donnell, J. Saulnier, T. E. Redlinger, J. Foster and R. W. Lenz (1992). "The supramolecular architecture of the polyhydroxyalkanoate inclusions in *Pseudomonas oleovorans*." FEMS Microbiology Reviews **9**(2-4): 279-288.

Galán, B., N. Dinjaski, B. Maestro, L. I. de Eugenio, I. F. Escapa, J. M. Sanz, J. L. García and M. A. Prieto (2011). "Nucleoid-associated PhaF phasin drives intracellular location and segregation of polyhydroxyalkanoate granules in *Pseudomonas putida* KT2442." Molecular Microbiology **79**(2): 402-418.

Gao, T., H. Chang, M. Fan, X. Lu, Z. Wang, X. Zhang, X. Jing, Y. Shi and Z. Li (2014). Bio-modification of polyhydroxyalkanoates and its biocompatibility with chondrocytes. Zhong guo Xiu Fu Chong Jian Wai Ke Za Zhi (Chinese Journal of Reconstructive and Reparative Surgery) **28**(8): 1023-1029.

Garg, S., V. Swaminathan, S. Dhavala, M. A. Kiebish, R. Sarangarajan and N. R. Narain (2017). "CoQ10 selective miscibility and penetration into lipid monolayers with lower lateral packing density." Biochimica et Biophysica Acta (BBA) - Biomembranes **1859**(7): 1173-1179.

Gerngross, T., P. Reilly, J. Stubbe, A. Sinskey and O. Peoples (1993). "Immunocytochemical analysis of poly-beta-hydroxybutyrate (PHB) synthase in *Alcaligenes eutrophus* H16: localization of the synthase enzyme at the surface of PHB granules." Journal of Bacteriology **175**(16): 5289-5293.

Giner-Casares, J. J., G. Brezesinski and H. Möhwald (2014). "Langmuir monolayers as unique physical models." Current Opinion in Colloid & Interface Science **19**(3): 176-182.

Goormaghtigh, E., V. Cabiaux and J. M. Ruysschaert (1994). "Determination of soluble and membrane protein structure by Fourier transform infrared spectroscopy. III. Secondary structures." Subcellular Biochemistry **23**: 405-450.

Govindarajan, S. and O. Amster-Choder (2016). "Where are things inside a bacterial cell?" Current Opinion in Microbiology **33**: 83-90.

Griebel, R., Z. Smith and J. M. Merrick (1968). "Metabolism of poly(β-hydroxybutyrate). I. Purification, composition, and properties of native poly(β-hydroxybutyrate) granules from *Bacillus megaterium*." Biochemistry **7**(10): 3676-3681.

Grünberg, K., E.-C. Müller, A. Otto, R. Reszka, D. Linder, M. Kube, R. Reinhardt and D. Schüler (2004). "Biochemical and proteomic analysis of the magnetosome membrane in *Magnetospirillum gryphiswaldense*." Applied and Environmental Microbiology **70**(2): 1040-1050.

Guermeur, Y., C. Geourjon, P. Gallinari and G. Deleage (1999). "Improved performance in protein secondary structure prediction by in homogeneous score

combination." Bioinformatics **15**(5): 413-421.

Han, M., S. J. Park, J. W. Lee, B. Min, S. Y. Lee, S. Kim and J. S. Yoo (2006). "Analysis of poly(3-hydroxybutyrate) granule-associated proteome in recombinant *Escherichia coli*." Journal of Microbiology and Biotechnology **16**(6): 901.

Hanahan, D., J. Jessee and F. R. Bloom (1991). "Plasmid transformation of *Escherichia coli* and other bacteria." Methods in Enzymology **204**: 63-113.

Hänisch, J., M. Wältermann, H. Robenek and A. Steinbüchel (2006). "The *Ralstonia eutropha* H16 phasin PhaP1 is targeted to intracellular triacylglycerol inclusions in *Rhodococcus opacus* PD630 and *Mycobacterium smegmatis* mc2155, and provides an anchor to target other proteins." Microbiology **152**(Pt 11): 3271-3280.

Harbury, P. B., T. Zhang, P. S. Kim and T. Alber (1993). "A switch between two-, three-, and four-stranded coiled coils in GCN4 leucine zipper mutants." Science **262** (5138): 1401-1407.

Hauf, W., M. Schlebusch, J. Hüge, J. Kopka, M. Hagemann and K. Forchhammer (2013). "Metabolic changes in *Synechocystis* PCC6803 upon nitrogen-starvation: excess NADPH sustains polyhydroxybutyrate accumulation." Metabolites **3**(1): 101-118.

Hauf, W., B. Watzer, N. Roos, A. Klotz and K. Forchhammer (2015). "Photoautotrophic polyhydroxybutyrate granule formation is regulated by cyanobacterial phasin PhaP in *Synechocystis sp.* strain PCC 6803." Applied and Environmental Microbiology **81**(13): 4411-4422.

Hazer, B. and A. Steinbüchel (2007). "Increased diversification of polyhydroxyalkanoates by modification reactions for industrial and medical applications." Applied Microbiology Biotechnology **74**(1): 1-12.

Hazer, D. B., E. Kılıçay and B. Hazer (2012). "Poly(3-hydroxyalkanoate)s: diversification and biomedical applications: a state of the art review." Materials Science and Engineering: **32**(4): 637-647.

Hlady, V., J. Buijs and H. P. Jennissen (1999). [26] Methods for studying protein adsorption. Methods in Enzymology, Elsevier. **309:** 402-429.

Huisman, G. W., E. Wonink, R. Meima, B. Kazemier, P. Terpstra and B. Witholt (1991). "Metabolism of poly(3-hydroxyalkanoates) (PHAs) by *Pseudomonas oleovorans*. Identification and sequences of genes and function of the encoded proteins in the synthesis and degradation of PHA." Journal of Biological Chemistry **266**(4): 2191-2198.

Jagoda, A., P. Ketikidis, M. Zinn, W. Meier and K. Kita-Tokarczyk (2011). "Interactions of Biodegradable Poly([R]-3-hydroxy-10-undecenoate) with 1,2-Dioleoyl-sn -glycero-3-phosphocholine lipid: A monolayer study." Langmuir **27**(17): 10878-10885.

Jendrossek, D. (2009). "Polyhydroxyalkanoate granules are complex subcellular organelles (carbonosomes)." Journal of Bacteriology **191**(10): 3195-3202.

Jendrossek, D. and R. Handrick (2002). "Microbial degradation of polyhydroxyalkanoates." Annual Review of Microbiology **56**(1): 403-432.

Jendrossek, D. and D. Pfeiffer (2014). "New insights in the formation of polyhydroxyalkanoate granules (carbonosomes) and novel functions of poly(3-hydroxybutyrate)." Environmental Microbiology **16**(8): 2357-2373.

Jo, N.-J., T. Iwata, K. T. Lim, S.-H. Jung and W.-K. Lee (2007). "Degradation behaviors of polyester monolayers at the air/water interface: Alkaline and enzymatic degradations." Polymer Degradation and Stability **92**(7): 1199-1203.

Kadouri, D., E. Jurkevitch, Y. Okon and S. Castro-Sowinski (2005). "Ecological and agricultural significance of bacterial polyhydroxyalkanoates." Critical Reviews Microbiology **31**(2): 55-67.

Käll, L., J. D. Canterbury, J. Weston, W. S. Noble and M. J. MacCoss (2007). "Semi -supervised learning for peptide identification from shotgun proteomics datasets." Nature Methods **4**(11): 923-925.

Kanintronkul, Y., T. Srikhirin, C. Angsuthanasombat and T. Kerdcharoen (2005). "Insertion behavior of the *Bacillus thuringiensis* Cry4Ba insecticidal protein into lipid monolayers." Archives of Biochemistry and Biophysics **442**(2): 180-186.

Karimova, G., J. Pidoux, A. Ullmann and D. Ladant (1998). "A bacterial two-hybrid system based on a reconstituted signal transduction pathway." Proceedings of the National Academy of Sciences (PNAS) **95**(10): 5752-5756.

Karimova, G., A. Ullmann and D. Ladant (2000). "A bacterial two-hybrid system that exploits a cAMP signaling cascade in *Escherichia coli*." Methods in Enzymology **328**: 59-73.

Katti, D. S., R. Vasita and K. Shanmugam (2008). "Improved biomaterials for tissue engineering applications: surface modification of polymers." Current topics in medicinal chemistry **8**(4): 341-353.

Kim, Y. B. and R. W. Lenz (2001). Polyesters from microorganisms. Biopolyesters, Springer**:** 51-79.

Kniewel, R., O. Revelles Lopez and M. A. Prieto (2017). "Biogenesis of medium-chain-length polyhydroxyalkanoates." Biogenesis of Fatty Acids, Lipids and Membranes: 1-25.

Koller, M. (2018). "Biodegradable and Biocompatible Polyhydroxy-alkanoates (PHA): auspicious microbial macromolecules for pharmaceutical and therapeutic

applications." Molecules **23**(2): 362.

Krishna, O. D. and K. L. Kiick (2010). "Protein-and peptide-modified synthetic polymeric biomaterials." Biopolymers **94**(1): 32-48.

Kuchta, K., L. Chi, H. Fuchs, M. Pötter and A. Steinbüchel (2007). "Studies on the influence of phasins on accumulation and degradation of PHB and nanostructure of PHB granules in *Ralstonia eutropha* H16." Biomacromolecules **8**(2): 657-662.

Kyte, J. and R. F. Doolittle (1982). "A simple method for displaying the hydropathic character of a protein." Journal of Molecular Biology **157**(1): 105-132.

La Rosa, R., F. de la Peña, M. A. Prieto and F. Rojo (2014). "The Crc protein inhibits the production of polyhydroxyalkanoates in *Pseudomonas putida* under balanced carbon/nitrogen growth conditions." Environmental Microbiology **16**(1): 278-290.

Lambeek, G., E. J. Vorenkamp and A. J. Schouten (1995). "Structural study of Langmuir-Blodgett mono- and multilayers of poly(beta-hydroxybutyrate)." Macromolecules **28**(6): 2023-2032.

Lau, S. Y., A. K. Taneja and R. S. Hodges (1984). "Synthesis of a model protein of defined secondary and quaternary structure. Effect of chain length on the stabilization and formation of two-stranded alpha-helical coiled-coils." Journal of Biological Chemistry **259**(21): 13253-13261.

Li, X., H. Chang, H. Luo, Z. Wang, G. Zheng, X. Lu, X. He, F. Chen, T. Wang, J. Liang and M. Xu (2015). "Poly(3-hydroxybutyrate-co-3-hydroxyhexanoate) scaffolds coated with PhaP-RGD fusion protein promotes the proliferation and chondrogenic differentiation of human umbilical cord mesenchymal stem cells *in vitro*." Journal of Biomedical Materials Research A **103**(3): 1169-1175.

Li, Z., J. Yang and X. J. Loh (2016). "Polyhydroxyalkanoates: opening doors for a sustainable future." NPG Asia Materials **8**(4): e265.

Lim, S.-P., S.-N. Gan and I. K. Tan (2005). "Degradation of medium-chain-length polyhydroxyalkanoates in tropical forest and mangrove soils." Applied Biochemistry and Biotechnology **126**(1): 23.

Lin, Y., L. Wang, P. Zhang, X. Wang, X. Chen, X. Jing and Z. Su (2006). "Surface modification of poly(l-lactic acid) to improve its cytocompatibility via assembly of polyelectrolytes and gelatin." Acta Biomaterialia **2**(2): 155-164.

Liu, W., S. Li, Z. Wang, E. C. Yan and R. M. Leblanc (2017). "Characterization of surface-active biofilm protein BslA in self-assembling langmuir monolayer at the air–water interface." Langmuir **33**(30): 7548-7555.

Lórenz-Fonfría, V. A., C. Bamann, T. Resler, R. Schlesinger, E. Bamberg and J. Heberle (2015). "Temporal evolution of helix hydration in a light-gated ion channel correlates with ion conductance." Proceedings of the National Academy of Sciences (PNAS) **112**(43): E5796-E5804.

Lu, J., R. C. Tappel and C. T. Nomura (2009). "Mini-review: biosynthesis of poly (hydroxyalkanoates)." Journal of Macromolecular Science, Part C: Polymer Reviews **49** (3): 226-248.

Lupas, A., M. Van Dyke and J. Stock (1991). "Predicting coiled coils from protein sequences." Science **252**(5009): 1162-1164.

Maehara, A., Y. Doi, T. Nishiyama, Y. Takagi, S. Ueda, H. Nakano and T. Yamane (2001). "PhaR, a protein of unknown function conserved among short-chain-length polyhydroxyalkanoic acids producing bacteria, is a DNA-binding protein and represses *Paracoccus denitrificans phaP* expression in vitro." FEMS microbiology letters **200**(1): 9-15.

Maehara, A., S. Taguchi, T. Nishiyama, T. Yamane and Y. Doi (2002). "A repressor protein, PhaR, regulates polyhydroxyalkanoate (PHA) synthesis via its direct interaction with PHA." Journal of Bacteriology **184**(14): 3992-4002.

Maehara, A., S. Ueda, H. Nakano and T. Yamane (1999). "Analyses of a polyhydroxyalkanoic acid granule-associated 16-kilodalton protein and its putative regulator in the *pha* locus of *Paracoccus denitrificans*." Journal of Bacteriology **181**(9): 2914-2921.

Maestro, A., F. Ortega, R. G. Rubio, M. A. Rubio, J. Kragel and R. Miller (2011). "Rheology of poly(methyl methacrylate) Langmuir monolayers: percolation transition to a soft glasslike system." Journal of Chemistry and Physics **134**(10): 104704.

Maestro, B., B. Galán, C. Alfonso, G. Rivas, M. A. Prieto and J. M. Sanz (2013). "A new family of intrinsically disordered proteins: structural characterization of the major phasin PhaF from *Pseudomonas putida* KT2440." PLOS ONE **8**(2): 15.

Maestro, B. and J. M. Sanz (2017). "Polyhydroxyalkanoate-associated phasins as phylogenetically heterogeneous, multipurpose proteins." Microbial Biotechnology **20** (10): 1751-7915.

Mason, J. M. and K. M. Arndt (2004). "Coiled coil domains: stability, specificity, and biological implications." Chembiochem **5**(2): 170-176.

Mathew, S., S. Baudis, A. T. Neffe, M. Behl, C. Wischke and A. Lendlein (2015). "Effect of diisocyanate linkers on the degradation characteristics of copolyester urethanes as potential drug carrier matrices." European Journal of Pharmaceutics and Biopharmaceutics **95**: 18-26.

Mato, A., N. A. Tarazona, A. Hidalgo, A. Cruz, M. Jimenez, J. Perez-Gil and M. A. Prieto (2018). "Interfacial activity of phasin PhaF from *Pseudomonas putida* KT2440 at hydrophobic-hydrophilic biointerfaces." Langmuir **35**(3): 678-686.

Mayer, F. and M. Hoppert (1997). "Determination of the thickness of the boundary layer surrounding bacterial PHA inclusion bodies, and implications for models describing the molecular architecture of this layer." Journal of Basic Microbiology **37**(1): 45-52.

Mezzina, M. P. and M. J. Pettinari (2016). "Phasins, multifaceted polyhydroxyalkanoate granule-associated proteins." Appl Environ Microbiol **82**(17): 5060-5067.

Mezzina, M. P., D. E. Wetzler, M. V. Catone, H. Bucci, M. Di Paola and M. J. Pettinari (2014). "A Phasin with Many Faces: Structural Insights on PhaP from *Azotobacter sp*. FA8." PLOS ONE **9**(7): e103012.

Miller, J. H. (1972). Experiments in Molecular Genetics, Cold Spring Harbor Laboratory.

Moldes, C., G. P. Farinós, L. I. de Eugenio, P. García, J. L. García, F. Ortego, P. Hernández-Crespo, P. Castañera and M. A. Prieto (2006). "New tool for spreading proteins to the environment: Cry1Ab toxin immobilized to bioplastics." Applied Microbiology and Biotechnology **72**(1): 88-93.

Moldes, C., P. Garcia, J. L. Garcia and M. A. Prieto (2004). "In vivo immobilization of fusion proteins on bioplastics by the novel tag BioF." Applied Environmental Microbiology **70**(6): 3205-3212.

Mozejko-Ciesielska, J., D. Dabrowska, A. Szalewska-Palasz and S. Ciesielski (2017). "Medium-chain-length polyhydroxyalkanoates synthesis by *Pseudomonas putida* KT2440 relA/spoT mutant: bioprocess characterization and transcriptome analysis." Amb Express **7**(1): 92-92.

Murat, D., M. Byrne and A. Komeili (2010). "Cell biology of prokaryotic organelles." Cold Spring Harbor Perspectives in Biology **2**(10).

Murphy, D. J. (1993). "Structure, function and biogenesis of storage lipid bodies and oleosins in plants." Progress in Lipid Research **32**(3): 247-280.

Narancic, T., E. Scollica, G. Cagney and K. E. O'Connor (2018). "Three novel proteins co-localise with polyhydroxybutyrate (PHB) granules in *Rhodospirillum rubrum* S1." Microbiology **164**(4): 625-634.

Neff, J. A., K. D. Caldwell and P. A. Tresco (1998). "A novel method for surface modification to promote cell attachment to hydrophobic substrates." Journal of Biomedical Materials Research **40**(4): 511-519.

Nelson, K., C. Weinel, I. Paulsen, R. Dodson, H. Hilbert, V. M. dos Santos, D. Fouts, S. Gill, M. Pop and M. Holmes (2002). "Complete genome sequence and comparative analysis of the metabolically versatile *Pseudomonas putida* KT2440." Environmental Microbiology **4**(12): 799-808.

Neumann, L., F. Spinozzi, R. Sinibaldi, F. Rustichelli, M. Pötter and A. Steinbüchel (2008). "Binding of the major phasin, PhaP1, from *Ralstonia eutropha* H16 to poly(3-hydroxybutyrate) granules." Journal of Bacteriology **190**(8): 2911-2919.

Nikel, P. I., E. Martinez-Garcia and V. de Lorenzo (2014). "Biotechnological domestication of pseudomonads using synthetic biology." Nature Reviews Microbiology **12**(5): 368-379.

Nobes, G. A. R., D. A. Holden and R. H. Marchessault (1994). "Spreading of poly(β-hydroxylalkanoate)s at the air-water interface: a model system for the nascent lyotropic state of bacterial polyesters." Polymer **35**(2): 435-437.

Nogales, J., B. Ø. Palsson and I. Thiele (2008). "A genome-scale metabolic reconstruction of *Pseudomonas putida* KT2440: i JN746 as a cell factory." BMC systems biology **2**(1): 79.

Obruca, S., P. Sedlacek, F. Mravec, O. Samek and I. Marova (2016). "Evaluation of 3-hydroxybutyrate as an enzyme-protective agent against heating and oxidative damage and its potential role in stress response of poly(3-hydroxybutyrate) accumulating cells." Applied Microbiology and Biotechnology **100**(3): 1365-1376.

Park, H., M. Radisic, J. O. Lim, B. H. Chang and G. Vunjak-Novakovic (2005). "A novel composite scaffold for cardiac tissue engineering." *In Vitro* Cellular & Developmental Biology - Animal **41**(7): 188-196.

Pederson, E. N., C. W. McChalicher and F. Srienc (2006). "Bacterial synthesis of PHA block copolymers." Biomacromolecules **7**(6): 1904-1911.

Pfeiffer, D. and D. Jendrossek (2011). "Interaction between poly(3-hydroxybutyrate) granule-associated proteins as revealed by two-hybrid analysis and identification of a new phasin in *Ralstonia eutropha* H16." Microbiology **157**(Pt 10): 2795 -2807.

Pfeiffer, D. and D. Jendrossek (2012). "Localization of poly(3-Hydroxybutyrate) (PHB) granule-associated üroteins during PHB granule formation and identification of two new phasins, PhaP6 and PhaP7, in *Ralstonia eutropha* H16." Journal of Bacteriology **194**(21): 5909-5921.

Pfeiffer, D. and D. Jendrossek (2013). "Development of a transferable bimolecular fluorescence complementation system for the investigation of interactions between poly (3-Hydroxybutyrate) granule-associated proteins in Gram-negative bacteria." Applied

and Environmental Microbiology **79**(9): 2989-2999.

Pfeiffer, D., A. Wahl and D. Jendrossek (2011). "Identification of a multifunctional protein, PhaM, that determines number, surface to volume ratio, subcellular localization and distribution to daughter cells of poly(3-hydroxybutyrate), PHB, granules in *Ralstonia eutropha* H16." Molecular Microbiology **82**(4): 936-951.

Poblete-Castro, I., I. F. Escapa, C. Jäger, J. Puchalka, C. M. C. Lam, D. Schomburg, M. A. Prieto and V. A. M. dos Santos (2012). "The metabolic response of *P. putida* KT2442 producing high levels of polyhydroxyalkanoate under single-and multiple-nutrient-limited growth: Highlights from a multi-level omics approach." Microbial cell factories **11**(1): 34.

Pötter, M., M. H. Madkour, F. Mayer and A. Steinbüchel (2002). "Regulation of phasin expression and polyhydroxyalkanoate (PHA) granule formation in *Ralstonia eutropha* H16." Microbiology **148**(8): 2413-2426.

Pötter, M., H. Müller, F. Reinecke, R. Wieczorek, F. Fricke, B. Bowien, B. Friedrich and A. Steinbüchel (2004). "The complex structure of polyhydroxybutyrate (PHB) granules: four orthologous and paralogous phasins occur in *Ralstonia eutropha*." Microbiology **150**(Pt 7): 2301-2311.

Prieto, A., I. F. Escapa, V. Martinez, N. Dinjaski, C. Herencias, F. de la Pena, N. Tarazona and O. Revelles (2016). "A holistic view of polyhydroxyalkanoate metabolism in *Pseudomonas putida*." Environmental Microbiology **18**(2): 341-357.

Prieto, M. A., B. Buhler, K. Jung, B. Witholt and B. Kessler (1999). "PhaF, a polyhydroxyalkanoate-granule-associated protein of *Pseudomonas oleovorans* GPo1 involved in the regulatory expression system for *pha* genes." Journal of Bacteriology **181** (3): 858-868.

Puchalka, J., M. Oberhardt, M. Godinho, A. Bielecka, D. Regenhardt, K. Timmis and J. Papin "Martins, dS, V (2008). Genome-scale reconstruction and analysis of the *Pseudomonas putida* KT2440 metabolic network facilitates applications in biotechnology." PLoS Computational Biology **4**: e1000210.

Qi, Q., A. Steinbüchel and B. H. A. Rehm (2000). "*In vitro* synthesis of poly(3-hydroxydecanoate): purification and enzymatic characterization of type II polyhydroxyalkanoate synthases PhaC1 and PhaC2 from *Pseudomonas aeruginosa*." Applied Microbiology and Biotechnology **54**(1): 37-43.

Rai, R., T. Keshavarz, J. A. Roether, A. R. Boccaccini and I. Roy (2011). "Medium chain length polyhydroxyalkanoates, promising new biomedical materials for the future." Materials Science and Engineering: R: Reports **72**(3): 29-47.

Regenhardt, D., H. Heuer, S. Heim, D. U. Fernandez, C. Strompl, E. R. Moore and

K. N. Timmis (2002). "Pedigree and taxonomic credentials of *Pseudomonas putida* strain KT2440." Environmental Microbiology **4**(12): 912-915.

Rehm, B. H. (2010). "Bacterial polymers: biosynthesis, modifications and applications." Nature Reviews Microbiology **8**(8): 578.

Rehm, F. B., S. Chen and B. H. Rehm (2016). "Enzyme engineering for *In Situ* immobilization." Molecules **21**(10).

Ren, Q., G. de Roo, K. Ruth, B. Witholt, M. Zinn and L. Thöny-Meyer (2009). "Simultaneous accumulation and degradation of polyhydroxyalkanoates: futile cycle or clever regulation?" Biomacromolecules **10**(4): 916-922.

Ren, Q., N. Sierro, B. Witholt and B. Kessler (2000). "FabG, an NADPH-dependent 3-ketoacyl reductase of *Pseudomonas aeruginosa*, provides precursors for medium-chain -length poly-3-hydroxyalkanoate biosynthesis in *Escherichia coli*." Journal of Bacteriology **182**(10): 2978-2981.

Robichon, C., G. Karimova, J. Beckwith and D. Ladant (2011). "Role of leucine zipper motifs in association of the *Escherichia coli* cell division proteins FtsL and FtsB." Journal of Bacteriology **193**(18): 4988-4992.

Rogalska, E., R. Bilewicz, T. Brigaud, C. El Moujahid, G. Foulard, C. Portella and M. -J. Stébé (2000). "Formation and properties of Langmuir and Gibbs monolayers: a comparative study using hydrogenated and partially fluorinated amphiphilic derivatives of mannitol." Chemistry and Physics of Lipids **105**(1): 71-91.

Rost, B., G. Yachdav and J. Liu (2004). "The PredictProtein server." Nucleic Acids Research **32**(Web Server issue).

Ruiz, J. A., N. I. López, R. O. Fernández and B. S. Méndez (2001). "Polyhydroxyalkanoate degradation is associated with nucleotide accumulation and enhances stress resistance and survival of *Pseudomonas oleovorans* in natural water microcosms." Applied and Environmental Microbiology **67**(1): 225-230.

Ruiz, J. A., N. I. López and B. S. Méndez (2004). "*rpoS* gene expression in carbon-starved cultures of the polyhydroxyalkanoate-accumulating species *Pseudomonas oleovorans*." Current microbiology **48**(6): 396-400.

Russell, A. J., S. L. Baker, C. M. Colina, C. A. Figg, J. L. Kaar, K. Matyjaszewski, A. Simakova and B. S. Sumerlin (2018). "Next generation protein-polymer conjugates." AIChE Journal.

Ruth, K., G. d. Roo, T. Egli and Q. Ren (2008). "Identification of two acyl-CoA synthetases from *Pseudomonas putida* GPo1: one is located at the surface of polyhydroxyalkanoates granules." Biomacromolecules **9**(6): 1652-1659.

Ryan, W. J., N. D. O'Leary, M. O'Mahony and A. D. Dobson (2013). "GacS dependent regulation of polyhydroxyalkanoate synthesis in *Pseudomonas putida* CA-3." Applied and Environmental Microbiology: AEM. 02962-02912.

Sambrook, J. and D. W. Russell (2001). "Molecular cloning: a laboratory manual." Cold Spring Harb Lab Press Cold Spring Harb NY.

Sandoval, A., E. Arias-Barrau, M. Arcos, G. Naharro, E. R. Olivera and J. M. Luengo (2007). "Genetic and ultrastructural analysis of different mutants of *Pseudomonas putida* affected in the poly-3-hydroxy-n-alkanoate gene cluster." Environmental Microbiology **9**(3): 737-751.

Schöne, A. C., S. Falkenhagen, O. Travkova, B. Schulz, K. Kratz and A. Lendlein (2015). "Influence of intermediate degradation products on the hydrolytic degradation of poly [(rac-lactide)-co-glycolide] at the air–water interface." Polymers for Advanced Technologies **26**(12): 1402-1410.

Schöne, A. C., K. Richau, K. Kratz, B. Schulz and A. Lendlein (2015). "Influence of Diurethane Linkers on the Langmuir Layer Behavior of Oligo[(rac-lactide)-co-glycolide]-based Polyesterurethanes." Macromolecular Rapid Communications **36**(21): 1910-1915.

Schöne, A. C., T. Roch, B. Schulz and A. Lendlein (2017). "Evaluating polymeric biomaterial-environment interfaces by Langmuir monolayer techniques." Journal of the Royal Society Interface **14**(130).

Shen, X. W., Z. Y. Shi, G. Song, Z. J. Li and G. Q. Chen (2011). "Engineering of polyhydroxyalkanoate (PHA) synthase $PhaC2_{Ps}$ of *Pseudomonas stutzeri* via site-specific mutation for efficient production of PHA copolymers." Applied Microbiology and Biotechnology **91**(3): 655-665.

Shimoshige, H., H. Kobayashi, T. Mizuki, Y. Nagaoka, A. Inoue and T. Maekawa (2015). "Effect of polyethylene glycol on the formation of magnetic nanoparticles synthesized by *Magnetospirillum magnetotacticum* MS-1." PloS one **10**(5): e0127481.

Steinbüchel, A., K. Aerts, W. Babel, C. Follner, M. Liebergesell, M. H. Madkour, F. Mayer, U. Pieper-Fürst, A. Pries, H. E. Valentin and et al. (1995). "Considerations on the structure and biochemistry of bacterial polyhydroxyalkanoic acid inclusions." Canadian Journal of Microbiology **1**: 94-105.

Sudesh, K., H. Abe and Y. Doi (2000). "Synthesis, structure and properties of polyhydroxyalkanoates: biological polyesters." Progress in Polymer Science **25**(10): 1503-1555.

Sultana, A. and J. E. Lee (2001). Measuring protein-protein and protein-nucleic acid interactions by biolayer interferometry. Current Protocols in Protein Science, John Wiley & Sons, Inc.

Szklarczyk, D., J. H. Morris, H. Cook, M. Kuhn, S. Wyder, M. Simonovic, A. Santos, N. T. Doncheva, A. Roth, P. Bork, L. J. Jensen and C. von Mering (2017). "The STRING database in 2017: quality-controlled protein-protein association networks, made broadly accessible." Nucleic Acids Research **45**(D1): D362-D368.

Sznajder, A., D. Pfeiffer and D. Jendrossek (2015). "Comparative proteome analysis reveals four novel polyhydroxybutyrate (PHB) granule-associated proteins in *Ralstonia eutropha* H16." Applied Environmental Microbiology **81**(5): 1847-1858.

Tallawi, M., E. Rosellini, N. Barbani, M. G. Cascone, R. Rai, G. Saint-Pierre and A. R. Boccaccini (2015). "Strategies for the chemical and biological functionalization of scaffolds for cardiac tissue engineering: a review." Journal of the Royal Society Interface **12**(108): 20150254.

Tan, G.-Y. A., C.-L. Chen, L. Li, L. Ge, L. Wang, I. M. N. Razaad, Y. Li, L. Zhao, Y. Mo and J.-Y. Wang (2014). "Start a research on biopolymer polyhydroxyalkanoate (PHA): a review." Polymers **6**(3): 706-754.

Toimil, P., G. Prieto, J. Minones, Jr., J. M. Trillo and F. Sarmiento (2012). "Monolayer and Brewster angle microscopy study of human serum albumin-dipalmitoyl phosphatidyl choline mixtures at the air-water interface." Colloids and Surfaces B: Biointerfaces **92**: 64-73.

Tronin, A., T. Dubrovsky, C. De Nitti, A. Gussoni, V. Erokhin and C. Nicolini (1994). "Langmuir-Blodgett films of immunoglobulines IgG. Ellipsometric study of the deposition process and of immunological activity." Thin Solid Films **238**(1): 127-132.

Truebestein, L. and T. A. Leonard (2016). "Coiled-coils: The long and short of it." Bioessays **38**(9): 903-916.

Uchino, K., T. Saito, B. Gebauer and D. Jendrossek (2007). "Isolated poly(3-hydroxybutyrate) (PHB) granules are complex bacterial organelles catalyzing formation of PHB from acetyl coenzyme A (CoA) and degradation of PHB to acetyl-CoA." Journal of Bacteriology **189**(22): 8250-8256.

Venyaminov, S. Y. and N. N. Kalnin (1990). "Quantitative IR spectrophotometry of peptide compounds in water (H_2O) solutions. II. Amide absorption bands of polypeptides and fibrous proteins in α-, β-, and random coil conformations." Biopolymers **30**(13-14): 1259-1271.

Vincent, T. L., P. J. Green and D. N. Woolfson (2013). "LOGICOIL—multi-state prediction of coiled-coil oligomeric state." Bioinformatics **29**(1): 69-76.

Wahl, A., N. Schuth, D. Pfeiffer, S. Nussberger and D. Jendrossek (2012). "PHB granules are attached to the nucleoid via PhaM in *Ralstonia eutropha*." BMC Microbiology **12**: 262-262.

Wang, Y., A. Chung and G.-Q. Chen (2017). "Synthesis of medium-chain-length polyhydroxyalkanoate homopolymers, random copolymers, and block copolymers by an engineered strain of *Pseudomonas entomophila*." Advanced Healthcare Materials **6**(7): 1601017.

Wang, Z., H. Wu, J. Chen, J. Zhang, Y. Yao and G.-Q. Chen (2008). "A novel self-cleaving phasin tag for purification of recombinant proteins based on hydrophobic polyhydroxyalkanoate nanoparticles." Lab on a Chip **8**(11): 1957-1962.

Wei, D. X., C. B. Chen, G. Fang, S. Y. Li and G. Q. Chen (2011). "Application of polyhydroxyalkanoate binding protein PhaP as a bio-surfactant." Applied Microbiology and Biotechnology **91**(4): 1037-1047.

Wei, Q., T. Becherer, S. Angioletti-Uberti, J. Dzubiella, C. Wischke, A. T. Neffe, A. Lendlein, M. Ballauff and R. Haag (2014). "Protein interactions with polymer coatings and biomaterials." Angewandte Chemie International Edition in English **53**(31): 8004-8031.

Wieczorek, R., A. Pries, A. Steinbüchel and F. Mayer (1995). "Analysis of a 24-kilodalton protein associated with the polyhydroxyalkanoic acid granules in *Alcaligenes eutrophus*." Journal of Bacteriology **177**(9): 2425-2435.

Wilcox, K. E., E. W. Blanch and A. J. Doig (2016). "Determination of protein secondary structure from infrared spectra using partial least-squares regression." Biochemistry **55**(27): 3794-3802.

Xie, H., J. Li, L. Li, Y. Dong, G. Q. Chen and K. C. Chen (2013). "Enhanced proliferation and differentiation of neural stem cells grown on PHA films coated with recombinant fusion proteins." Acta Biomaterialia **9**(8): 7845-7854.

Xue, B., R. L. Dunbrack, R. W. Williams, A. K. Dunker and V. N. Uversky (2010). "PONDR-FIT: A meta-predictor of intrinsically disordered amino acids." Biochimica et biophysica acta **1804**(4): 996-1010.

Yamada, M., S. Takahashi, Y. Okahata, Y. Doi and K. Numata (2013). "Monitoring and kinetic analysis of the molecular interactions by which a repressor protein, PhaR, binds to target DNAs and poly [(R)-3-hydroxybutyrate]." Amb Express **3**(1): 6.

Yamada, M., K. Yamashita, A. Wakuda, K. Ichimura, A. Maehara, M. Maeda and S. Taguchi (2007). "Autoregulator protein PhaR for biosynthesis of polyhydroxybutyrate [P (3HB)] possibly has two separate domains that bind to the target DNA and P(3HB): functional mapping of amino acid residues responsible for DNA binding." Journal of Bacteriology **189**(3): 1118-1127.

Yang, Y., J. Gao, J. Wang, R. Heffernan, J. Hanson, K. Paliwal and Y. Zhou (2016). "Sixty-five years of the long march in protein secondary structure prediction: the final

stretch?" Briefings in Bioinformatics **19**(3): 482-494.

Yano, Y. F., T. Uruga, H. Tanida, Y. Terada and H. Yamada (2011). "Protein salting out observed at an air–water interface." The Journal of Physical Chemistry Letters **2**(9): 995-999.

Yao, Y. C., X. Y. Zhan, J. Zhang, X. H. Zou, Z. H. Wang, Y. C. Xiong, J. Chen and G. Q. Chen (2008). "A specific drug targeting system based on polyhydroxyalkanoate granule binding protein PhaP fused with targeted cell ligands." Biomaterials **29**(36): 4823-4830.

York, G. M., J. Stubbe and A. J. Sinskey (2001). "New insight into the role of the PhaP phasin of *Ralstonia eutropha* in promoting synthesis of polyhydroxybutyrate." Journal of Bacteriology **183**(7): 2394-2397.

York, G. M., J. Stubbe and A. J. Sinskey (2002). "The *Ralstonia eutropha* PhaR protein couples synthesis of the PhaP phasin to the presence of polyhydroxybutyrate in cells and promotes polyhydroxybutyrate production." Journal of Bacteriology **184**(1): 59-66.

You, M., G. Peng, J. Li, P. Ma, Z. Wang, W. Shu, S. Peng and G. Q. Chen (2011). "Chondrogenic differentiation of human bone marrow mesenchymal stem cells on polyhydroxyalkanoate (PHA) scaffolds coated with PHA granule binding protein PhaP fused with RGD peptide." Biomaterials **32**(9): 2305-2313.

Zhang, J. (2012). Protein-Protein Interactions in Salt Solutions.

Zhao, H., H. Wei, X. Liu, Z. Yao, M. Xu, D. Wei, J. Wang, X. Wang and G.-Q. Chen (2016). "Structural insights on PHA Binding protein PhaP from *Aeromonas hydrophila*." Scientific Reports **6**: 39424.

Zhao, M., Z. Li, W. Zheng, Z. Lou and G.-Q. Chen (2006). "Crystallization and initial X-ray analysis of polyhydroxyalkanoate granule-associated protein from *Aeromonas hydrophila*." Acta Crystallographica Section F: Structural Biology and Crystallization Communications **62**(8): 814-819.

Zinn, M. and R. Hany (2005). "Tailored material properties of polyhydroxyalkanoates through biosynthesis and chemical modification." Advanced Engineering Materials **7**(5): 408-411.

ANNEX 1.

PHOHHx detailed characterization

When octanoic acid (C8) is used as the sole carbon source, *P. putida* produces mcl-PHAs containing randomly distributed (*R*)-3-hydroxyoctanoate (C8) and (*R*)-3-hydroxyhexanoate (C6), PHO-co-PHHx copolymer (refer to as PHOHHx). The presence of shorter chains is an intrinsic characteristic of mcl-PHAs produced by β-oxidation of fatty acids. Monomer content of PHOHHx has been widely reported as ~94 mol % 3HO and ~6% 3HHx.[59] The monomeric composition of the polymer was further verified by nuclear magnetic resonance NMR. The spectra of ^{1}H- and ^{13}C-NMR of the purified PHOHHx and the assignment of the corresponding PHA by comparison with published data are depicted in Figure A1. The ^{1}H NMR spectra showed the different environments for mcl-PHA protons. Resonance signal at 0.88 ppm designated the presence of methyl group protons (-CH_3 group); the methylene proton resonance (-CH_2 group) was seen at 1.28, 1.59 and 2.54; and the resonance at 5.18 showed the methine proton of PHA. Eight peaks corresponding to the eight different environments for the carbon in HO monomers were obtained. The chemical-shifts at 169.38 ppm (C1, C=O group), 70.84 ppm (C3, –CH group), 39.10 ppm (C2, -CH_2 group), 22-34 ppm (C4-C7, -CH_2 group) and 13.94 ppm (C8, -CH_3 group) were consistent with those reported for the 3HO monomer.[28, 35] Additionally, chemical-shifts at 70.59 ppm (C3, –CH group), 35.87 ppm (C4 –CH_2 group), 18.29 ppm (C5 –CH_2 group) and 13.77 ppm (C6 –CH_3 group) confirmed that the PHA synthesized by *P. putida* KT2440 is a random copolymer of 3HO and 3HHx monomers. Polymer molecular weight after purification was determined by GPC as M_w: 166 500 g·mol^{-1} and PDI of 1.8, which is accepted as a low value for polymers produced by bacteria.

Figure. A1. ^{1}H- and ^{13}C-NMR spectra of poly[(3-*R*-hydroxyoctanoate)-*co*-(3-*R*-hydroxyhexanoate)] (PHOHHx)

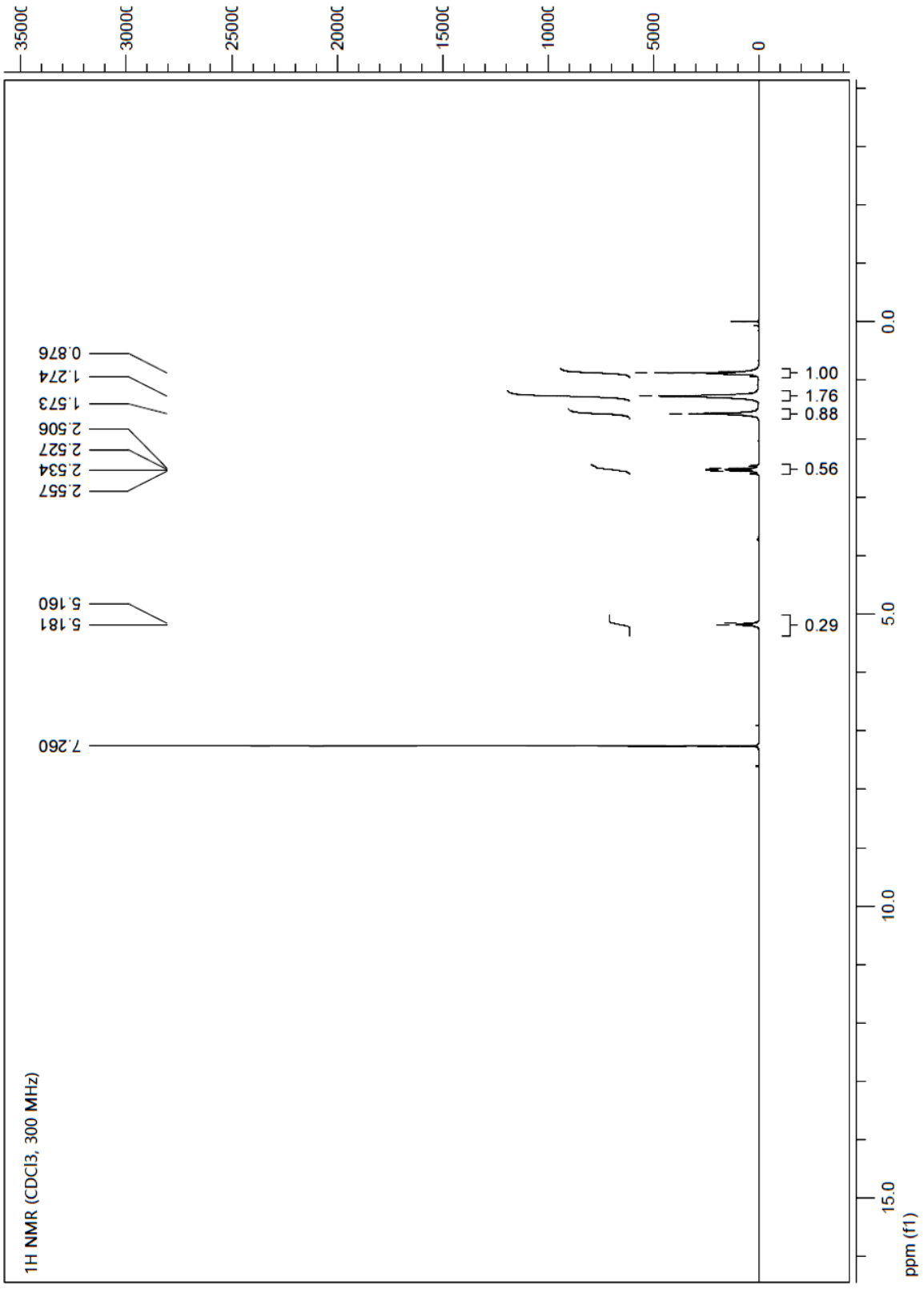

Figure. A1. ^{1}H- and ^{13}C-NMR spectra of poly[(3-*R*-hydroxyoctanoate)-*co*-(3-*R*-hydroxyhexanoate)] (PHOHHx)